THE UNIVERSITY OF CHICAGO

QUANTIFICATION OF THE ALLOSTERICALLY-DRIVEN UNFOLDING OF BTUB'S N-TERMINUS UPON B12 BINDING BY HDX-MS

A DISSERTATION SUBMITTED TO
THE FACULTY OF THE DIVISION OF THE BIOLOGICAL SCIENCES
IN CANDIDACY FOR THE DEGREE OF
DOCTOR OF PHILOSOPHY

GRADUATE PROGRAM IN BIOCHEMISTRY AND MOLECULAR BIOPHYSICS

BY
ADAM MACIEJ ZMYSLOWSKI

CHICAGO, ILLINOIS
DECEMBER 2021

"The true delight is in the finding out rather than in the knowing."

Isaac Asimov

TABLE OF CONTENTS

LIST OF FIGURES vi

ACKNOWLEDGMENTS vii

ABSTRACT ix

1 INTRODUCTION 1
1.1 TonB-dependent transporters (TBDTs) 1
1.1.1 The outer membrane (OM) environment and OM proteins 2
1.1.2 TBDTs in bactericidal and medical contexts 4
1.1.3 Evolution, structure, biogenesis, and regulation of TBDTs 6
1.1.4 Mechanism features common to TBDTs 9
1.2 BtuB, the *E. coli* vitamin B12 TBDT 10
1.2.1 The structure of BtuB 10
1.2.2 Early steps in BtuB transport 12
1.2.3 Models of pore formation in BtuB 12
1.3 Hydrogen deuterium exchange mass spectrometry (HDX-MS) at the outer membrane 14
1.3.1 Introduction to HDX-MS 14
1.3.2 Practical aspects of conducting HDX-MS 17
1.3.3 Applying HDX-MS at the outer membrane 21

2 CONFORMATIONAL RESPONSE OF BTUB TO LIGAND BINDING IN OUTER MEMBRANES (ZMYSLOWSKI ET AL 2021 25
2.1 Summary 26
2.2 Introduction 26
2.3 Results 33
2.3.1 OM sample preparation, sequence coverage 33
2.3.2 Reproducibility and heterogeneity 37
2.3.3 HDX formalism 38
2.3.4 Substrate binding loops 43
2.3.5 Destabilization of the Ionic Lock (IL) and Ton box upon B12 binding 43
2.3.6 Complex ligand effects in the third substrate binding loop, including destabilization by B12 45
2.3.7 Regions with no significant HDX differences 47
2.4 Discussion 47
2.4.1 B12-induced dynamics at the amino terminus of BtuB 48
2.4.2 Comparisons to existing models 49
2.4.3 Complex HDX behavior in the third substrate binding loop of BtuB . 50
2.5 Conclusions 51
2.6 Further Data 52
2.6.1 Supplemental Figures and Tables 52
2.6.2 Peptide assignment of BtuB and TonB 62

2.6.3 Offline proteolysis of BtuB assayed by SDS-PAGE . . . 68
2.6.4 Sequence analysis of BtuB . . . 75
2.7 Materials and Methods . . . 77
2.7.1 Bacterial strains and plasmids . . . 77
2.7.2 Protein expression and purification . . . 77
2.7.3 Proteolysis Assay . . . 80
2.7.4 Hydrogen Exchange Labeling Experiments . . . 81
2.7.5 Mass Spectrometry . . . 83
2.7.6 Data Processing . . . 84

3 FOLDING STUDIES OF TBDT PLUG DOMAINS . . . 85
3.1 Summary . . . 85
3.2 Introduction . . . 86
3.3 Results . . . 86
3.3.1 Identification and circular dichroism characterization of TBDTs with spontaneously folding plug domains . . . 87
3.3.2 SAXS studies of plug domains . . . 89
3.3.3 Kinetic folding studies of BtuB plug domain . . . 91
3.3.4 NMR studies of TBDT plug domains . . . 93
3.3.5 Pressure denaturation NMR . . . 95
3.3.6 Analysis of pressure denaturation NMR data . . . 97
3.3.7 T2 relaxation rate measurements of BtuB plug domain . . . 97
3.4 Discussion . . . 100
3.5 Supplemental Figures . . . 100
3.5.1 Structural analysis and sequence comparison of TBDT plug domains 101
3.5.2 Plug domain contact map analysis . . . 101
3.6 Methods . . . 104

4 CONCLUSIONS AND FUTURE DIRECTIONS . . . 106
4.1 Conclusions . . . 106
4.1.1 B12 binding allosterically unfolds the amino terminus of BtuB . . . 106
4.1.2 The unfolded state of BtuB's plug domain experiences significant non-structural environmental protection . . . 107
4.2 Future directions . . . 107
4.2.1 BtuB transport mechanism . . . 108
4.2.2 Towards more native HDX measurements in outer membranes . . . 113
4.2.3 Non-structural protection factors in outer membranes . . . 116

REFERENCES . . . 119

LIST OF FIGURES

1.1 Crystal structure of unliganded BtuB 11
1.2 Conformational changes in the amino terminus upon B12 binding 13

2.1 BtuB purification and HDX protocol 30
2.2 Detailed comparison of the Ionic Lock and IL Region in PDB structures 31
2.3 HDX-derived model of the BtuB plug domain's conformational response to ligand binding events 32
2.4 Effects of B12 binding on HDX 34
2.5 SDS-PAGE of OMP abundance and soluble pepsin digestion of BtuB in OMs . . 36
2.6 Multi-modal exchange in the third substrate binding loop 39
2.7 HDX in the Ionic Lock Region 40
2.8 Statistical summary plots 41
2.9 Outer membrane environment 46
2.10 Deuterium uptake plots 53
2.11 Biochemical and statistical details for each measured state 59
2.12 HDX peptide summary table 60
2.13 Peptide and resolution maps of BtuB in 8M urea 63
2.14 Peptide and resolution maps of BtuB in azolectin liposomes 64
2.15 Peptide and resolution maps of BtuB in DDM detergent 65
2.16 Peptide and resolution maps of BtuB in native-like OMs 66
2.17 Peptide and resolution maps of TonB 67
2.18 Urea- and temperature- dependence of BtuB offline proteolysis, part 1 69
2.19 Urea- and temperature- dependence of BtuB offline proteolysis, part 2 70
2.20 Detergent dependence of BtuB offline proteolysis, part 1 71
2.21 Detergent dependence of BtuB offline proteolysis, part 2 72
2.22 Optimization of urea concentration for HDX proteolysis, part 1 73
2.23 Optimization of urea concentration for HDX proteolysis, part 2 74
2.24 Multiple sequence alignment of BtuB 76

3.1 Normalized circular dichroism spectra of six different TBDT plug domains. . . . 88
3.2 SAXS studies of plug domains 90
3.3 Chevron plot for BtuB plug domain 92
3.4 ^{1}H-^{15}N HSQC NMR spectra of plug domains 94
3.5 Endpoint spectra of BtuB pressure ramp NMR experiments 96
3.6 Pressure denaturation NMR data analysis 98
3.7 Fitted transverse relaxation rates for BtuB plug domain 99
3.8 Cross-species sequence comparison of TBDTs 102
3.9 Contact map analysis of TBDTs 103

ACKNOWLEDGMENTS

This work was only possible with the aid of my colleagues in the Sosnick lab and throughout the department. Tobin Sosnick, my advisor, has structured his lab to be a pleasure to work in, and helped me develop the skills needed to succeed as a scientist. Whether as an instructor, imparting knowledge and introducing experimental techniques, a guide, facilitating contact with his counterparts from around the world, or a co-author, offering insights during the writing process, Tobin has always had interesting perspectives and tactful advice to share. His focus and dedication are qualities I strive to emulate.

The rest of the Sosnick lab has been a privilege to work with as well. Michael was a font of technical knowledge and an ideal partner for figuring out how to do HDX-MS. Isabelle cheerfully converted emails with primer sequences into *dozens of milligrams* of purified protein, often before I had finalized plans for how to use it. Joe showed me many interesting and practical aspects NMR. Josh was my big brother in the lab and first new friend in Hyde Park. Witnessing his successes inspired me in my early years or when things were difficult. Alex, Kevin, Zongan, Sheng, Nabil, Xiangda, John, Aiman, Darren, Kayvon, Wookyung, Abigail, Kourtney, Andrew, Yiheng, Hendrik, and Julia have all been fun to discuss science and occasionally work with. Collaborations and discussions with members of my cohort and others in the department, including Ben, Marta, and Michael have also been enjoyable and productive. Lastly, sharing my HDX knowledge with and seeing the successes of Kelly, Fraol, Wojciech, Ruofan and Xiaoxuan has been especially gratifying.

I would like to thank my sources of financial support. I have been supported by the Molecular and Cellular Biology training grant R01 GM055694 and T32 GM007183-41.

I would like to thank my family for their support during graduate school. They were patient with me when I was not in an ideal state to be around. I was always welcome back home, and visiting my childhood home was great for taking my mind off of work and remembering that the world outside still exists. Visits overseas to my extended family were also refreshing, and I thank them for their hospitality.

I am also grateful to my non-science friends for their support and companionship. Inspiration was not limited to my time in lab but rather came in a variety of contexts such as a late night fencing practice, weekend tennis match, or meal cooked together.

ABSTRACT

To import large metabolites across the outer membrane (OM) of Gram-negative bacteria, TonB dependent transporters (TBDTs) undergo significant conformational change. After substrate binding in BtuB, the *E. coli* vitamin B12 TBDT, TonB binds and couples BtuB to the inner membrane proton motive force which powers transport. The role of TonB in rearranging the plug domain to form a putative pore remains enigmatic. The aim of my thesis is to advance understanding of the substrate transport process in BtuB.

Chapter 1 is a review of the outer membrane environment, TBDT biology, and a survey of what is known about BtuB specifically. Models of BtuB pore formation and some of the recent experiments supporting them are introduced. Some studies focus on force-mediated unfolding while others propose force-independent pore formation by TonB binding leading to breakage of a salt bridge termed the "Ionic Lock". Additionally, an introduction is given to the technique of hydrogen deuterium exchange mass spectrometry (HDX-MS), with an emphasis on its application to outer membrane proteins.

Chapter 2 details work characterizing early steps in the BtuBs transport cycle, in a native OM context. Our hydrogen exchange measurements in *E. coli* outer membranes find that a region surrounding the Ionic Lock, far from the B12 site, is fully destabilized upon substrate binding. A comparison of the exchange between the B12- and B12+TonB-bound complexes indicates that B12 binding is sufficient to unfold the Ionic Lock region with binding of a TonB fragment having much weaker effects. TonB binding accelerates exchange in the third substrate binding loop, but pore formation does not obviously occur. This chapter provides a detailed structural and energetic description of the early stages of B12 passage that provides support both for and against current models of the transport process.

Chapter 3 presents a characterization of the independently folding plug domains found among a surveyed set of TBDTs. The plug domains of BtuB and CirA were found to contain substantial amounts of independently folding structure, and were characterized with a variety of techniques. Attempts at structure determination by NMR were unsuccessful due to poor

solution properties and rapid transverse relaxation rates. Initial experiments characterizing BtuB constructs with stabilizing disulfide and/or bi-histidine site mutations were suspended upon success of initial mass spectrometry HDX experiments, which were used to characterize the folding of BtuB in a more native context.

Chapter 4 summarizes the conclusions from chapter 2. From these conclusions, future directions are proposed to further advance understanding of BtuB biology, the mechanism of TBDTs in general, and to address an intriguing new question raised about apparent non-structural HDX protection conferred by the outer membrane. In summary, this thesis represents an advance in understanding the mechanism of BtuB and explores TBDT plug domain folding in various contexts. Additionally, it establishes a technique for routine acquisition of high-quality HDX data in a challenging but valuable context, the native outer membrane.

CHAPTER 1

INTRODUCTION

TonB-dependent transporters (TBDTs) are a family of proteins ubiquitously expressed in the outer membranes (OMs) of Gram-negative bacteria, critical to the biology of this class of microorganisms [1]. TBDTs serve to provide access across the OM, which Gram-positive bacteria (and most other organisms) lack. The unusual OM environment occupied by members of this protein family causes them to have an unusual structure and to employ a complicated mechanism to solve a simple problem, that of moving a substrate molecule from the outside of the cell to the periplasm.

Though these are interesting qualities and merit study on their own, there are also very practical reasons to understand TBDTs. TBDTs are present in many disease-causing organisms, and in some cases function as virulence factors, that is, the genes whose expression causes otherwise benign microbes to become pathogenic [2]. TBDTs have therefore long been the targets of drug design efforts, some of which are still ongoing. Progress in understanding the biology of TBDTs, and efforts at harnessing or altering these molecules to serve the needs of humanity have and will continue to rely on mechanistic knowledge of their function.

Despite substantial advances over the past few decades, key aspects of the TBDT mechanism remain unknown. This thesis advances the understanding of the TBDT transport mechanism from a protein folding perspective by bringing a powerful and yet-unapplied technique of hydrogen deuterium exchange mass spectrometry (HDX-MS) to bear on a series of related and long-standing questions: How does a TBDT's pore forming transport intermediate form, and what are its structural and dynamical properties?

1.1 TonB-dependent transporters (TBDTs)

Membranes are key to supporting and categorizing life. A cell cannot exist without some structure containing it. In nature this structure takes the form of membrane. Eukaryotes

enclose their DNA within a membrane-bound nucleus, while prokaryotes do not. Among prokaryotic bacteria, a major classification is into Gram-positives and Gram-negatives, referring to a method which by which bacteria are stained according to their membrane structure. The Gram-positives, which have the peptidoglycan ("cell wall") outside of their single membrane, retain the color of the stain upon subsequent washing, while Gram-negatives, whose peptidoglycan lies between their two membranes, do not. The double membrane structure of Gram-negatives lends them several advantages by introducing an extra layer of defense between the cell interior and the environment which the cells occupy. However, much like a fence or moat around a building [3], a double membrane also introduces problems of its own, most obviously by restricting transport across the cell envelope, complicating import of nutrients and export of waste or secreted products. It is in this intuitive context that the biology of TBDTs can be introduced to a general audience and interpreted.

1.1.1 The outer membrane (OM) environment and OM proteins

TBDTs serve to solve the problem of access into and out of the periplasm (the space between inner and outer membranes) for a certain class of molecules. The periplasm constitutes 10-20% of the bacterial cell volume [4, 5], but whether it counts as the "inside" the cell is a matter of definition. Just as a fence restricts access only to objects too large to fit between the pickets and rails, or a moat deters only entities incapable of traversing water, the OM is impermeable only to molecules with certain sizes and chemical characteristics. Small (lighter than 600 Da) hydrophilic molecules can diffuse through porins, such as OmpF for *E. coli*, which form non-specific pores in the OM. Consequently, the ionic strength and reduction potential of the periplasm are less controlled than that of the cytoplasm, with the cytoplasm considered to be an oxidizing environment [6]. Although no ATP is available in the periplasm [7], active transport (against diffusion potentials) must occur across the outer membrane in both directions [8, 9]. It is primarily for import of larger and more hydrophobic molecules, then, that one may expect TBDTs to be utilized. Indeed, many of the longest-studied

TBDTs have large metal-chelating molecules as their substrates, ranging in size from 660 to 1355 Da.

Besides lacking access to the cytoplasm on its inner face, the OM environment in which these proteins reside is also compositionally distinct from a eukaryotic cell membrane, or even the plasma membranes found in the same gram-negative bacteria. The inner leaflet of the OM is composed of similar lipids as the plasma membrane, although possibly with shorter distribution of acyl chain lengths [10], and the OM is undergirded on the periplasmic side by peptidoglycan. Also known as the cell wall, peptidoglycan is a network of linear oligosaccharides heavily crosslinked by short peptides [11] and covalently attached to the inner leaflet of the OM through a small trimeric α-helical protein known as Braun's lipoprotein [12, 13].

The OM outer leaflet is even more unusual, containing large amounts of lipopolysaccharide (LPS). LPS is a molecule composed of three parts: lipid A, core oligosaccharide, and O-antigen. Lipid A is a phosphorylated glucosamine disaccharide, with six alkyl chains of 14 to 16 carbons each [14]. The core oligosaccharide is a short, branched network of sugars, but can also include amino acids, ethanolamine, and phosphate components. The O-antigen is a large polymer of sugars which can vary within as well as between species [15]. Certain strains of *E. coli* (such as K-12) lack O-antigen completely, which dramatically changes their membrane properties [16]. LPS has a high anionic charge density and contains a significant amount of divalent metal ions to balance the negative charge. When Gram-negative organisms are treated with metal chelators such as EDTA or EGTA, the unbalanced anionic charge density resulting from removal of divalent ions can in certain cases lead to the ejection of the charged LPS molecules from the cell membrane into solution [17]. Finally, the OM is regarded to be less fluid than inner membranes, though there are exceptions to this trend [18]. The above features of OMs cause them to be occupied by a set of proteins with a β-barrel topology distinct from plasma membrane proteins.

Like the plasma membrane, the OM contains about a 50% mass fraction of proteins [19],

which collectively influence its properties. For example, the mechanical rigidity of OMs arises not only from their LPS and PG layers, but also from the resident outer membrane proteins (OMPs). Most [20]OMPs are β-barrels [21]. Though occasionally seen in soluble proteins, among MPs, β-barrels are only found in outer and mitochondrial membranes. The β-barrel domains of OMPs confers them high mechanical rigidity, with recent studies suggesting that OMPs [22] can significantly contribute to cellular stiffness, along with LPS [23]. Although oligomerization is common [24], most known OMPs have a single transmembrane β-barrel domain, however recent informatics work has provided evidence of multi-barrel sequences [25]. Additionally, there is emerging evidence that OMPs associate to form protein-dense regions within the OM, termed "OMP islands" [26]. BtuB, the protein which this thesis describes, is thought to engage in such interactions as well [27]. In summary, the outer membrane environment is intimately linked to TBDT function (and the function of OMPs generally) and it is a critical factor to consider when studying them. As reviewed below, the results of experiments performed on TBDTs often depend on the choice of specific membrane or membrane mimetic.

1.1.2 TBDTs in bactericidal and medical contexts

According to the US Centers for Disease Control and Prevention [28] millions of antibiotic-resistant infections occur each year in the USA, resulting in tens of thousands of deaths. Members of both Gram-positive and Gram-negative bacteria cause disease and death, with well-known examples (and the diseases they cause) including *S. pneumoniae* (pneumonia), *S. aureus* (MRSA), and *S. pharyngitis* (strep throat) for Gram-positives and *N. gonorrhoeae* (gonorrhea), *Y. Pestis* (bubonic plague), and *E. coli* (meningitis) for Gram-negatives [28]. Many TBDTs are expressed as virulence factors [29, 30, 31, 32, 33, 34], meaning the genes whose expression causes an organism to become pathogenic. Some TBDTs are engaged in evolutionary conflicts with the mammalian immune system. For example, as part of the innate immune response transferrin sequesters iron in the bloodstream, depriving pathogens

of this vital nutrient. However, in a process termed iron piracy, transferrin can be bound by *H. influenzae* TBDT TbpA and the iron cargo extracted, allowing the pathogen to survive an otherwise successful immune reaction. This process has significant enough effects on human health that evolutionary signatures have been detected in the proteins [35]. Likewise, the *N. meningitidis* TBDT ZnuD is employed to scavenge low-abundance zinc ions during host colonization [36]. Other TBDTs import siderophores (strong metal chelators) such as enterobactin, which bacteria use to scavenge iron from their surroundings and from each other [37]. Additionally, TBDTs can function in export of macromolecules, e.g., Oar, a *M. Xanuthis* TBDT responsible for the starvation-induced secretion of the extra cellular protease PopC [38]. In summary, TBDTs have multiple roles in the biology of Gram-negative bacteria and their impact on the health and disease states of not only humans but virtually all organisms these bacteria encounter.

TBDTs play roles in interbacterial interactions as well. Because TBDTs import essential nutrients, they influence bacterial cooperation, parasitism, and competition. In both cooperative and parasitic contexts, TBDTs can be used by an organism to take up a growth-limiting nutrient. For example, iron can be absorbed in the form of a siderophore even though an organism may not necessarily synthesize that siderophore [39].

In a purely adversarial context, TBDTs are the targets of various small molecules secreted to the inhibit growth of their competitors. Bacteriocins are one class of such molecules, discovered nearly a century ago [40], and are defined by being at least partially composed of proteins or peptides. This large category of bactericidal compounds is categorized into subclasses such as microcins (small bacteriocins) and colicins, which are bacteriocins made by, and specific for, organisms such as *E. coli* [41]. Crystal structures have been obtained for several TBDTs with attached colicins, and their mechanism of entry into cells is an active area of research. In addition to bacterial attacks, TBDTs can serve as receptors for viral entry to the cell [42], which is unsurprising given their ubiquity and essential role in nutrient acquisition.

Though progress has been made in reducing the morbidity from Gram-negative infections, there is still need for development of novel antibiotics. With inspiration provided by bacteriocin biology, multiple TBDTs have been targeted for a Trojan horse antibiotic strategy [43, 44, 45, 46, 47]. In this strategy an antibiotic payload is covalently fused to a natural TBDT substrate, resulting in a drug that the targeted bacterium spontaneously imports. Albomyicins are a natural class of such compounds [43] whose total synthesis was recently achieved [48]. Synthetic Trojan horse TBDT substrates have also been [49], and continue to be [50, 51] developed. One such drug, cefiderocol, was FDA approved to treat complicated urinary tract infections in 2019 [52, 53]. Additionally, TBDTs can be immunogenic [54], and have been targeted for vaccine development [55, 34]. Expanding the basic understanding of TBDT biology can aid in successfully employing these strategies.

1.1.3 Evolution, structure, biogenesis, and regulation of TBDTs

Outer membrane proteins' β-barrel structure places topological constraints on their biogenesis and appears to have resulted in a distinct mode of evolution [56]. Changes in OMP strand number appear to occur via conversion of extracellular loops to hairpins, or duplications of one or more hairpins at a time, each of which strictly increase strand number by multiples of two [57, 56]. Correspondingly, OMPs, and with a few exceptions limited to mitochondria [58, 59], transmembrane β-barrels in general have even numbers of β-strands, ranging from 8 to 36 [60], as the proteins are composed of hairpins inserted into the membrane from the periplasmic face. Unlike inner membrane proteins [61], OMPs follow a positive-outside rule [62]. TBDTs have sequence homology at the protein family and individual gene level, and horizontal gene transfer has been implicated in their evolution [29]. TBDTs specific for the same substrate across different species appear to share greater sequence identity than different TBDTs of the same organism **(Figure 3.8)**.

TBDTs have a prototypical domain structure composed of an amino terminal plug domain 130-150 residues in length, and a carboxy terminal β-barrel domain with 22 transmembrane

strands. The plug domain has a mixed α/β topology with a central 4-stranded β-sheet, and normally resides in the lumen of the β-barrel occluding it from forming a large pore. The lumen of TBDT β-barrels is substantially wider than that of nonspecific porins such as OmpF, which has 16 β-strands. Early studies comparing TBDTs to nonspecific porins led to the term "ligand-gated porin" [63]. All known TBDTs contain a Ton box sequence element at the amino terminus of the plug domain, with a 5- to 7-residue sequence defined by its ability to specifically bind the carboxy terminus of the TonB protein [64, 65]. TonB couples TBDTs to the energy source of the inner membrane (termed the "proton motive force") and allows them to function.

TBDT β-barrel domains have short turns connecting adjacent strands on the periplasmic face, and loops of variable length on the extracellular side of the membrane. These loops are often long enough to contain entire secondary structural elements and interact with the lipopolysaccharide extending from the OM outer leaflet. Some TBDT β-barrels are highly asymmetric, with certain strands far exceeding others in length, leading to non-parallel membrane planes for the inner and outer faces [66].

Biogenesis of TBDTs occurs in a similar manner as for most OMPs. The process begins as normal for a bacterial secreted protein, until export through the plasma membrane is initiated. While being exported through the SEC translocase [67], the nascent OMP polypeptide encounters periplasmic chaperones such as DegP, Spy, Skp, and SurA [68, 69]. These chaperones keep the unfolded OMP soluble until it reaches the Bam outer membrane insertase complex. Unlike many smaller *E. coli* OMPs whose folding has been reconstituted in vitro [70], TBDTs are not known to spontaneously fold into lipids, instead being fully reliant on a Bam complex for membrane insertion. The initial few strands of an OMP to be inserted are not stable on their own and a so templated folding mechanism is used to accommodate them until a critical number is reached. Briefly, during insertion, which is dependent on recognition of a β-signal sequence [71] and proceeds from the carboxy terminus, the BamA protein opens at a labile seam and accommodates the extra strands of the nascent OMP into

its own barrel structure. The composite barrel grows as the client protein is inserted, one hairpin at a time, until it is large enough that the nascent OMP can pinch off and form its own independent structure. Much of the progress towards understanding the Bam complex has been achieved in the last several years, and no adequate review was found as of the preparation of this thesis [72, 73, 74, 75, 76, 77, 78, 79, 80, 81, 82, 83]. Additionally, for at least some TBDTs, the plug domain appears to play a role in biogenesis. FhuA with a deleted plug domain was expressed and inserted into the outer membrane, although at lower levels, suggesting a biogenesis defect [84]. Expression of the plug domain as a separate polypeptide restored the biogenesis and function.

Some TBDTs have a small, soluble regulatory domain appended to their amino terminus that resides in the periplasm. In the well-studied case of FecA [85], the periplasmic domain is involved in detecting the binding of metal-free substrate at the extracellular face of the transporter. The regulatory domain of FecA engages in interactions with other periplasmic proteins which transduce the signal across the inner membrane to regulate transcription [86]. Transcription of many *E. coli* iron siderophore TBDTs is regulated through a common fur transcriptional repressor [87], whereas for BtuB, a riboswitch is involved [88]. In this manner, the activity of TBDTs regulates their own biogenesis and that of the ExbB/ExbD/TonB complex members [45, 89, 90], which are subject to some of the same transcriptional controls. Signal transduction affecting transcription of metal-acquisition genes by TBDT periplasmic regulatory domains appears to be conserved [91], with evolutionary signatures present in the distributions of amino acids found at multiple sites in these domains [92]. In addition, TBDTs within the same cell can compete with each other for TonB function [93], with overexpression of a transporter and addition of its substrate causing inhibition of the uptake of other siderophores. The overexpression of TonB can relieve this inhibition [93], though some organisms have multiple TonB genes [94] suggesting that regulation of TBDT function is exerted at multiple levels.

1.1.4 Mechanism features common to TBDTs

TBDTs having large substrates such as vitamin B12 (1355 Da), enterobactin (670 Da), and ferrichrome (741 Da) are among the best studied members of the family, however, they are not its only members. Other TBDTs import smaller substrates such as citrate, chitin, and a general class of molecules termed "dissolved organic matter" [95] Though TBDTs specific for polysaccharides [96] are not as well studied biophysically, metaproteome studies have shown that TBDTs are among the most abundant proteins in oceans rich in nutrients [97, 98]. TBDTs function as components of multi-protein complexes, with partners at the inner and outer membranes, as well as in the periplasm. Pore dimensions seem likely to be variable among TBDTs of such various substrates, but this remains unproven as the full mechanism of pore formation has not yet been characterized for any TBDT.

The transport cycle of TBDTs begins with binding of the substrate on the extracellular side of the transporter. Upon substrate binding, an allosteric signal is transmitted to the inner face of the membrane with the Ton box becoming available for binding. The Ton box can subsequently be engaged by the carboxy terminal domain (CTD) of TonB. TonB is an integral inner membrane protein [99] and has a relatively rigid 110 residue linker connecting its amino and carboxy terminal domains. The linker is rich in charged and proline residues and EPR experiments [100] have shown that it prefers to exist in an extended conformational ensemble which is capable of spanning the periplasm. The CTD of TonB can dimerize [101, 102, 103] and engage in interactions with peptidoglycan when not binding to TBDTs [104, 105, 106, 107, 108].

Additionally, TonB is a peripheral member of the ExbB/ExbD complex, which harvests energy from the inner membrane proton gradient. The complex shares sequence, structural, and functional homology with the Mot and Tol motor systems, which transduce the inner membrane proton gradient into torque [109]. Substantial progress has recently been made on determining the structure and functional stoichiometry of the ExbB/ExbD complex [110, 111, 112] but the nature of the motions this inner membrane complex undergoes remains

unclear. ExbD possesses a folded periplasmic domain which interacts with the periplasmic linker of TonB [113, 114]. This interaction is thought to transduce the energy of the inner membrane proton gradient, possibly in the form of a force which is then applied by TonB onto the bound TBDT. The TonB CTD is involved in interactions with both ExbD and bound TBDTs. However, the nature of a complex where TonB simultaneously engages both ExbD and a TBDT remains unknown.

After passage through the outer membrane, TBDT substrates often interact with periplasmic regulatory domains [85] and are bound by periplasmic shuttle proteins [115]. The shuttle proteins, which can be positioned near the OM by TonB [116], carry the substrates to specialized ABC transporters residing in the inner membrane [117, 118, 119].

1.2 BtuB, the *E. coli* vitamin B12 TBDT

BtuB was identified in 1973 as being responsible for B12 transport and as residing in the outer membrane [120, 121]. The importance of TonB for BtuB's function followed four years later [122]. Since that early work, a variety of experimental techniques has been used to probe the structure and function of BtuB, making it one of, if not *the* best-studied TBDTs.

1.2.1 The structure of BtuB

Many crystal structures of BtuB have been solved in a variety of both membrane mimetic environments and ligand states. The 1NQE [123], 1NQH [123], and 2GSK [124] structures were all solved in detergent, and represent the apo **(Figure 1.1)**, B12-bound, and B12-and-TonB-bound states of the protein, respectively. In addition, the structure has been solved in a lipidic mesophase (2GUF [125]), bound to colicin E2 and E3 receptor binding domains (2YSU [126], 1UJW [127], respectively), bound to calcium ions (1NQG [123]), and in a subset of the above states with spin labels attached (3M8B [128], 3M8D [128], 3RGM [129], 3RGN [129]). The inner and outer membrane planes of BtuB, defined by its aromatic girdles of

Figure 1.1: **Crystal structure of unliganded BtuB (PDBID: 1NQE)** Residues 6-137 comprising the plug domain are shown in solid grey, and residues 138-594 comprising the β-barrel domain are shown as a light transparency.

tyrosine and tryptophan residues [130], are more than 10 degrees away from parallel to each other [66], reflective of the β-barrel's asymmetry.

1.2.2 Early steps in BtuB transport

The first step in the transport pathway of BtuB involves binding of B12 to the outer face of the transporter. The affinity of BtuB for B12 is increased from the low μM to the low nM range in the presence of saturating amounts of Ca^{2+} ions, for which BtuB has two specific binding sites [131]. Upon B12 binding there is an allosteric change in BtuB which results in the disengagement of amino terminal residues including the Ton box from their native position. In POPC, this disengagement results in the relocation of these residues 20-30 Å into the periplasm [132]. Once exposed to the periplasm, the Ton box can be bound by TonB. Disengagement of the amino terminus may be regulated by a salt bridge termed the "Ionic Lock," which has recently been proposed to be broken by TonB binding *in vivo* [133]. The structure of BtuB with B12 (in the absence of the TonB CTD) has the Ionic Lock broken in the rigorous sense that the distance between the carboxylate and guanidinium moiety carbon atoms of the two involved residues, Arg14 and Asp316, increases from 4.9 to 7.8 Å away from each other in 1NQH and 1NQE structures, respectively. However, the backbone conformation of residues 11-23 is essentially unchanged, with a C_α RMSD of 0.31 Å. The backbone dihedral angles for residues 6-9, comprising the amino terminal half of Ton box, are mildly affected, but even this fragment of the protein is found in a similar position in the two structures, with a C_α RMSD of 3.0 Å. **Figure 1.2** shows the extent of conformational change at the amino termini of the apo and B12-liganded crystal structures of BtuB.

1.2.3 Models of pore formation in BtuB

The longest-standing and most popular models of pore formation in BtuB, and in TBDTs generally, posit that TonB causes pore formation by applying a force onto the plug domain via its linkage with the Ton box [134]. Experimental evidence supporting these models

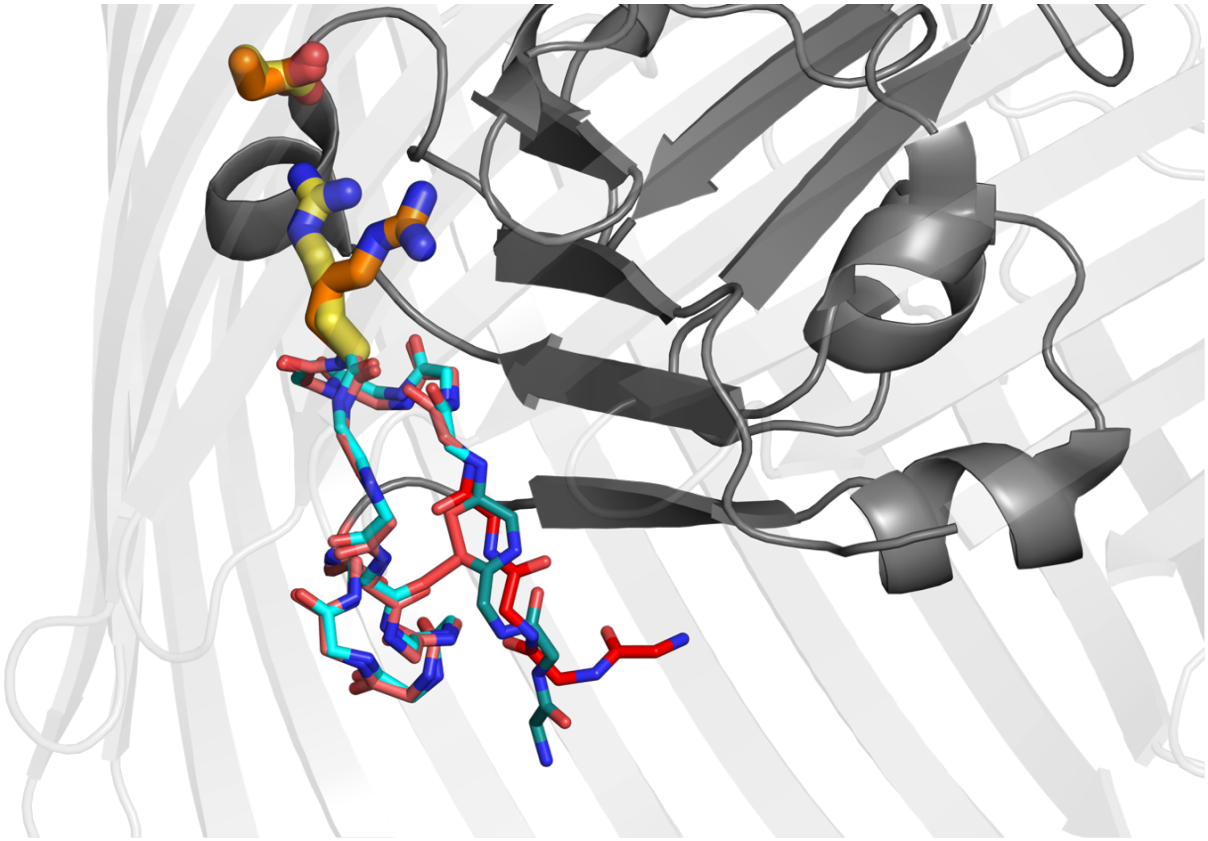

Figure 1.2: **Conformational changes in the amino terminus upon B12 binding** For the apo (1NQE) and B12-liganded (1NQH) crystal structures of BtuB, the main chain atoms of residues 6-9 are shown in dark red and dark teal, residues 10-23 are shown in light red and cyan, and the side chains of residues Arg14 and Asp316 are shown in yellow and orange, respectively. As in **Figure 1.1**, the remainder of the plug domain is shown as a dark grey cartoon representation, and the barrel domain is shown as a transparent cartoon. Residues 1-5 are not resolved in either structure.

includes fluorescence [108, 135] and atomic force [136] microscopy studies. Despite reconstitution of pore formation (via unfolding of the amino terminal half of the plug sequence) by both chemical denaturation [137] and force-induced methods, aspects of the model remain problematic. For example, in the reconstituted force microscopy system, the distance which the amino terminus of the TBDT had to be extended was longer than the width of the periplasm.

Simulations have offered additional support for a force-dependent model [136, 138, 139, 140], though spontaneous transport has not been modeled, with simulated passage of B12 through the membrane relying on steered molecular dynamics techniques to apply forces and drag the substrate through the pore. Models not involving pulling have also been considered [141]. These models are further reviewed in Subchapter 2.2.

1.3 Hydrogen deuterium exchange mass spectrometry (HDX-MS) at the outer membrane

1.3.1 Introduction to HDX-MS

Hydrogen deuterium exchange (HDX) is a technique where the rate of uptake or loss of hydrogen isotopes is used to infer structural or dynamic information about a molecule. HDX has been used to study protein folding for well over half a century [142, 143]. Though early studies measured exchange via radioactivity from tritium incorporation [144], density of solutions into which deuterated proteins were placed [144], or infrared spectroscopy [145], modern approaches employ nuclear magnetic resonance (NMR) spectroscopy [146] and mass spectrometry. HDX-NMR is well established as one of the leading techniques for studying protein dynamics [147], with HDX-mass spectroscopy (HDX-MS) enjoying more recent growth. Although HDX-NMR can yield amino acid resolution at nearly every site in a protein, this remains a difficult feat for HDX-MS but it has been achieved with soluble proteins such as RNAse H [148] and Maltose Binding Protein [149]. Counterbalancing this

lower resolution is the ability of HDX-MS to handle samples of a more complicated composition, and the reliance of HDX-NMR data interpretation on peak assignments, which can be difficult to obtain. The lack of a size limit (imposed onto NMR techniques by signal loss due to slow molecular tumbling) has also made HDX-MS the technique of choice for many proteins. Having undergone a growth in popularity in recent decades, HDX-MS has by now been applied to a variety of systems, including membrane transporters [150]. The HDX-MS technique has also emerged as one of the more popular methods to characterize protein-protein interactions in industry, especially in the case of antibody epitope mapping [151, 152]. Contributing to the popularity of HDX-MS is that deuterium labeling is essentially non-perturbative, meaning that the incorporation of label does not significantly affect protein folding or function [153]. HDX-MS has experienced sufficient growth in popularity that leaders in the field have recently proposed a set of standards [154] for carrying out, reporting, and analyzing experiments.

Proteins or peptides can be labeled by exposure to any environment with a hydrogen isotopic composition differing from their own. HDX-MS is most commonly applied in solution, though performing exchange in the gas and [155, 156] and solid [157, 158] phases is possible. The chemistry forming the basis of HDX-MS is well established [159], and in most cases for proteins (pH $>$ 2.5) is catalyzed by abstraction of an amide proton by hydroxide. Because of this, the intrinsic hydrogen exchange rate (see section 2.3.3) in a reaction can be controlled by altering pH as well as temperature, and to a lesser extent ionic strength. This allows not only for control of labeling times at the experimenter's convenience, but also for sampling a wider range of time scales than would otherwise be reasonable. Pulsed exchange methods accomplished with rapid mixing techniques and serial dilution allow for labeling times as short as milliseconds [160], and there is no upper limit on length of labeling experiments, although for practical reasons (including complication of interpretation by exchange at side chain groups [161]) labeling is usually not carried out for longer than a few days.

After labeling, usually by dilution into a solution containing a high fraction of D_2O,

the protein is broken into short peptides for measurement of localized deuterium uptake. Conversion of the protein into peptides can be achieved by two means: fragmentation inside the spectrometer ("Top-down HDX-MS") or proteolytic digestion ("Bottom-up HDX-MS"), or a combination of the two ("Middle-down HDX-MS") [162]. Of these, bottom-up HDX-MS is the most commonly used due to issues with fragmentation rearranging the occupancy of deuterium on a protein's amides in a process termed "hydrogen scrambling" [163]. Bottom-up HDX-MS relies on nonspecific proteolysis under cold acidic conditions, usually followed by rapid desalting and separation of the peptides to minimize loss of label from a process termed "back exchange". Separation of the peptides is usually achieved by reversed phase high performance liquid chromatography (RP-HPLC, sometimes shortened to "LC") or ultra-performance liquid chromatography (UPLC) [164], although other techniques such as size exclusion chromatography (SEC) have also been employed [165].

The need for multiple steps to occur rapidly under controlled conditions has led to the development of a standardized fluidics approach used by many HDX-MS labs. In a typical system, protein is handled on injected into a loop attached to a computer-controlled valve, used to synchronize the various elements of the automated sampling system. The injection may be performed by a human, commercially available fluid handling robot, or custom-built device designed to accommodate specific needs, e.g., short label times for pulsed labeling studies [166, 167]. After injection, protein is passed across a nonspecific acid-compatible protease column to generate peptides (low pH is typically used to quench exchange). Columns are commercially available or can be obtained by functionalizing a protease of choice onto an appropriate resin [168, 169]. The low cost and high activity of porcine pepsin [170, 171], *A. saitoi* fungal protease XIII [172], and *Rhozipus* fungal protease XVIII [173] have made them popular choices for HDX-MS, though other hardy proteases such as nepenthesin (used by tropical pitcher plants to digest insects) [174] or *A. niger* prolyl endopeptidase [175] have also been explored as specialized tools to increase peptide coverage. Furthermore, proteases may be combined to increase general or specifically targeted cleavage as desired [176, 177].

Additionally, in order to minimize deuterium (D) signal loss from "back-exchange" [178] to hydrogen (H) during the proteolysis and LC steps, the protein is usually "quenched" by dilution into an ice-cold solution strongly buffered at pH 2.5 immediately after labeling. The rate of back exchange depends on temperature and pH, so both parameters are controlled for the entirety of the period between quenching and ionization. Back exchange rates are faster at higher temperatures, so the entire chromatographic system is usually encased in a refrigerated chamber kept near 0 ^{o}C, from the sample injection loop to the end of the analytical LC column. The choice of pH 2.5 (2.25 at low ionic strengths) is made to minimize acid- and base-catalyzed exchange [178], such that lowering pH any further results in increases in back exchange rates. With the proper instrumentation, organic additives maybe used to achieve separation at temperatures below the freezing point of water to further slow back exchange [164]. If protein is not rapidly diluted into nearly 100% H solution after quenching, results may be significantly affected by a process analogous to back-exchange, but which proceeds in the forward direction. This process is termed "in-exchange" [179], and can be accounted for by performing pseudo-zero time labeling control experiments. In such experiments, the quench and label solutions are first mixed to simulate the protein spending an infinitesimally short time in the label solution and going directly to the quenched state. The practical aspects of peptide generation, separation, and measurement have been the subject of intense study and the Sosnick lab has largely adopted the practices established by the Englander group [180], as well as some specialized approaches developed for membrane proteins [181]. For further details and a more up to date review, see the following [182]. Analysis of HDX data includes concepts such as the protection factor, and EX1 & EX2 exchange regimes. These topics are covered in detail in Chapter 2.

1.3.2 Practical aspects of conducting HDX-MS

Assignment of peptides is carried out by tandem mass spectrometry, also known as "MS-MS" or "MS2" (more generally "MSn", referring to n rounds of subsequent fragmentation

and mass analysis) experiments. In these experiments, signals in the primary mass spectral scans ("MS1") likely arising from unlabeled peptides (identified by their distinctive isotopic patterns, ideally in charge states z = 2, 3, or 4) are automatically analyzed by the mass spectrometer. If certain conditions are met (e.g., signal intensity, and a peptide-like isotopic pattern), a putative peptide's ion envelope is isolated and subjected to secondary mass spectral scans after fragmentation by collisions with an inert gas (collision-induced dissociation, or CID). The CID energy is chosen to balance optimal fragmentation against the possibility of deuterium label rearrangement by the collision energy. The fragments' mass spectra ("MS2") are later compared to assign the sequence of the parent, using proteomic search algorithms commonly used for protein identification [183]. To maximize the number of peptides identified per assignment run, several MS2 scans can be triggered from a single MS1 scan. Additionally, after a peptide ion candidate is sent to MS2, it is usually placed on a "dynamic exclusion list" (usually lasting 30 seconds to a few minutes) to prevent constant re-assignment of the most dominant peptide signals. Despite such measures, after analysis of a peptide assignment experiment, it is good practice to place the assigned peptides on a permanent exclusion list. The permanent list is coded into the MS2 method and instructs the instrument to reject known candidate ions for fragmentation and MS2 scans, freeing them up for less abundant peptides which were not chosen previously. This process of placing contaminants or assigned peptides on an exclusion list is repeated until most or all plausible peptide signals present in the data have been identified, and it is judged that no candidate ions are being missed by insufficient opportunities for selection into MS2 scans.

Though peptide assignment requires more protein per injection than runs measuring deuterium uptake, assignments are usually obtained at an early stage in an HDX-MS project to evaluate feasibility. If peptide coverage is low in regions of interest, or those critical to success of a project, coverage must be improved via optimization of some combination of the digestion, separation, or measurement processes. Some iteration between assignment and uptake measurement stages is to be expected, as spectral overlap can change when isotopic

envelopes begin to move as the peptides acquire deuterium, and certain peptides may not show up well in deuterated data. However, as a rule of thumb, obtaining a number of unique peptides equal to the length of a target protein is a good starting point. With more peptides, site resolution can increase, meaning that the size of regions with amides exchanging together shrinks, down to an ideal of individual residues. Additionally, a greater number of peptides affords greater redundancy, meaning an increase in the number of peptides covering a site of interest, which can increase confidence in the measured uptake. Many assigned peptides often fail to give interpretable uptake data and for various reasons such dropout can be heavily biased to occur within certain regions. Therefore, extensive peptide coverage is a good indicator of success for the HDX-MS project.

Once a dataset is collected, the first stage of analysis is to search the MS/MS data against a protein sequence library and match the masses which were measured to those calculated from the expected sequences. Computationally, allowing for post-translational protein modifications (either during biogenesis, or from chemical damage, e.g., deamidation or oxidation of side chains) can increase coverage but also lead to a greater number of false positives and misassigned peptides. The use of very short peptides in the search can also cause problems, as they are less likely to have a unique source and may be generated from different parts of a protein's sequence, depending on the repetitiveness of the sequence. Where to place the cut-off for filtering peptides by length largely project-specific, but a safe default to begin with can be 5-30 residues in length. Similarly to using the known features of peptide assignment run mass spectral data to filter assignments, data from labeling experiments is filtered and processed using a variety of techniques designed to prevent interference from contaminants and increase confidence in measured deuterium uptake. Examples of such algorithms are given in publications describing the original EXMS package, and more were added in a recently updated version, EXMS2 [184, 185]. Briefly, data are checked for common issues, potentially problematic cases flagged for manual review, and the isotopic envelopes are fitted to a chosen model of isotopic envelope. Extension modules such as HDSite can then be used

to compare the data from overlapping peptides to deduce the behavior of regions where the peptides differ. In some cases, this process is capable of achieving individual amide site resolution, and even when it does not it can reduce the size of sub-peptide segments whose amides' exchange cannot be deconvoluted, termed "switchable regions".

Lastly, more data is not always strictly better. Despite automated analysis packages being capable of construction of global exchange profiles with individually resolved amides, human intervention is often needed to prevent obvious errors. Too much data, (particularly data of low quality, if filtering thresholds are relaxed) can lead to onerous workloads when manually inspecting every peptide. For nearly every HDX project undertaken in the Sosnick laboratory so far, initially generated global exchange profiles (such as "heat maps" which map the globally computed uptake over time to a sequence or structure) have contained several nonphysical features such as non-monotonic uptake. This has been the case even after optimization of m/z and retention time boundaries for a project. Though most of the problematic features seen in such heat maps are due to poor integration of a peptide's elution profile, peptide misassignments can also cause issues even if data for every peptide is individually internally consistent and physically plausible. Comparison of isotopic data from multiple peptides (and different charge states of the same peptide) is critical to forming confident conclusions about HDX-MS data, and an important stage of any project is cross-checking all peptide data to ensure that it is self-consistent. Many commonly used software packages for analyzing HDX-MS data are incapable of automatically detecting all the ways in which data can fail to be self-consistent. Therefore, it is recommended to become familiar with the most important uptake curves (and raw data behind them) as early in a project as possible, as this is likely to result in time savings through identification and exclusion of misassigned peptides.

1.3.3 Applying HDX-MS at the outer membrane

As outlined above, HDX-MS is a technique well suited to studying proteins in their complex native environment, provided that suitably labeled peptides can be obtained and measured. The application of HDX-MS to membrane proteins (MPs) has necessitated development of specialized protocols. Membrane proteins are insoluble in the absence of a membrane or a membrane mimetic.

Unfortunately, many of the mimetics used to solubilize MPs have poor compatibility with reversed phase HPLC and MS systems. Many early studies on MPs were conducted in simple, bespoke systems such as lipid vesicles [186] and detergent micelles [187]. A major difficulty in applying HDX-MS to MPs has been the effect of excessive quantities of lipids and detergents on both the performance of the chromatographic system and the ionization efficiency. Small amounts of detergents, especially if nonionic, appear to be well tolerated by LCMS systems used in HDX-MS and are in sometimes used to clean columns and other fluidics elements between sample injections. In such cases the primary effects of the detergent seem to be the modification of retention times and introduction of modest chromatographic peak tailing.

However, at high multiples of the critical micelle concentration (CMC), even otherwise benign detergents can have a deleterious effect on signal intensity. For example, if injected at a concentration below CMC, n-dodecyl-β-D-maltoside (DDM), one of the less structure-perturbing and more MS-compatible detergents in use, will elute primarily as a single late eluting peak. If nearly all of the measured DDM signal is confined to this peak, which is found at higher fractions of organic mobile phase than peptides are, flow from the LC system can safely be diverted to waste after most of the peptides have eluted. On the other hand, if DDM is in excess of its CMC is injected, signals of not only the monomer but also a mix of dimers, trimers, tetramers, and hexamers (the latter three can also be detected as doubly positively charged ions) will be present in scans throughout the entire elution profile. The presence of oligomers of detergent in mass spectral data may support the notion that micelles

are preserved throughout the chromatographic separation, and peptides sequestered within such micelles may fail to bind the stationary phase of the desalting column. Therefore, if a membrane protein is kept soluble in DDM for a labeling experiment and digestion, if possible the sample should be diluted to below CMC prior to injection. Though mitigation of detergent and lipid effects can be achieved via several methods, the most effective is removal of most of the detergents or lipids prior to injection onto the LC system.

The early 2010s saw the introduction of techniques for routine detergent and lipid removal. These include organic solvent extraction of detergents [188], spin column filtration through resins capable of binding detergents [189], and chemical precipitation of the phospholipids. Organic solvent extraction, in this context usually employing dichloromethane or chloroform, separates molecules by hydrophobicity, and thus is usually applied after digestion of the membrane protein, as the resulting peptides are less hydrophobic than the intact protein. Since MP-derived peptides, particularly those covering the transmembrane regions, can still be hydrophobic, the use of organic solvent extraction often resulted in loss of coverage for transmembrane regions, even with optimization of proteolysis to minimize peptide hydrophobicity.

Spin column detergent removal has been adopted in proteomics [190] and crystallography [191] studies, but incompatibility with quench conditions (the resin does not function above pH 5) has precluded its use in HDX-MS. The chemical precipitation technique involves the use of beads coated with zirconium oxide, which acts as a Lewis acid to bind the phosphate moiety of lipids. Though only applicable to phosphate-containing molecules, zirconia treatment has proven to be an effective tool for removing phospholipids from solutions containing labeled proteins or peptides [192], with recent years seeing an integration into automated sample handling systems [193]. Thanks to the popularization of these techniques, MPs have in the past decade been studied in a wider variety of membrane mimetics [164], including bicelles [194], nanodiscs [184], styrene maleic acid lipid particles (SMALPs) [195], and outer membrane vesicles (OMVs) [196]. Despite the increased array of options for handling MPs,

many of the HDX studies on integral membrane proteins have achieved only modest coverage of the transmembrane regions. Reported signals are usually concentrated in juxtamembrane loops connecting the transmembrane segments, or in soluble, membrane-tethered domains. As of the writing of this thesis, the outer membrane vesicle study remains the only report of HDX measurements of an outer membrane protein in a context where it can interact with lipopolysaccharide, a critical component of outer membranes.

In that work, outer membrane vesicles were obtained by filtration and ultracentrifugation of the supernatant left over from harvesting a culture of log-phase from a culture of *E. coli* [196]. Unfortunately, BtuB does not express well in outer membrane vesicles, and attempts to measure BtuB peptide signals from OMVs prepared by following the protocols described in that publication were unsuccessful. Consequently, a preparation of OMs derived from *E. coli* cells was required for the desired HDX-MS measurement of BtuB. OMs were obtained by a method involving repeated centrifugation and a brief extraction with sarkosyl, a detergent which dissolves IMs but not lipopolysaccharide [183].

When optimizing proteolysis for coverage of the BtuB plug domain, (and during testing of the LCMS system on CirA plug domain, see Chapter 3), many proteolytic conditions were assayed. For denaturant- and detergent-solubilized BtuB samples, use of a protease column gave adequate coverage, but these conditions were not ultimately used because BtuB failed to exhibit any evidence of ligand binding. For membrane-embedded BtuB, use of soluble protease under denaturing conditions was found to give superior peptide coverage to passage over a protease column. The plug domain is known to sequentially unfold from the amino terminus at denaturant concentrations tolerated by pepsin [137], and since the unfolded polypeptide likely exits the membrane under denaturing conditions, a soluble protease is better able to access the protein for proteolysis than if the protease were immobilized on a column. Rather than having an immobilized protease, which target protein molecules must diffuse over for proteolysis to occur, the membrane protein may be kept immobilized in the outer membranes, and the protease brought to it. This strategy has the additional

benefits of relieving the need for extraction of BtuB from membranes prior to proteolysis and minimizing the amount of membrane components introduced to the LC system. Many of the results in Chapter 2 relied on off-column in-membrane digestion, and its importance to the success of the project cannot be overstated.

CHAPTER 2

CONFORMATIONAL RESPONSE OF BTUB TO LIGAND BINDING IN OUTER MEMBRANES (ZMYSLOWSKI ET AL 2021

The following chapter appears as work submitted to be published in 2021, followed by related unpublished results. This work represents the first high-resolution HDX-MS study of an outer membrane protein embedded in the native outer membrane environment. In addition to advancing the understanding of the BtuB transport cycle, this work identifies an environmental protection effect which may be common to all HDX-MS experiments performed on integral membrane proteins. The method described represents a step towards expanding the technique to study proteins in a difficult yet important context.

Michael Baxa maintained the mass spectrometry system and assisted in measurements and data interpretation. Isabelle Gagnon assisted with cloning, expression, and purificaiton of protein samples. Professors Robert Nakamoto, Heedeok Hong, and Nicholas Noinaj provided materials and valuable advice on the project, as well as feedback on the manuscript during preparation.

I designed, cloned, expressed, and purified all protein constructs. I performed all mass spectrometry experimental design, conducted experiments, and analyzed data. I designed and performed the offline proteolysis assays.

2.1 Summary

HDX-MS performed on BtuB in E. coli Outer Membranes Delineates the Luminal Domain's Allostery and Unfolding upon B12 and TonB Binding.

Authors:

Adam M. Zmyslowski, Michael C. Baxa, Isabelle A. Gagnon, Tobin R. Sosnick.

To import large metabolites across the outer membrane of Gram-negative bacteria, TonB dependent transporters undergo significant conformational change. After substrate binding in BtuB, the E. coli vitamin B12 TBDT, TonB binds and couples BtuB to the inner membrane proton motive force which powers transport. The role of TonB in rearranging the plug domain to form a putative pore remains enigmatic. Some studies focus on force-mediated unfolding while others propose force-independent pore formation by TonB binding leading to breakage of a salt bridge termed the "Ionic Lock". Our hydrogen exchange measurements in E. coli outer membranes find that a region surrounding the Ionic Lock, far from the B12 site, is fully destabilized upon substrate binding. A comparison of the exchange between the B12- and B12+TonB-bound complexes indicates that B12 binding is sufficient to unfold the Ionic Lock region with binding of a TonB fragment having much weaker effects. TonB binding accelerates exchange in the third substrate binding loop, but pore formation does not obviously occur. This study provides a remarkably detailed structural and energetic description of the early stages of B12 passage that provides support both for and against current models of the transport process.

2.2 Introduction

TonB-dependent transporters (TBDTs) are ubiquitously found in the outer membranes (OMs) of Gram-negative bacteria where they import scarce nutrients [95]. Some members of

the family function as virulence factors, counteracting nutrient sequestration by the innate immune response [197]. Aspects of the transport mechanism remain unclear, especially the nature of the structural changes involved in the creation of the pore required for substrate passage through the transmembrane β-barrel [110]. Pore formation in each TBDT is tailored to its substrate, which can range in size from 56 Da (iron) to 1.4 kDa (cyanocobalamin, "B12"). In some TBDTs, the large extracellular loops close behind the substrate and prevent back-diffusion upon formation of a pore [198]. Therefore, formation of a pore through the lumen of the barrel need not imply bi-directional diffusion. Alternatively, the pore may be formed in stages, with no single conformation allowing for unrestricted diffusion across the length of the membrane. Though the individual mechanisms may be substrate-specific, pore formation generally involves conformational changes within the plug domain that normally occludes the lumen of the β-barrel.

BtuB is a prototypical *E. coli* TBDT that has been studied extensively in both functional and biophysical contexts **(Figure 2.1)** [199, 124, 123]. B12 is a relatively large substrate which places constraints on the minimum pore size. In proposed models of pore formation [136, 133], B12 binding initiates an allosteric signaling event that leads to the release of the 7 residue, amino terminal "Ton box" [132] into the periplasm where it binds the periplasmic carboxy terminal domain (CTD) of TonB (TonB_{CTD}), an inner membrane (IM) protein [104].

The binding of TonB_{CTD} enables the energetic and possibly mechanical coupling between the IM and OM that is necessary for transport against a B12 gradient [200]. In the periplasm, TonB interacts with the ExbB/ExbD complex, which harvests the proton motive force of the IM [113]. The steps leading from TonB_{CTD}-Ton box binding to the formation of a pore are currently under debate. Though many structures of the TonB/ExbB/ExbD complex have recently been solved, the relationship between the transport mechanism and the assumed rotation of this inner membrane complex on TBDTs remains ambiguous [110]. In force-dependent models, TonB transduces energy from the IM either by pulling the plug domain's

amino terminus towards the periplasm [134, 136, 124] or by applying a torque [201]. These forces are proposed to remodel the plug to form a pore, as seen in simulations [136, 140]. Other steered MD simulations have characterized the interactions of B12 as it was pulled through the lumen [138].

Alternatively, pore formation has been proposed to be regulated in a force-independent manner by the Ionic Lock *(IL)*, a conserved salt bridge between Arg14 on the plug and Asp316 on the nearby inner surface of the transmembrane β-barrel [202, 133]. In the force-independent model, TonB binding need only disengage the *IL* to allow pore-forming motions in the third substrate binding loop (SB3) when B12 is present [133].

In the B12-bound crystal structure of BtuB (PDBID 1NQH [123]), the *IL* region adopts a very similar backbone conformation to the apo state (PDBID 1NQE). The major change in the *IL* region is the rotation of the Arg14 sidechain and the loss of the salt bridge with Asp316. **(Figure 2.2)** However, the *IL* is fully broken and the Arg14 Cα atom moves by 30.2 Å in the ternary complex with TonB_{CTD} (PDBID 2GSK, [124]). This breakage occurs along with the residues immediately carboxy terminal to the Ton box adopting an extended conformation, which permits them to exit the lumen and bind TonB_{CTD} **(Figure 2.2)**.

Cafiso and coworkers have suggested that the folded *IL* region in B12-bound BtuB (1NQH) is a crystallographic artifact, as the B12 was soaked into crystals (grown in detergent) rather than added before crystallization [128]. This potentially crucial difference leaves unresolved the actual conformation of the *IL* region in the B12 bound state in the native membrane context. Determining when the *IL* region unfolds is important as it has been recently proposed that the subsequent binding of TonB is the critical event that breaks the Ionic Lock rather than the binding of B12 [133]. This ambiguity on how the amino terminal region of BtuB responds to B12 and subsequent TonB binding events is the focus of the present work.

Studying the forces that promote transport experimentally in the context of the intact cell envelope is desirable but so far has been prohibitively difficult. Hence, most biophysical

measurements of BtuB have been performed in reconstituted, single bilayer systems. However, the results of these experiments have depended on the choice of environment, which have included detergents, liposomes, supported bilayers, OMs, or recently even live *E. coli* [203]. The pore-forming intermediate state of BtuB has proven difficult to characterize, and efforts have relied on either extraction from native membranes, use of cysteine mutants and spin labels, or a combination thereof [136, 203].

Here we present a label-free investigation of the effects of B12 and TonB_{CTD} binding on the conformation of BtuB plug domain using hydrogen-deuterium exchange (HDX) in OMs **(Figure 2.1)**. As anticipated, we find that binding of B12 slows down HDX on the plug's three substrate binding (SB) loops **(Figure 2.1, blue)**. Upon the binding of B12 alone, however, HDX is increased by 10^2-10^3-fold (i.e., destabilized) for at least a dozen residues surrounding the *IL*. These residues stretch from the carboxy terminal side of the Ton box to the beginning of the first β-strand **(Figure 2.1, red)**, supporting the proposal [133] that a binding event breaks the *IL* as a prerequisite to transport. However, we find that the binding of B12 by itself, rather than TonB, can accomplish this *IL* disruption. Accordingly, we propose that B12 binding leads to an allosterically-induced unfolding of BtuB's amino terminus via breakage of the *IL*, which in turn enables TonB to bind the newly-exposed Ton box **(Figure 2.1, red)**. In addition, we observe a mild acceleration within a four-residue segment located between the *IL* and the B12-contacting apex of the SB3 loop, which is near a recently proposed site for pore formation [133]. This co-localization suggests that B12 initiates only the first step in a cascade of events that promotes its own transport **(Figure 2.3)**. The binding of TonB is a subsequent step, but our results suggest that it too, may be insufficient to cause pore formation in the absence of coupling to an active ExbB/ExbD complex.

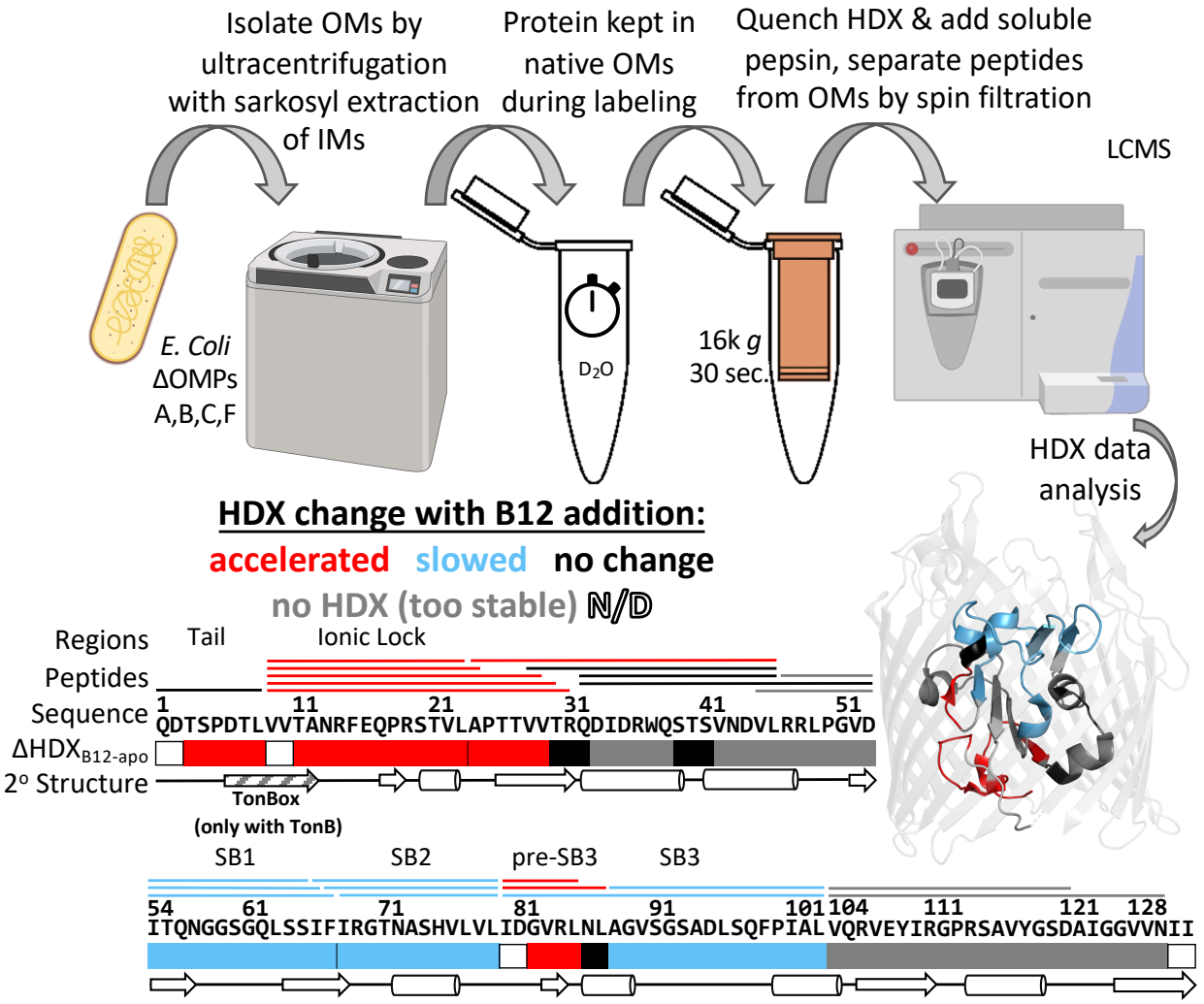

Figure 2.1: **BtuB purification and HDX protocol** Sample preparation in outer membrane (OM) involves no chromatography, only repeated centrifugation and resuspension with a sarkosyl extraction step to remove inner membranes (IM). All steps except HDX labeling on ice. Structure shown is for the apo state of BtuB (PDBID: 1NQE [123]), with the β-barrel domain displayed transparently to highlight regions of the plug domain. N/D refers to residues whose deuterium uptake could not be determined due to rapid back exchange (see main text). Cartoons made with BioRender.com.

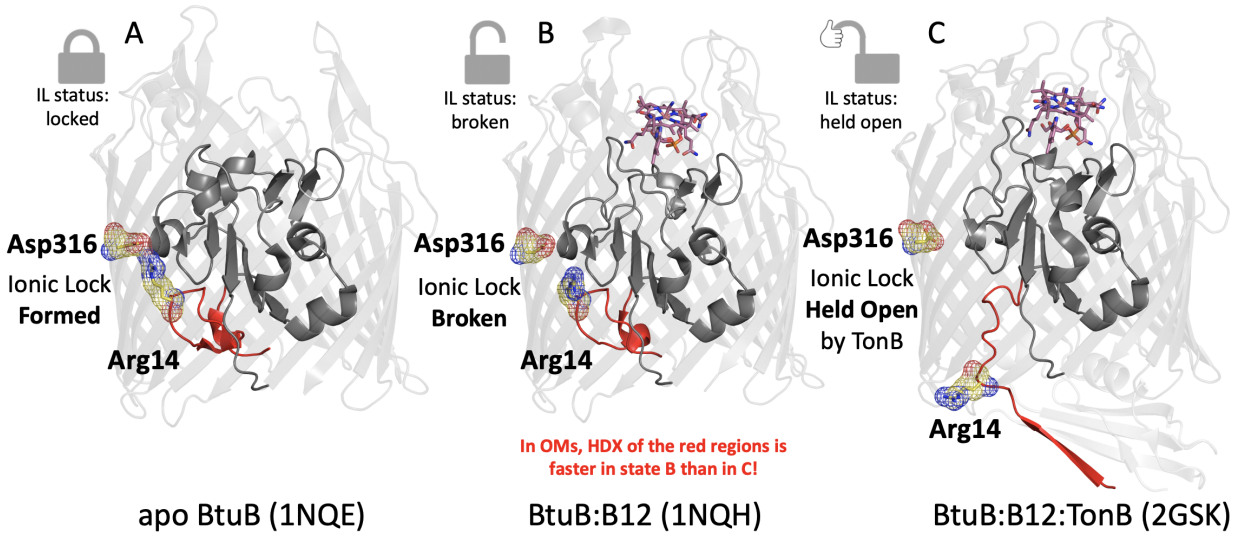

Figure 2.2: **Detailed comparison of Ionic Lock and IL Region in PDB structures** A) apo BtuB (PDBID: 1NQE [123]) B) BtuB:B12 complex (PDBID: 1NQH [123]) C) BtuB:B12:TonBCTD complex (PDBID: 2GSK [124]) structures. The amino terminal tail through the *ILR* is colored red. The *IL* is shown as yellow sticks and mesh

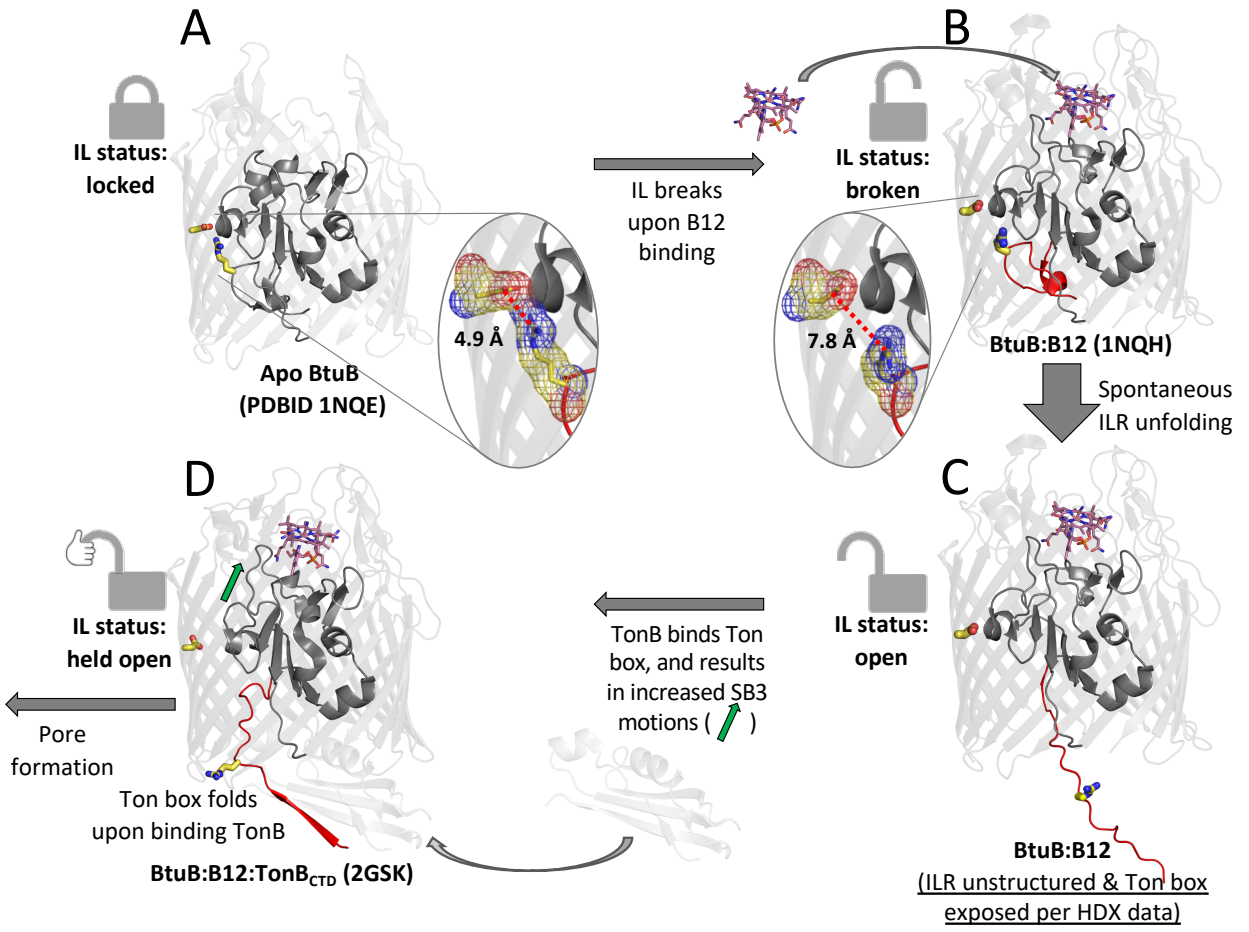

Figure 2.3: **HDX-derived model of the BtuB plug domain's conformational response to two ligand binding events** A), C), D) are the three major steps identified by the HDX data whereas B) is a structure with bound B12 observed by crystallography but not observed in our data. The Ionic lock sidechains are shown as yellow sticks, with oxygen and nitrogen atoms colored in red and blue, respectively. Inset ovals show an expanded mesh representation of the IL in states A) and B) with bolded numbers corresponding to the distance between Arg14 guanidinium and Asp316 carboxylate carbon atoms.

2.3 Results

We first present the protocols and reproducibility of our HDX measurements in OMs, followed by data for regions where stability increases due to B12 binding, focusing on SB1-SB3 **(Figure 2.4, shades of blue/green)**. We next describe the large decrease in stability observed near the IL and the smaller stability losses for regions at the nearby amino terminus, first strand, and start of the SB3 loop **(Figure 2.4, red shading)**. We conclude with an examination of the regions where minimal changes in HDX are seen upon B12 binding. To allow access to the HDX data of this study, the HDX data summary table **(Table S1)** and the HDX data table **(Table S2)** are included in the supporting information [154].

2.3.1 OM sample preparation, sequence coverage

We measured deuterium uptake at pD 7.2 (pD_{read} = 6.8), 22 ^{o}C for apo, B12- and $TonB_{CTD}$ -liganded states of BtuB in native-like OMs from three biological replicates. To study the effects of $TonB_{CTD}$ binding, we used $TonB_{\Delta N}$, a construct containing the CTD and periplasmic linker, lacking only the amino terminal transmembrane helix (hereafter referred to as TonB within the context of our experiments). OMs and OM proteins (OMPs) are significantly more stable than their IM counterparts, and thus the protocols used to study OMPs employ strategies not commonly used for IM proteins.

To our knowledge, the only published HDX-MS study of OMPs performed in a native OM-like environment was conducted on OmpF in *E. coli* OM vesicles [196]. BtuB, however, did not express well in OM vesicles, so we adapted protocols used in the EPR studies of BtuB embedded in native-like OMs [204]. Based on a strategy employed on FhuA [205], a BtuB construct was created with five histidines, glycine, and two serines inserted after His449 on the apex BtuB's seventh extracellular loop. This construct and the wild-type were overexpressed in *E. coli*, and after lysis, total membranes were separated using ultracentrifugation followed by extraction with sarkosyl to selectively remove the IMs. Initially, the OMPs were

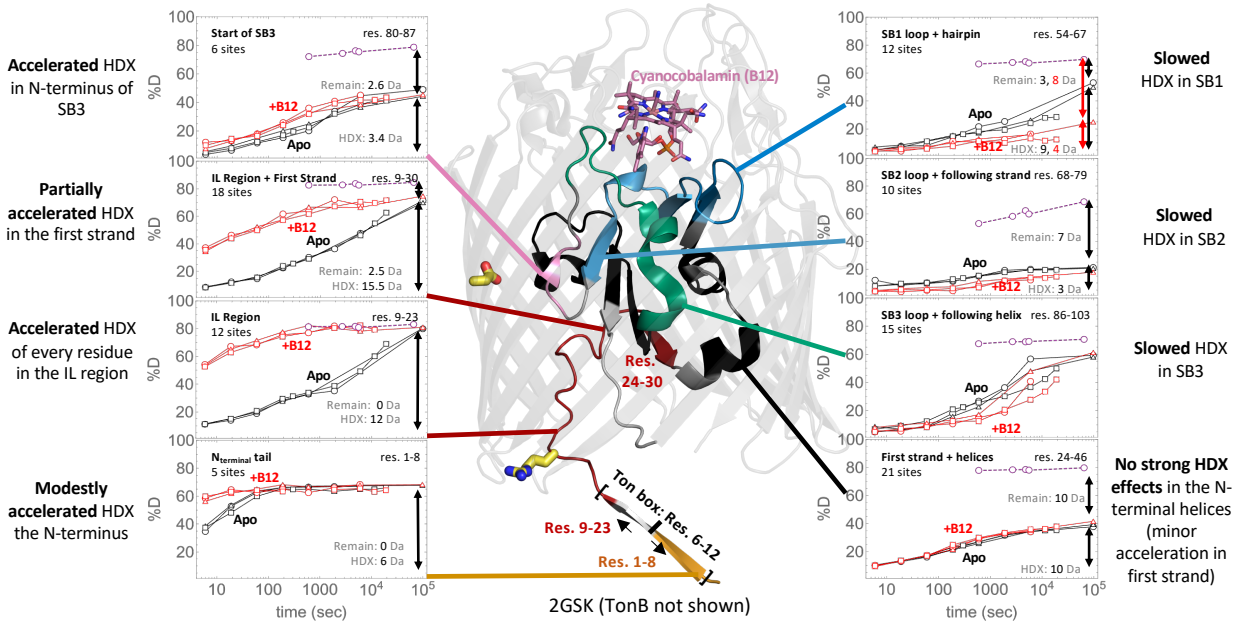

Figure 2.4: **Effects of B12 binding on HDX** Uptake plots show biologically triplicated data (circles, triangles, and squares) for BtuB measured in apo (black) and B12-bound (red) states. Insets contain uptake curves for the peptides depicted by the colored regions on the BtuB structure. The number of exchangeable sites is assumed to be the number of non-proline residues minus two. The exchanged and remaining masses at the last time point are given in grey, after correcting for back exchange by normalizing to unfolded controls which assumed to be fully deuterated (purple circles with dashed lines). On the structure, black corresponds to regions with undetectably slow exchange, dark grey to regions with exchange unaffected by B12 and/or TonB binding, and pale grey to regions with no data available.

extracted with detergent, but detergent-solubilized BtuB failed to exhibit evidence of B12 binding in the ILR by HDX, consistent with earlier findings that detergent solubilization perturbs the folding of the amino terminus [206]. Hence, BtuB was left in its native OM environment for our HDX studies.

Accordingly, our workflow was altered to allow HDX labeling of BtuB still embedded in the OM preparations. After HDX labeling, we added denaturant and soluble pepsin in the HDX quench buffer rather than employing an in-line protease column as typically done in HD-XMS measurements. This change afforded us greater control over the cleavage conditions while eliminating fouling of the chromatographic system as it was no longer necessary to extract BtuB from OMs. We optimized digestion for redundant and nearly complete peptide coverage of the plug domain, in part by decreasing β-barrel cleavage **(Figures 2.1, 2.5B)**. Consistent with the known trends of BtuB unfolding in response to denaturant [140], the proteolysis was best near the amino-terminus. Pepsin's weak preference to cleave after hydrophobic residues caused the peptides to cluster into regions with similar boundaries, with peptides within each region exhibiting similar HDX behavior. In our nomenclature, regions are capitalized while the sequence bounds are denoted in subscript, with important peptides following in parentheses, e.g., BtuB's amino terminus is covered by Region_{3-8} (Peptide_{1-8}).

The imperfect correspondence between peptide and region boundaries is caused by an effect common to all HDX-MS studies: The intrinsic exchange rate (k_{chem}) for the first two residues on any given peptide is sufficiently fast that the residues undergo essentially complete back exchange and do not measurably impact the deuterium uptake level [207]. Consequently, we defined regions to start at the third residue of the most amino terminal peptide of the cluster, except for situations where other peptides can provide information for those residues. Our partitioning of the plug domain into regions mapped well to the secondary structure boundaries. Areas previously reported to undergo distinct motions usually separated into distinct regions **(Figure 2.4)** [139]. Despite each region having

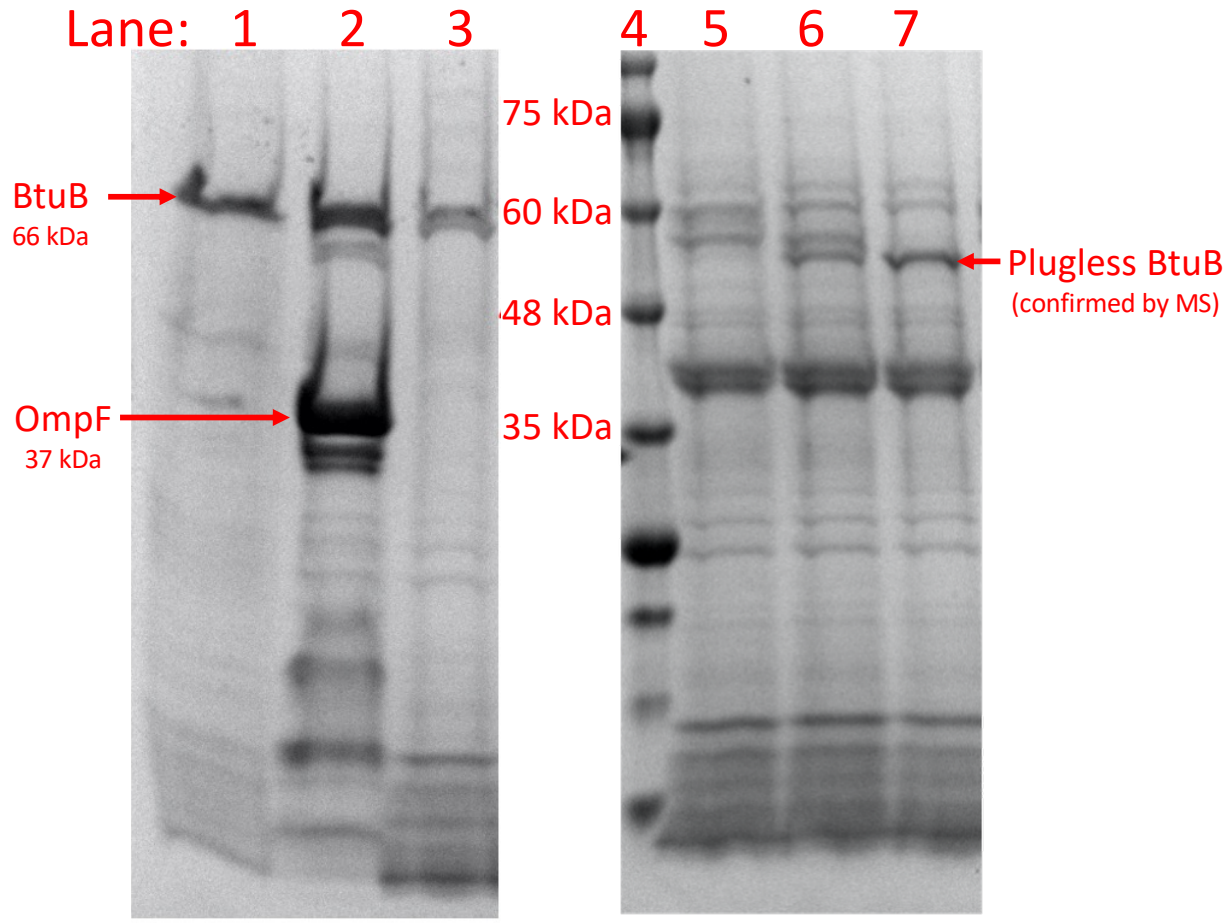

Figure 2.5: **SDS-PAGE of A) OMP abundance and B) soluble pepsin digestion of BtuB in OMs A**) Total OMP content of the three OM samples used in this study. Lanes 1 and 3, duplicates prepared from OMs of ΔABCF *E. coli*, that lack several naturally abundant OMPs, e.g., OmpF. Lane 2 is prepared from OM of wild-type *E. coli*. **B)** Digestion of BtuB in OM by pepsin under HDX quench conditions, with lanes 5, 6, and 7 corresponding to digestion times of 1, 3, and 10 minutes, respectively. Lane 4 is a molecular weight marker. Note the progressive weakening of the intact BtuB band and the appearance of a plugless BtuB band (whose identity was confirmed by tryptic digest experiments performed at an independent facility), along with several intermediates. A digestion time of 3 minutes was used for HDX samples.

markedly different exchange behavior, peptides within a region were internally consistent with respect to their deuteration levels. Peptides spanning more than one region displayed intermediate effects, weighted by the number of amide protons in each region **(SI)**.

2.3.2 Reproducibility and heterogeneity

Three biological replicates were initially prepared, two from a quadruple OMP knockout strain of *E. coli*, with a third replicate using unmodified BL12 (DE3) *E. coli* to examine the potential effects of the knockout strain [208]. Use of the knockout strain did not significantly perturb HDX results **(Figure 2.7)** although it did reduce the non-BtuB OMP content as intended **(Figure 2.5A)**. One of the two knockout replicates had high levels of non-native signals, complicating the analysis. Although the slowly exchanging subpopulations matched the other samples, this replicate was excluded from analysis to simplify data processing and a fourth knockout sample was prepared to take its place.

For most peptides, the slowest exchanging population was dominant and hence, was considered to represent the natively folded protein. For certain peptides, however, we observed multiple populations with distinct exchange kinetics. Their isotopic envelopes remained separated even in our longest measurements of 10^5 seconds implying that the underlying populations do not interconvert on this time scale. The heterogeneity generally was manifested as bimodal isotopic envelopes that varied in relative intensity for different peptides but exhibited a systematic correlation within a bioreplicate.

When minor populations were present, they usually exchanged much faster than the major population. Several of their features, including their insensitivity to B12, suggested that these fast populations represent unfolded or damaged proteins **(Expanded data)**. The uptake trends of the minor populations were similar to membraneless controls measured in 0.5 M urea. These controls were prepared using a BtuB construct lacking a signal sequence that was expressed in inclusion bodies and purified in 8 M urea so that the β-barrel was unlikely to have ever folded properly. By comparing our main dataset to this control, we identified

and excluded populations of peptides that likely arose from non-native BtuB and focused our analysis on the major, slowly exchanging population. The minor subpopulations were computationally isolated or suppressed using the bimodal fitting capability of the HDExaminer 3.1 program and were not plotted in the main figures but are shown in the supplement **(Figure 2.6 and Expanded data)**. We additionally required consistency between multiple peptides and replicates in constructing our comprehensive profile of the plug domain's behavior.

Our conclusions regarding B12 binding hold for every presented peptide across all replicates, though minor features of HDX uptake trends varied between bio-replicates **(Figure 2.7)**. For the major population, the only significant difference between biological replicates is that one had a diminished effect of $\text{TonB}_{\Delta\text{N}}$ binding **(Figure 2.7B)**. Optimization of integration bounds for our data using HDE3 program resulted in average apo state standard deviations of approximately 0.24 Da, averaged across the 35 presented peptides. Table S3 provides estimates of mass differences significant at the 98% confidence level for each peptide. These intervals varied from 0.17 (Peptide_{45-53}) to 8.30 Da (Petide_{80-103}) and had a mean of 1.14 Da and median of 0.62 Da. The average level of back exchange observed in our data was 25.1%, with an interquartile range of 9.0%. Further plots summarizing the reproducibility are provided in **Figure 2.8**.

2.3.3 HDX formalism

In apo-BtuB, substrate binding loops SB1-SB3 exchanged slowly with most associated peptides retaining greater than 50% of their H-level even after 10^5 seconds, the longest measured time point. This slow exchange translates to an HDX protection factor (PF) $> 10^5$, where PF is defined as the relative slowing of the observed HDX rate (k_{obs}) compared to the intrinsic chemical exchange rate for an exposed amide proton (k_{chem}), i.e., $PF = k_{chem}/k_{obs}$. In this commonly used formalism, exchange is assumed to occur when an H-bond is broken in a transient open state, and the amide is exposed to solvent [210].

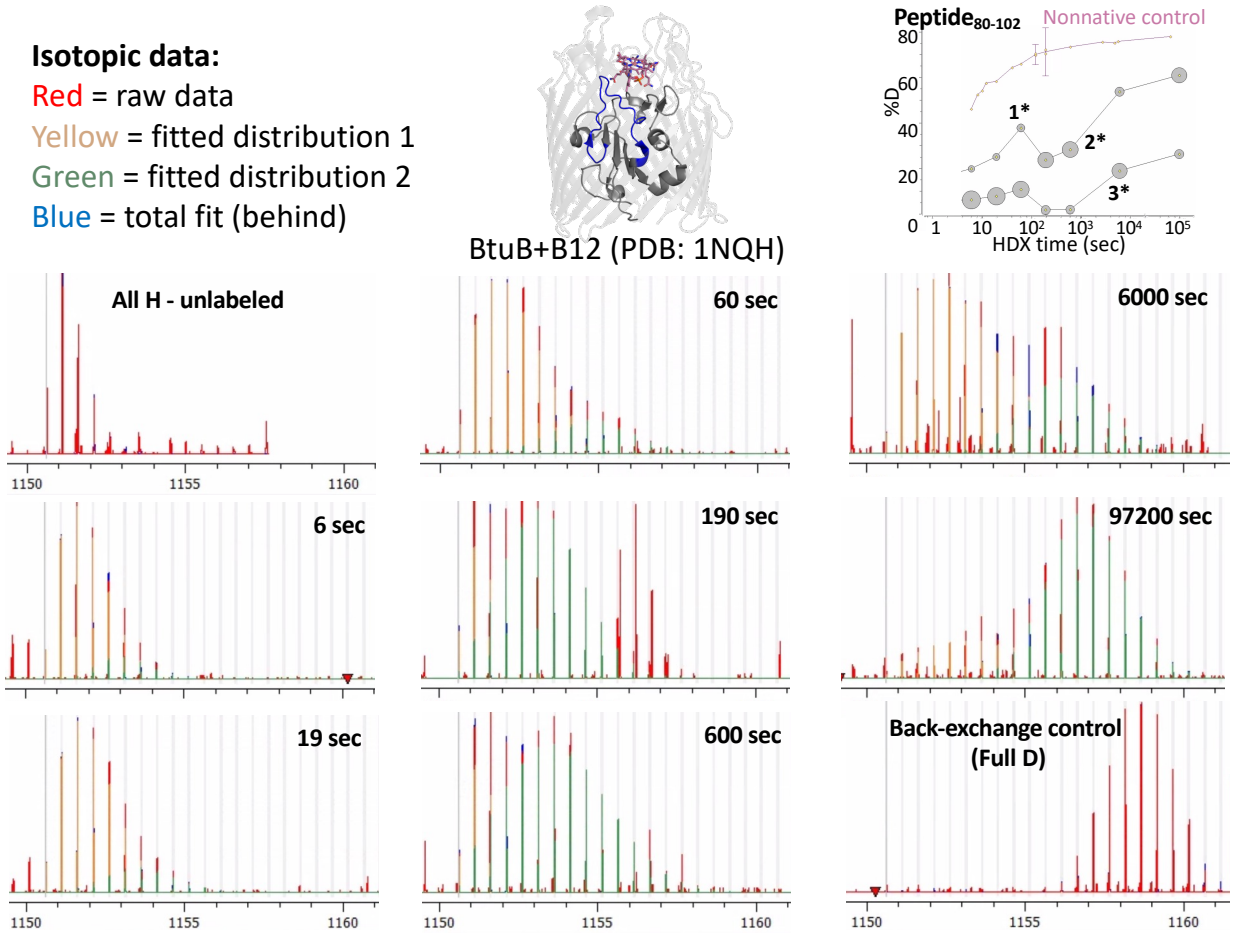

Figure 2.6: **Multi-modal exchange in the third substrate binding loop Left:** undeuterated, in-exchange, and back-exchange controls. **Middle & Right:** Raw mass spectral data (red) and fitted populations (yellow and green, left and right subpopulations, respectively, blue, total fitted distribution) for all time points of one apo state bioreplicate. Grey bars indicate masses comprising the peptide's isotopic envelope, calculated according to $(m_{monoisotopic} + \frac{n}{z}$, where $m_{monoisotopic}$ and z are the monoisotpic mass and charge of the peptide, respectively, and n are whole numbers. **Top Right:** uptake plot for the presented data, indicating fitted populations by 1*, 2*, and 3*. Circle sizes correspond to fitted population weights.

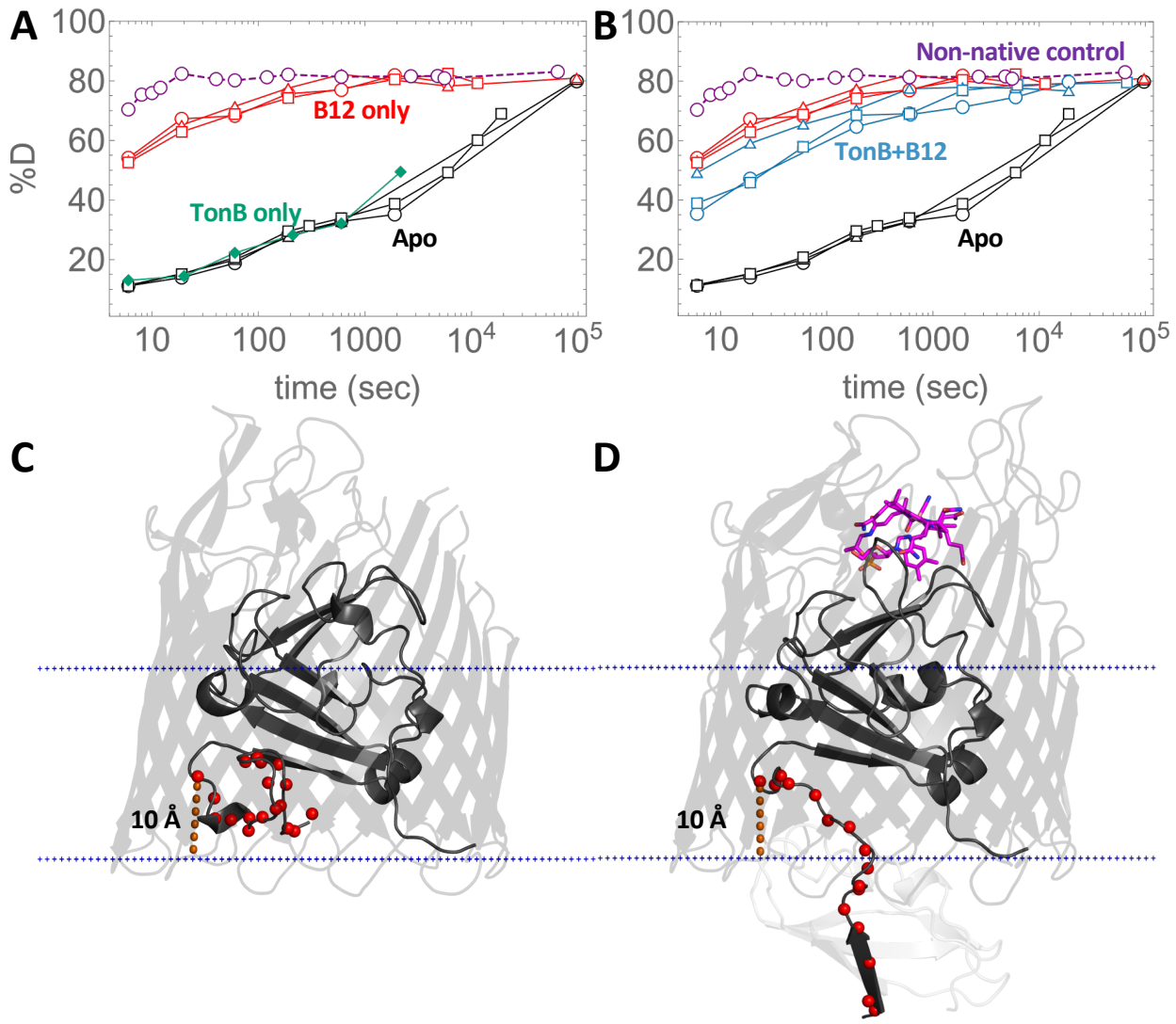

Figure 2.7: **HDX in the Ionic Lock Region A, B)** Uptake plots for Peptide$_{9-23}$, three biological replicates (black), and (red), and TonB$_{\Delta N}$ (green). Four long points of an unfolded control shown in purple. **B)** Uptake plots for Peptide$_{9-23}$, apo (black), B12 (red), and B12+TonB$_{\Delta N}$ (blue) **C) & D)**: Position of the amino terminal regions relative to the membrane plane. **C)** apo (PDBID: 1NQE) and **D)** BtuB:B12:TonB complex (PDBID: 2GSK) crystal structures, taken from the OPM database [209]. N atoms for residues 6-23 are shown as red spheres. Distances from Leu23's N atom to the nearest membrane plane dummy atom are shown as dashed red lines, in both cases about 10 Å.

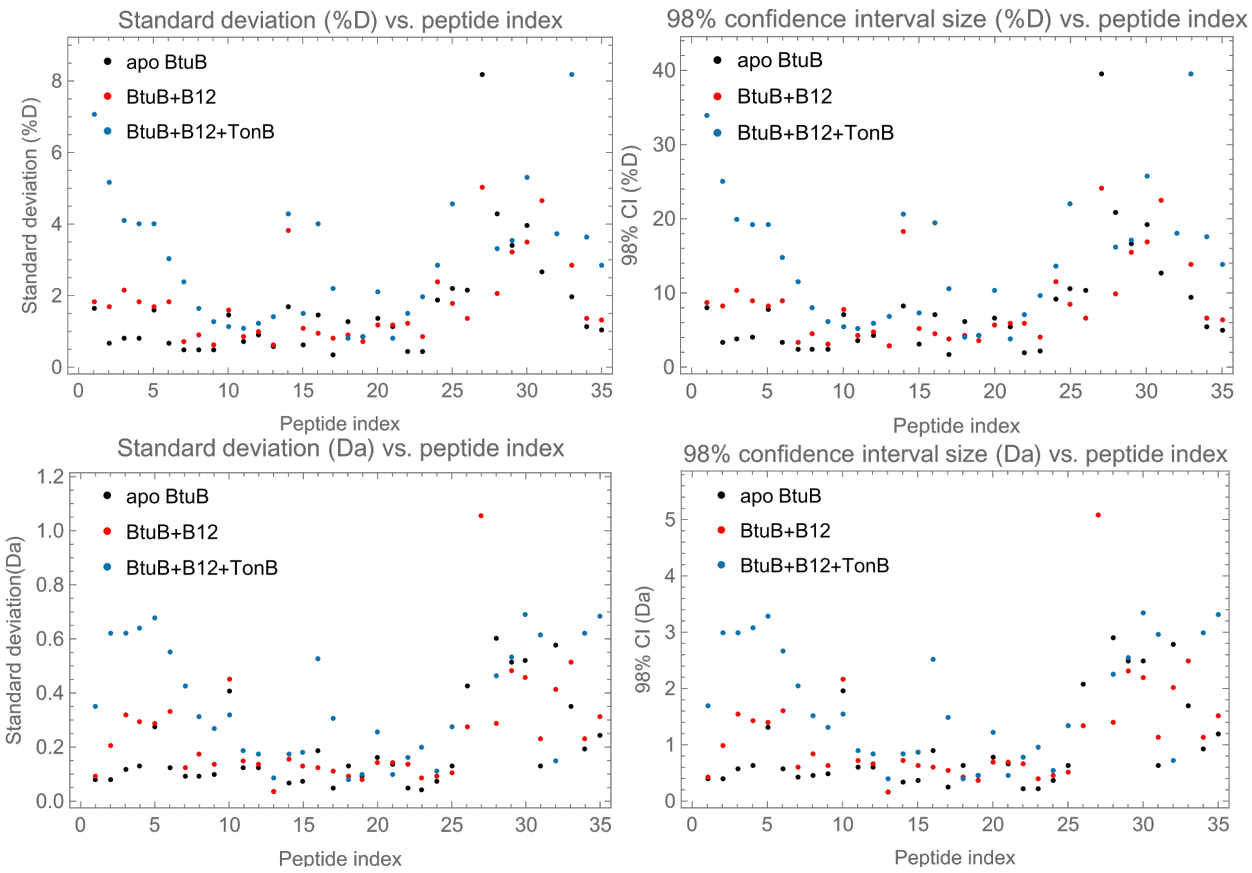

Figure 2.8: **Statistical summary plots** Scatterplots show the reproducibility as standard deviations (left) or 98% confidence intervals (right), in terms of %D (top) or Daltons (bottom). Peptides are ordered sequentially by amino terminus. Peptide index 26, where reproducibility begins to decrease, corresponds to Peptide_{80-102}, the first to cover the SB3 loop apex.

$$\text{H-bond formed} \underset{k_{close}}{\overset{k_{open}}{\rightleftharpoons}} \text{H-bond broken} \xrightarrow{k_{chem}} \text{H-D exchange} \tag{2.1}$$

where k_{open} and k_{close} are the opening and closing rates, respectively. In general, the observed HDX rate for this reaction is given by

$$k_{obs} = \frac{k_{chem} \cdot k_{open}}{k_{close} + k_{open} + k_{chem}} \tag{2.2}$$

Under the so-called EX2 condition where $k_{close} >> k_{chem}$, the PF is directly related to the equilibrium stability according to [159]:

$$\Delta G_{HX} = RT \cdot \ln(K_{eq}) = RT \cdot \ln(\frac{[closed]}{[open]}) = RT \cdot \ln(\frac{[k_{closed}]}{[k_{open}]}) = RT \cdot \ln(PF - 1) \tag{2.3}$$

In the EX1 limit where $k_{close} << k_{chem}$, every opening event produces a concerted exchange for all exposed amide protons with the observed rate equal to the opening rate, $k_{obs} = k_{open}$. Unfortunately, we cannot use the $k_{close} >> k_{chem}$ criterion to test for EX2 behavior as commonly employed in site-resolved NMR studies [210] because we lack explicit information on k_{close} for BtuB. However, we can take advantage of the behavior of HDX/MS isotopic envelopes to identify whether our measurements are in the EX1 or EX2 limit. Specifically, in the EX1 limit, the concreted exchange should produce a decreasing protonated isotopic envelope and the concomitant rise in the corresponding deuterated isotopic envelope [211]. In the EX2 limit, however, the isotopic envelope for a peptide should exhibit a continuous increase in mass as a function of time, as exchange at each residue in the peptide is uncorrelated. The D uptake is consistent with EX2 behavior for the presented peptides and we therefore interpret the data as occurring in the EX2 limit.

2.3.4 Substrate binding loops

As noted above, the three SB loops exchanged slowly with >50% of the H-level remaining after 10^5 second. In addition, the presence of 20 μM B12 further slowed exchange. An examination of overlapping peptides indicated that this slowing was concentrated in the residues nearer to the B12 binding site. SB1 exhibited the largest slowing effect, followed by SB2 and SB3 **(Figure 2.4)**. The observed slowing for SB2 was relatively small, about 10-fold, although most amides on the associated peptides already exchanged very slowly in the apo state making any changes difficult to detect. Whereas the overall exchange for SB3 was slowed only 5-fold, some peptides displayed complex behavior, and exchange for other peptides was even accelerated, as will be discussed later. Otherwise, the general slowing of HDX by B12 in each of the SB loops indicates that binding stabilizes each of the regions contacting the B12 binding site.

2.3.5 Destabilization of the Ionic Lock (IL) and Ton box upon B12 binding

Our major finding is that upon B12 binding, exchange drastically increased for the *IL* Region_{11-23} ($\text{Peptides}_{9-23,\,9-27,\,9-28,\,9-29,\,9-30}$). The *IL* region contains the Arg14-Asp316 salt bridge that connects the plug domain to the inner wall of the β-barrel **(Figures 2.7, 2.12)**. In addition, exchange was mildly increased for the amino terminal tail Region_{3-8} **(Figure 2.12, Peptide_{1-8})**. Specifically, peptides in the *IL* region exchanged up to 10^3-fold faster with B12, with a majority of the exchange occurring in the 6 second dead-time of the measurement. For the tail region, deuterium uptake increased mildly, with the uptake increasing from 50% to 80% at 6 seconds. From this widespread acceleration of HDX, we infer that both regions are unfolded in the B12 bound state and that upon B12 binding the amino terminus partially exits the lumen. The smaller acceleration for the tail region is the result of it being less stable in the apo state to begin with.

We interpret the sizable B12 effect on the HDX of the *IL* region to be a result all residues within the region losing specific interactions with the β-barrel, most importantly the Arg14-

Asp316 salt bridge. This disruption results in the exit of the Ton box from the lumen into the periplasm. Residues 1, 2, 9, and 10 are unobservable due to HD back exchange (an inherent HDX-MS issue occurring during sample handling). These four residues likely are also unstructured given the rapid exchange of every observable residue surrounding them (e.g., $\text{Peptides}_{1-8 \text{ and } 9-23}$). Notwithstanding, the data provide strong evidence that BtuB's first 23 residues undergo a complete or near-complete loss of native structure in response to B12 binding.

Our inference that both the *IL* region and the Ton box were unfolded upon B12 binding alone is further supported by our finding that the addition of $\text{TonB}_{\Delta\text{N}}$ did not further accelerate exchange. The binding of TonB (specifically the carboxy terminal domain) to the Ton box requires that the Ton box extend into the periplasm, which in turn necessitates that the *IL* be broken. Therefore, if the *IL* region remained folded after B12 binding and then unfolded when $\text{TonB}_{\Delta\text{N}}$ bound, one would have expected a marked increase in exchange for the *IL* region upon $\text{TonB}_{\Delta\text{N}}$ binding. However, exchange did not markedly increase upon $\text{TonB}_{\Delta\text{N}}$ addition (in fact, exchange even slowed for a few residues, which provides direct evidence of TonB binding, **Figure 2.9, right)**. This minimal response is in the opposite direction than expected if B12 binding were insufficient for lock breakage. Therefore, the *IL* region was already unfolded prior to $\text{TonB}_{\Delta\text{N}}$ binding and B12 binding alone was sufficient to unfold the *IL* region.

In ostensible disagreement with this conclusion is that the *IL* region does retain a significant amount of HDX protection even after B12 binding. The approximate PF is 10^2 when referenced to the intrinsic exchange rate (k_{chem}) determined for peptides in bulk solution [207]. This reference rate may be inappropriate in the present situation as the *IL* region's carboxy terminus is located 10 Å within the barrel lumen, which prevents portions of the region from fully exiting into bulk solvent. In this partially confined state inside the barrel, the access of OD- to peptide backbone is reduced, and the residues which do exit into the periplasm may be subject to a milder but similar effect from interactions with the nearby

peptidoglycan **(Figure 2.9)**. In addition, the effective [OD^-] should be lower in the barrel than in the bulk solvent as the anion prefers to be hydrated rather than reside in the lumen's lower dielectric environment [212]. Both the reduced access to the backbone and lower [OD^-] concentration will retard exchange and, hence, may account for the slower than expected HDX observed for the *IL* and for other regions especially those further inside the barrel.

Our B12 results imply that the extent of conformational change in the amino terminus of BtuB is greater than previously inferred. Early EPR studies probing the Ton box found that B12 binding caused the first residue within the Ton box, Asp6, to project 20-30 Å into the periplasm [132]. Whereas the authors modeled the first 15 residues as exiting the lumen, we observed rapid deuteration of every observable amide on $\text{Peptides}_{1-8 \text{ and } 9-23}$ suggesting that an additional eight residues are affected by the same B12 binding event. A comparison of Peptide_{9-23} with overlapping $\text{Peptides}_{9-27,\, 9-28,\, 9-29, \text{ and } 9-30}$ found that acceleration of HDX was also occurring in some additional residues between 24-29, which encompass BtuB's first β-strand **(Figure 2.10)**. The acceleration in Residues_{24-29} did not affect all five exchangeable residues equally, however. Some residues within BtuB's first β-strand remained very slow to exchange, implying that the strand remains folded, while its exposed face becomes more solvent exposed when B12 binds. Thus, our data identify the B12 sensitive region as being at least eight residues (>50%) larger than previously proposed.

2.3.6 Complex ligand effects in the third substrate binding loop, including destabilization by B12

In sharp contrast to the generally slowed exchange observed for the substrate binding loops, the amino terminus of SB3, i.e., Region_{82-85}, exhibited accelerated exchange upon B12 binding **(Figure 2.10)**. The apparent exchange timescale for the fastest amide among Residues_{82-85} on Peptide_{80-85} was approximately 2,000 s, and B12 binding increased exchange of this single amide by about 5-fold. Other amides within Region_{82-85} remained

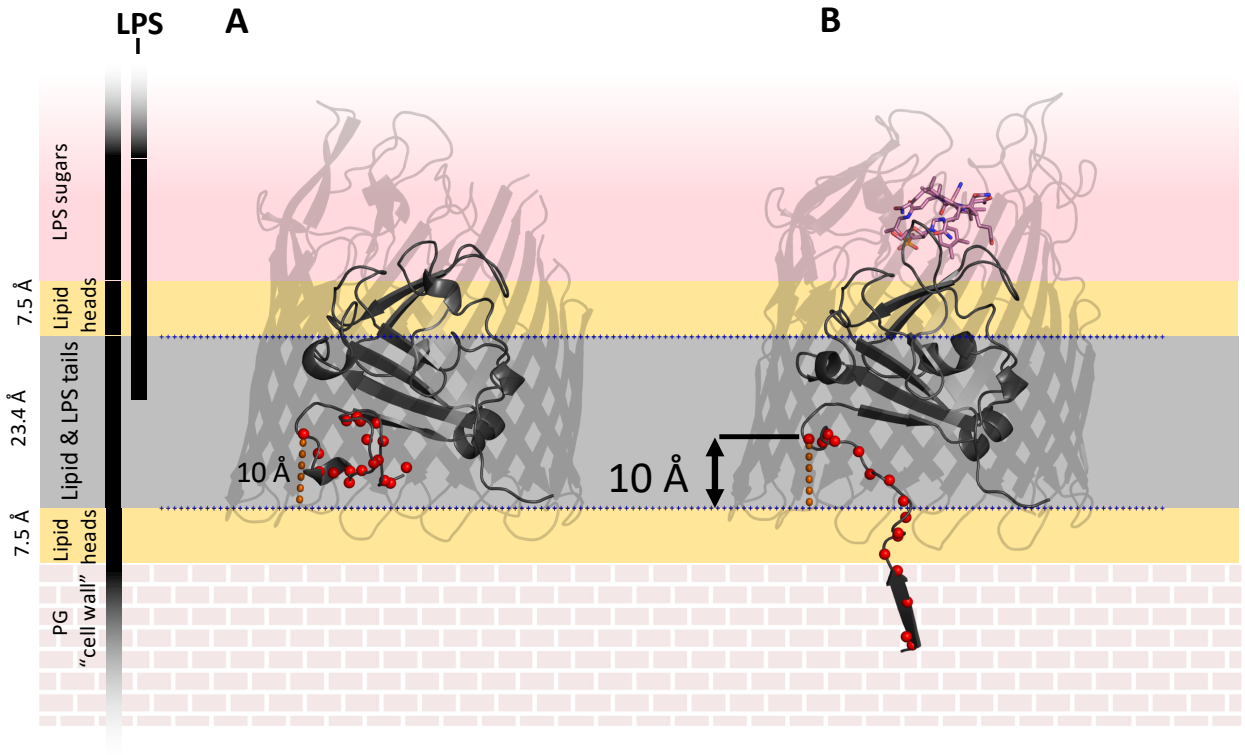

Figure 2.9: **Outer membrane environment** Structures of A) apo BtuB (PDBID: 1NQE) and B) BtuB:B12:TonB ternary complex (PDBID: 2GSK) highlighting amide nitrogen atoms of Residues_{6-23} as red spheres. The 10 Å distance from Leu23 to the membrane plane defined by OPM [209] is shown as a dashed orange line. The shaded background shows approximate zones of various outer membrane layers. Dark grey indicates lipid tails, yellow indicates the headgroup region, solid pale red indicates extracellular lipopolysaccharide, and brick indicates peptidoglycan (the cell wall). The lipid zone thickness value of 23.4 Å is taken from OPM, the headgroup value of 7.5 Å is taken from [66], although the model presented here with parallel planes is an oversimplification. The membrane plane has been measured to be significantly distorted around BtuB in lipid vesicles as the hydrophobic thickness varies significantly around the circumference of the β-barrel. However, regardless of membrane plane tilt, several amides on the amino terminus exit the lumen into the periplasmic zone occupied by peptidoglycan where $[OD^-]$ apparently is lower than in bulk solvent, based on our findings that HDX for this region remains 10^2 slower than k_{chem} in the presence of B12.

too protected to be seen exchanging in our experiments, so the data are agnostic regarding whether these positions were affected by B12, unlike the remaining portion of SB3 (Region_{86-103}) and the other SBs, which were affected **(Figures 2.10)**. Though the change in HDX upon B12 binding was relatively mild compared to that seen at the amino terminus of the protein, Region_{82-85} was unique in having its exchange further enhanced beyond the already B12-accelerated rates by addition of $\text{TonB}_{\Delta\text{N}}$. **(Figure 2.10)**. Hence, this region allosterically responds to distal B12 as well as TonB binding events, supporting it as potentially important for TonB-dependent pore formation [133].

2.3.7 Regions with no significant HDX differences

The HDX of the three remaining regions of the plug domain did not display a significant response to B12 binding **(Figure 2.10)**. Two of these ($\text{Regions}_{30-46 \text{ and } 47-53}$) lie between the *IL* and SB1, and the third, ($\text{Region}_{104-128}$) is carboxy terminal to SB3. Comparison of overlapping peptides within Region_{30-46} **(Figure 2.10**, $\text{Peptides}_{24-46 \text{ to } 31-46}$) confirmed the mild response to B12 within Residues_{26-29} discussed earlier and showed that residues flanking BtuB's first stable helix do not respond to B12. $\text{Regions}_{47-53 \text{ and } 104-128}$ **(Figure 2.10**, $\text{Peptides}_{103-121 \text{ to } 104-128}$) exhibited almost no exchange, indicating extremely high stability. The high overall stability for these regions and lack of a response to ligand binding indicate that rearrangements in the plug domain during ligand binding are restricted to the areas surrounding the *IL* and SB3.

2.4 Discussion

Our major finding is that the binding of B12 promotes the complete breaking of the Ionic Lock [212], a critical salt bridge connecting the amino terminal end of the plug domain to the inner surface of the β-barrel (Arg14-Asp316). The breakage results in all of the residues within Region_{11-23} unfolding, which enables TonB binding. Upon subsequent TonB binding

to the B12-bound state, we did not observe evidence of pore formation or further unfolding of the *IL* region. In fact, TonB binding alone only produced subtle HDX changes throughout the plug domain, suggesting that its full function in pore formation requires an energized inner membrane, or some other factor only present in live cells.

2.4.1 B12-induced dynamics at the amino terminus of BtuB

Binding of B12 alone resulted in stability changes throughout the plug domain, both increasing and decreasing the HDX rates. We observed the anticipated slowing of exchange for the loops that directly contact B12. But the addition of B12 also resulted in a dramatic acceleration of HDX by up to 10^3-fold for all amide protons in the *IL* Region (e.g., Peptide_{9-23}), even approaching the rapid exchange rates seen in BtuB's labile amino terminus (Peptide_{1-8}). The large change in HDX rates upon B12 binding for the Ton box residues reflects the disruption of the entire *IL* region (11-23) in response to B12 alone. We believe this disruption is responsible for exposing the Ton box thereby regulating TonB binding.

The IL is over 20 Å away from the B12 binding site, implying an allosteric mechanism is involved in the breaking of this salt bridge. The amino terminal segment of SB3, Region_{82-85}, is located near the *IL* and also is accelerated by B12, pointing to the involvement of SB3 in the allosteric mechanism. Additionally, HDX of Region_{82-85} is further accelerated by the binding of TonB to the Ton box, suggesting a bi-directional coupling of one or both Ton box-containing regions with the SB3 loop. The movement of SB3 upon B12 binding likely is a critical initial step in the signal propagation downwards to the *IL*, and our data support the notion that SB3 may undergo further motions upon TonB binding [133].

As discussed earlier, even with a 10^2-10^3-fold increase in exchange rate for the *IL* Region_{11-23} upon binding B12, exchange is still 10^2-fold slower than k_{chem}. One might consider that this protection is indicative of residual structure in the *IL* region; however, there is direct evidence that this region is indeed unfolded. Because the binding of $\text{TonB}_{\Delta N}$ showed no further unfolding of the *IL* region after B12 binding, the *IL* must already have been broken in

the B12 bound state. Therefore, we propose that the 10^2-fold residual protection arises from other factors including restricted access to the peptide backbone as the region is tethered inside the lumen as well as a reduction of the local [OD^-] inside the lower dielectric environment [212]. Additionally, hydrogen bonding interactions with the peptidoglycan network that normally undergirds the inner surface of the OM may be conferring protection even to an otherwise unstructured chain.

2.4.2 Comparisons to existing models

Current models of BtuB transport can be broadly separated into two categories depending on the location and energetics of pore formation, including whether it is force-independent (FI) or force-dependent (FD). In both models, either implicitly or explicitly, the binding of B12 is necessary for exposure of the Ton box and subsequent TonB binding. In the FI model [133], TonB binding provides the energy for subsequent plug remodeling events, which are sufficient to open a pore near the *IL* region and permit B12 transport. By contrast, a recent FD model proposed that TonB binding establishes a mechanical linkage that transmits the force to unfold the "mechanically weak subdomain" within the plug [136]. This partial unfolding of the plug forms a substrate channel, although some uncertainty exists regarding whether this mechanism applies *in vivo*.

While the results of our experiments do not fundamentally disagree with either model, our HDX data demonstrate that binding of B12 alone is sufficient to disrupt the IL region and expose the Ton box. However, our data find that neither the individual B12 nor TonB binding events are sufficient to destabilize the substantial fraction of the plug domain, which is postulated to unfold under the FD model ($\text{Regions}_{31-46,\ 47-53,\ \text{and}\ 54-67}$). Peptides in Region_{45-53} did not exchange in the duration of our measurements (10^5 sec), implying a very high stability (Peptide_{45-53}; PF $> 10^7$). Flanking regions that unfold in the FD model (as observed in the atomic force microscopy study [136]) were either unaffected (Peptide_{31-46}; PF = 10^4) or even stabilized (Peptide_{54-67}; PF = 10^3-10^6) by B12 binding. We find this

high stability to be unexpected, but not impossible within the FD model [136]. Our data corroborate an argument [133] deployed against FD models related to the application of a torque to BtuB by TonB [201]. We found that in the ternary complex of BtuB with both B12 and TonB, nearly a dozen residues between the Ton box and BtuB's stably folded core are unstructured, consistent with what was reported for FhuA [213]. For these residues, the free rotation of their (ϕ, ψ) backbone torsion angles likely precludes the transmission of a torque from the Ton box to the plug.

Our HDX results also differ with the FI model regarding the effects of ligand binding. We find that the *IL* is broken by B12 binding alone whereas Cafiso et al. [133] found *in vivo* that the *IL* is partially broken by B12 and only completely broken by TonB, based on the conformational response of the SB3 loop to B12 binding. Specifically, mutations that broke the *IL* (e.g., Arg14Ala, Asp316Ala) enabled a 20 Å movement in SB3 and were thus reported to mimic TonB binding. In OMs, however, we find that the *IL* fully breaks in response to B12 binding, and, additionally, the *IL* is not broken by TonB binding at a concentration of 26 μM when B12 is absent. When B12 is added, however, we find the *IL* is sufficiently destabilized that subsequent TonB binding does not cause a significant slowing of the HDX for the *IL* region. In our view, the Ton box is normally sequestered in the lumen of the β-barrel and becomes available for binding only when B12 binding allosterically induces breakage of the *IL*. In this mechanism, the rest of the steps required to gate the pore cannot begin before the initial B12 binding event.

2.4.3 Complex HDX behavior in the third substrate binding loop of BtuB

Instead of the large conformational change observed in SB3 by Cafiso et al. [133], we detected only subtle HDX changes for this region upon TonB binding aside, from the substrate-induced slowing common to all SB loops (**Figure 2.10**, Peptides$_{80-85\text{ to }80-87}$). The contrast between the 10^3-fold increase seen in the *IL* region against the lack of a large effect on peptides covering the apex of SB3 is difficult to reconcile with large scale motions occurring in SB3.

Possible explanations for the difference include our use of sarkosyl to remove IMs [133] and the EPR study's use of live cells where endogenous TonB is presumably energized by the IM proton gradient. The introduction of TonB and formation of the ternary complex reduced the signal quality for certain peptides due to chromatographic overlap and mass spectral crowding. Interestingly, for certain SB3 peptides, deuterium uptake trends became complex even with B12 alone (tri-modal exchange), possibly reflecting increased heterogeneity where the apo state splits into multiple slowly interconverting populations upon ligand binding **(Figure 2.6)**. Further study of the complex HDX behavior of the SB3 loops may shed light on the allosteric mechanism.

2.5 Conclusions

Using HDX, we identified regions of the BtuB plug domain that both increase and decrease stability upon substrate binding. Most notably, the binding of B12 is sufficient to initiate an allosteric pathway involving the disruption of a dozen residues located up to 20 Å away from the B12 binding site. The process involves the unfolding of the *IL* region to permit the binding of TonB to the Ton box.

The remaining steps in the transport process are less clear. Potentially, an exit channel forms that follows a route from the B12 binding site past SB3 and out through the space formerly occupied by the *IL* region. Alternatively, TonB binding may initiate the force-induced unfolding of the plug core to create a substrate channel. This latter mechanism is appealing in its simplicity and generalizability, as one can envision the role of substrate binding is simply to release the Ton box into solution where forces are applied by TonB, and the channel is then formed by the unfolding of approximately half of the plug domain core. However, the HDX data indicate that the core of the plug remains extremely stable even when B12 and TonB are bound, providing a powerful example of how HDX's ability to access local thermodynamic information can help identify mechanism. Besides the study of mutations that constitutively break the *IL* or disrupt potential allosteric pathways that

cross the membrane, the measurement of the denaturant dependence of the HDX [207] could further define the conformational changes resulting from binding and force.

Because results across multiple techniques have depended on the membrane environment, future BtuB studies should be performed in as native-like a context as possible. Our application of HDX/MS in native OMs is a compromise between working in live cells and in reconstituted systems such as detergents (which do not bind B12) or liposomes (which are compositionally very different from OMs). The use of OMs provides both a native-like bilayer and high yield, which may enable the ambitious goal of performing HDX in live cells.

2.6 Further Data

Here I present large supplemental figures and unpublished data related to the above manuscript. Small supplemental figures have been incorporated into the sections above. These findings detail the development of the methods employed and offer supporting data for application of HDX-MS to outer membranes.

2.6.1 Supplemental Figures and Tables

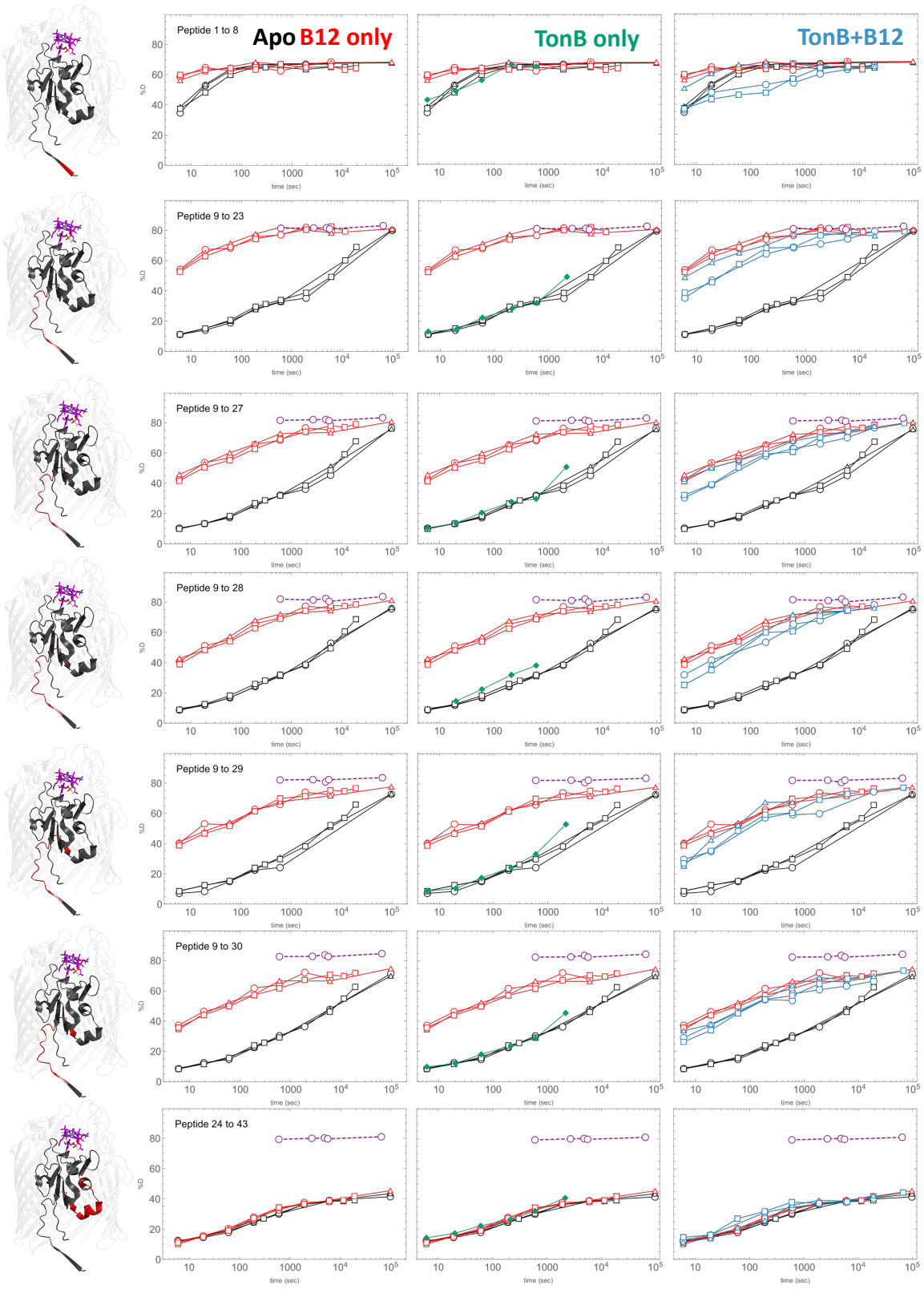

Figure 2.10: **Deuterium uptake plots** Peptides$_{1-8\text{ to }24-43}$. Continued on next page.

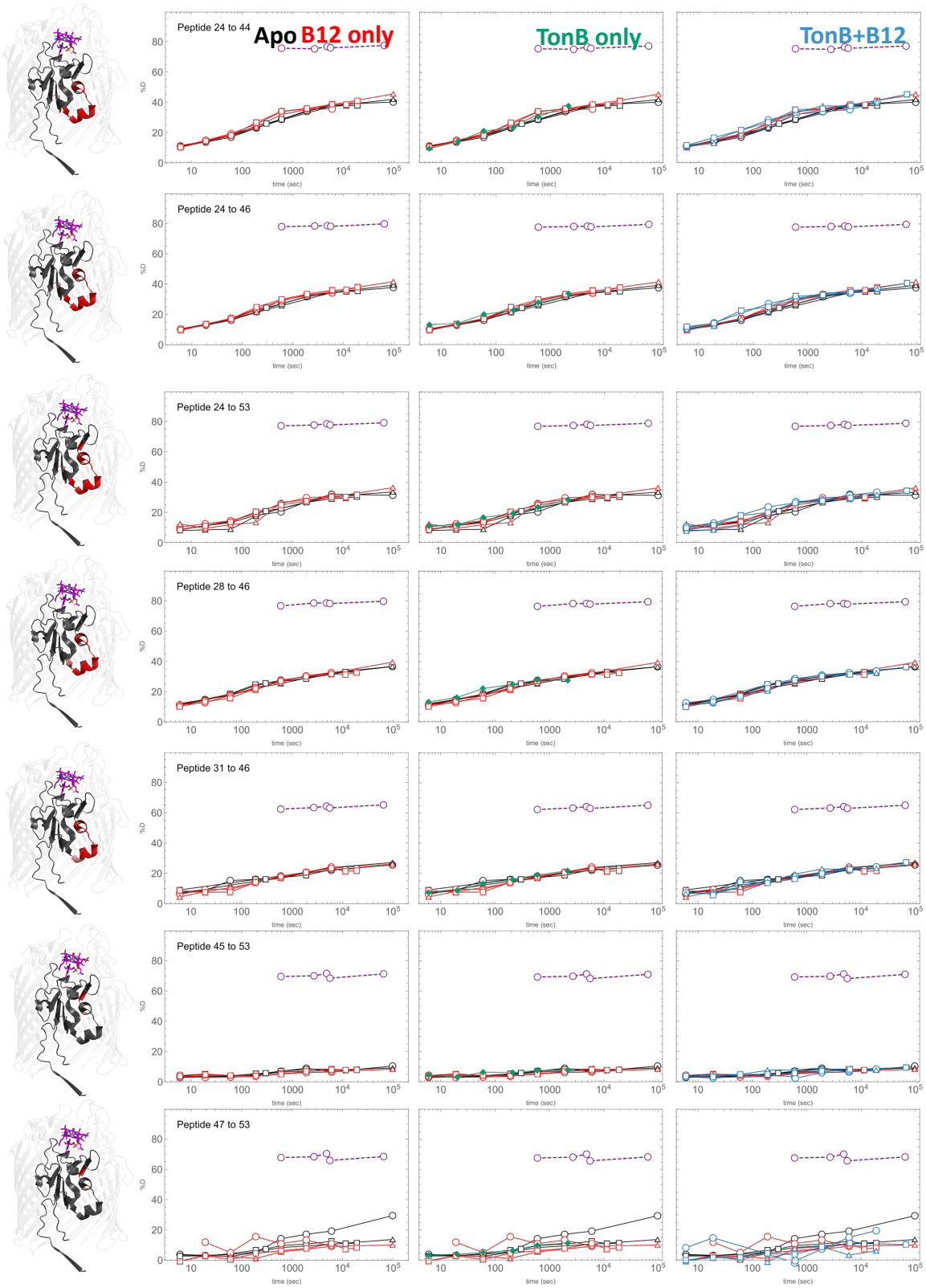

Figure 2.10 continued: Peptides$_{24-44\text{ to }45-57}$. Continued on next page.

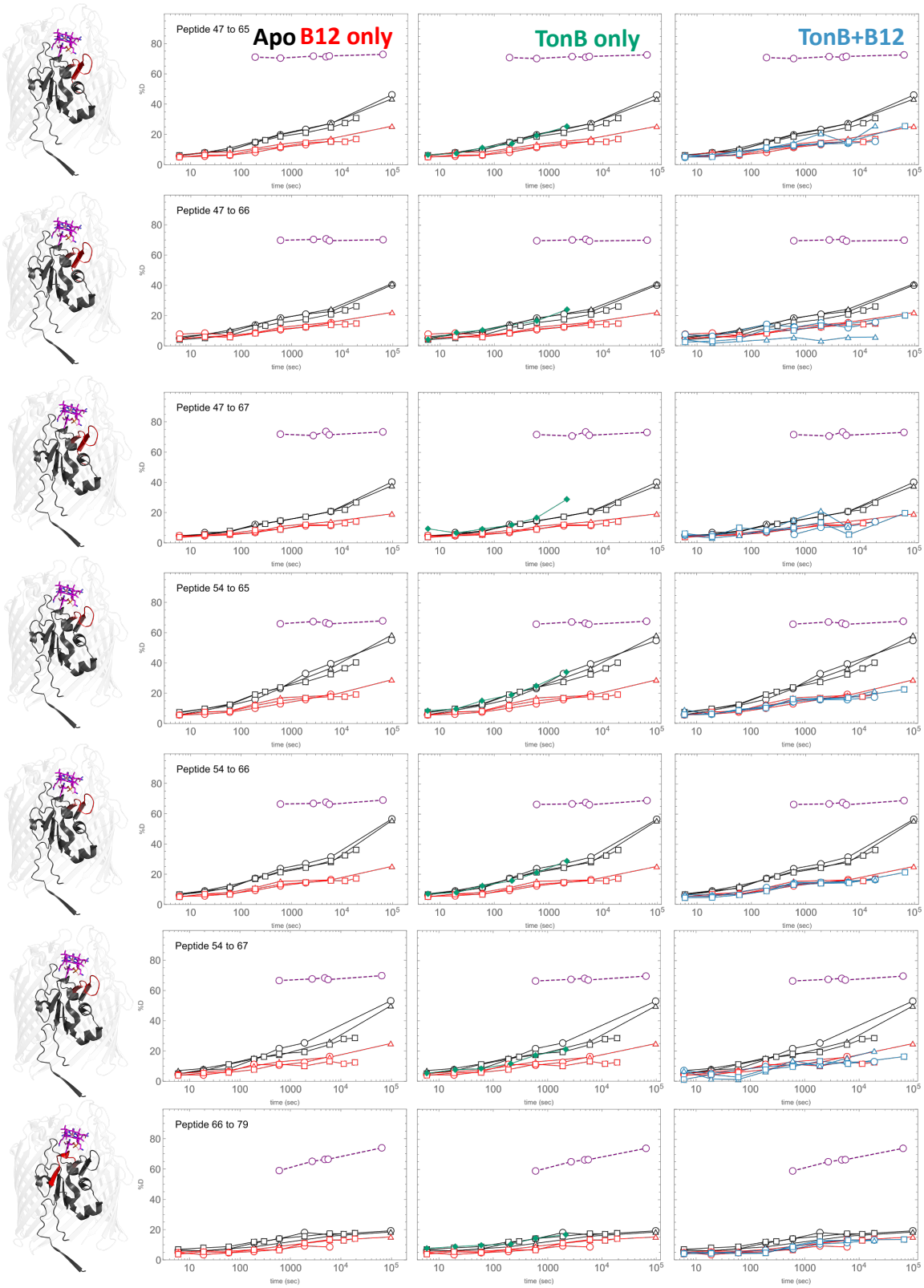

Figure 2.10 continued: Peptides$_{47-65\text{ to }66-79}$. Continued on next page.

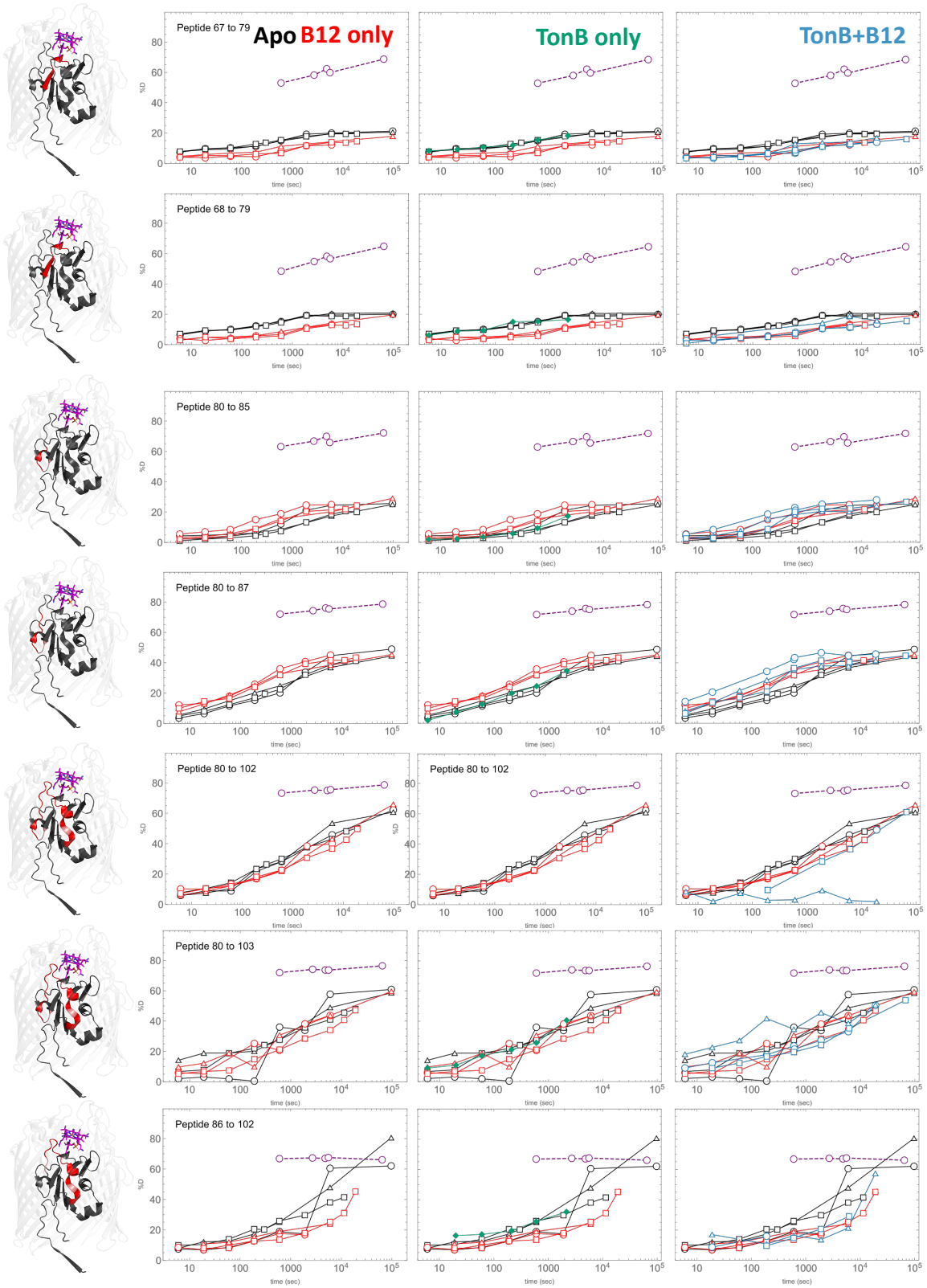

Figure 2.10 continued: Peptides$_{67-79\text{ to }86-102}$. Continued on next page.

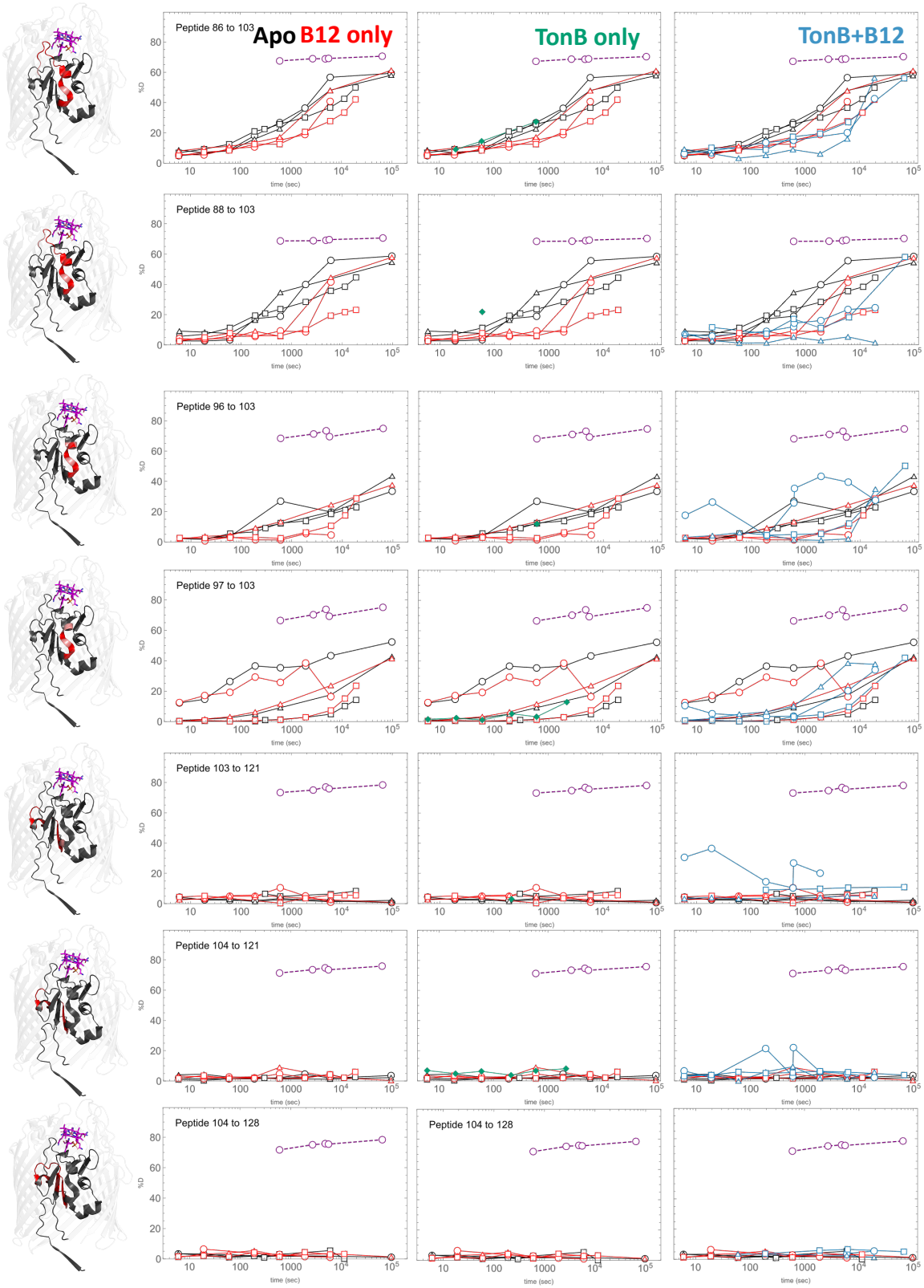

Figure 2.10 continued: Peptides$_{80-103 \text{ to } 104-128}$. Continued on next page.

Figure 2.10 continued: Three deuterium uptake plots are shown for each peptide, together with a structure highlighting the peptide in red. The first two residues of a peptide, which are non-observable due to rapid back exchange, are colored a brighter shade of red to distinguish them. Deuterium uptake plot color scheme is as follows: Apo BtuB (black), BtuB+B12 (red), BtuB+B12+TonB (blue), BtuB+TonB, (green), and nonnative BtuB only control (purple). For clarity, only the last 5 points for the nonnative control are shown.

Data Set	apo BtuB	BtuB + B12	BtuB + TonB	BtuB + B12 + TonB (Ternary)
HDX reaction details	46.7 mM Na_2HPO_4, 0.6 mM Tris, pD_{read} = 6.80, 22 °C	46.7 mM Na_2HPO_4, 0.6 mM Tris, pD_{read} = 6.80, 20 µM B12, 1 mM $CaCl_2$, 22 °C	46.7 mM Na_2HPO_4, 0.6 mM Tris, pD_{read} = 6.80, 22 °C	46.7 mM Na_2HPO_4, 0.6 mM Tris, pD_{read} = 6.80, 2 µM B12, 1 mM $CaCl_2$, 22 °C
HDX time course (min)	0.1, 0.316, 1.0, 3.16, 10, 31.6, 100, 316, 1620	0.1, 0.316, 1.0, 3.16, 10, 31.6, 100, 316, 1620	0.1, 0.33, 1.0, 3.5, 10, 36	0.1, 0.316, 1.0, 3.16, 10, 31.6, 100, 316
HDX control samples	Maximally-labeled control (LH4 construct, his-tagged on extracellular loop)	Maximally-labeled control (LH4 construct, his-tagged on extracellular loop)	Maximally-labeled control (LH4 construct, his-tagged on extracellular loop)	Maximally-labeled control (LH4 construct, his-tagged on extracellular loop)
Back-exchange (mean / IQR)	25.1% / 9.0%	25.1% / 9.0%	25.1% / 9.6%	24.9% / 9.3%
# of Peptides	35	35	29	31
Sequence coverage	95.4% (of 130 residues covering Nterminus & plug domain) 21.2% (whole protein)	95.4% (of 130 residues covering Nterminus & plug domain) 21.2% (whole protein)	90% (of 130 residues covering Nterminus & plug domain) 19.7% (whole protein)	90% (of 130 residues covering Nterminus & plug domain) 19.7% (whole protein)
Average peptide length / Redundancy	16.5 / 0.7	16.5 / 0.7	16.5 / 0.7	15.9 / 0.6
Replicates	3 (biological)	3 (biological)	1	3 (biological)
Repeatability	2% / 0.24 Da (average standard deviation)	2% / 0.24 Da (average standard deviation)	N/A	3.2% / 0.37 Da (average standard deviation)
Significant differences in HDX (ΔHDX > X Da)	1.14 Da (98% confidence interval)	1.16 Da (98% confidence interval)	N/A	2.66 Da (98% confidence interval)

Figure 2.11: **Biochemical and statistical details for each measured state**.

Peptide Index	Peptide Length	Start	End	Number of observable sites	Standard deviation (S.D.) of apo points (%D)	Number of triplicated apo points	S.D. of BtuB+B12 points (%D)	Number of triplicated BtuB+B12 points
1	8	1	8	5	1.65	6	1.81	6
2	15	9	23	12	0.69	5	1.69	5
3	19	9	27	15	0.80	5	2.14	5
4	20	9	28	16	0.83	6	1.85	6
5	21	9	29	17	1.61	5	1.69	6
6	22	9	30	18	0.67	6	1.84	6
7	20	24	43	18	0.50	6	0.69	6
8	21	24	44	19	0.49	6	0.91	6
9	23	24	46	21	0.47	6	0.64	6
10	30	24	53	28	1.45	6	1.61	6
11	19	28	46	17	0.72	6	0.86	6
12	16	31	46	14	0.88	4	0.98	6
13	9	45	53	6	0.60	6	0.60	6
14	7	47	53	4	1.69	6	3.81	5
15	19	47	65	12	0.63	6	1.07	6
16	20	47	66	13	1.44	6	0.95	6
17	21	47	67	14	0.37	4	0.80	6
18	12	54	65	10	1.29	6	0.90	6
19	13	54	66	11	0.86	6	0.72	6
20	14	54	67	12	1.35	5	1.17	6
21	14	66	79	12	1.12	6	1.20	6
22	13	67	79	11	0.42	6	1.24	6
23	12	68	79	10	0.44	6	0.85	6
24	6	80	85	4	1.89	6	2.38	6
25	8	80	87	6	2.20	6	1.77	6
26	23	80	102	20	2.14	6	1.39	6
27	24	80	103	21	8.18	6	5.01	5
28	17	86	102	14	4.50	6	2.06	4
29	18	86	103	15	3.42	6	3.21	6
30	16	88	103	13	3.98	5	3.51	6
31	8	96	103	5	4.27	5	4.66	5
32	7	97	103	4	14.39	6	10.38	6
33	19	103	121	18	1.95	2	2.87	3
34	18	104	121	17	1.14	6	1.37	5
35	25	104	128	24	1.02	4	1.37	4
Average of peps 1-35	16.49			13.60	2.00	5.54	2.00	5.63

Figure 2.12: **HDX peptide summary table** Part 1. Continued on next page.

S.D. of BtuB+B12 +TonB points (%D)	Number of triplicated BtuB+B12+ TonB points	S.D. of BtuB+B12 +TonB points (%D)	S.D. of apo points (Da)	S.D. of BtuB+ B12 points (Da)	S.D. of BtuB+B12 +TonB points (Da)	%D in last urea ctrl. point (100 - back exchange)	98% Confidence interval (CI) for apo state (Da)	98% C.I. for BtuB+B12 state (Da)	98% C.I. for BtuB+B12+ TonB state (Da)
7.05	5	7.05	0.08	0.09	0.35	NAN	0.40	0.44	1.70
5.16	5	5.16	0.08	0.20	0.62	83.03	0.40	0.98	2.99
4.12	5	4.12	0.12	0.32	0.62	83.32	0.58	1.55	2.99
3.99	4	3.99	0.13	0.30	0.64	83.63	0.64	1.43	3.09
4.00	4	4.00	0.27	0.29	0.68	83.58	1.32	1.39	3.28
3.06	5	3.06	0.12	0.33	0.55	84.54	0.58	1.60	2.66
2.37	5	2.37	0.09	0.13	0.43	80.99	0.43	0.60	2.06
1.64	5	1.64	0.09	0.17	0.31	77.49	0.45	0.84	1.51
1.28	5	1.28	0.10	0.13	0.27	79.72	0.48	0.64	1.30
1.14	4	1.14	0.41	0.45	0.32	79.13	1.96	2.17	1.54
1.10	5	1.10	0.12	0.15	0.19	79.66	0.59	0.71	0.90
1.23	4	1.23	0.12	0.14	0.17	65.19	0.60	0.66	0.83
1.42	5	1.42	0.04	0.04	0.09	71.20	0.17	0.17	0.41
4.28	5	4.28	0.07	0.15	0.17	68.38	0.33	0.74	0.83
1.51	4	1.51	0.08	0.13	0.18	72.81	0.36	0.62	0.87
4.03	5	4.03	0.19	0.12	0.52	70.10	0.91	0.59	2.53
2.18	5	2.18	0.05	0.11	0.31	73.37	0.25	0.54	1.48
0.82	5	0.82	0.13	0.09	0.08	67.80	0.62	0.44	0.40
0.87	5	0.87	0.10	0.08	0.10	69.01	0.46	0.38	0.46
2.13	5	2.13	0.16	0.14	0.26	69.76	0.78	0.68	1.23
0.81	5	0.81	0.13	0.14	0.10	74.01	0.65	0.70	0.47
1.49	4	1.49	0.05	0.14	0.16	68.70	0.22	0.66	0.79
1.99	2	1.99	0.04	0.09	0.20	64.84	0.21	0.41	0.96
2.84	5	2.84	0.08	0.10	0.11	72.18	0.37	0.46	0.55
4.57	5	4.57	0.13	0.11	0.27	78.64	0.64	0.51	1.33
21.19	NAN	NAN	0.43	0.28	NAN	78.74	2.07	1.34	NAN
10.17	4	10.17	1.72	1.05	2.14	76.42	8.30	5.08	10.32
3.53	NAN	NAN	0.63	0.29	NAN	66.09	3.04	1.40	NAN
3.53	3	3.53	0.51	0.48	0.53	70.58	2.48	2.32	2.56
5.33	4	5.33	0.52	0.46	0.69	70.63	2.50	2.20	3.34
12.30	3	12.30	0.21	0.23	0.62	74.92	1.03	1.13	2.97
3.74	4	3.74	0.58	0.42	0.15	75.04	2.78	2.00	0.72
8.16	NAN	NAN	0.35	0.52	NAN	78.38	1.69	2.49	NAN
3.64	5	3.64	0.19	0.23	0.62	75.84	0.93	1.13	2.98
2.86	NAN	NAN	0.25	0.33	NAN	78.40	1.19	1.58	NAN
3.99	4.48	3.35	0.24	0.24	0.40	75.08	1.15	1.16	1.94

Figure 2.12 continued: **HDX peptide summary table** Part 2. Continued on next page.

Figure 2.12 continued: **HDX peptide summary table.** Standard deviations, number of triplicated points in each condition, and sizes of 98% confidence interval sizes are provided for each peptide. Some peptides in conditions with TonB present were excluded due to poor signal quality and are marked with NAN.

2.6.2 Peptide assignment of BtuB and TonB

Can the transmembrane β-barrel and extracellular loops of BtuB be studied by HDX-MS? How well is BtuB digested by pepsin while embedded in the OM? To address the possibility of digesting extracellular loops and segments of the β-barrel, peptide assignments were carried out on BtuB in a variety of membrane and membrane mimetic environments. The best results, per unit protein, were obtained on detergent-solubilized BtuB, but due to a failure of B12 to bind in detergent, digestion in OMs was attempted. The ease of producing large quantities of BtuB-rich OMs allowed for use of very high protein concentrations, which gave the best overall assignment results after the optimizations in **Figures 2.18-2.23** were carried out.

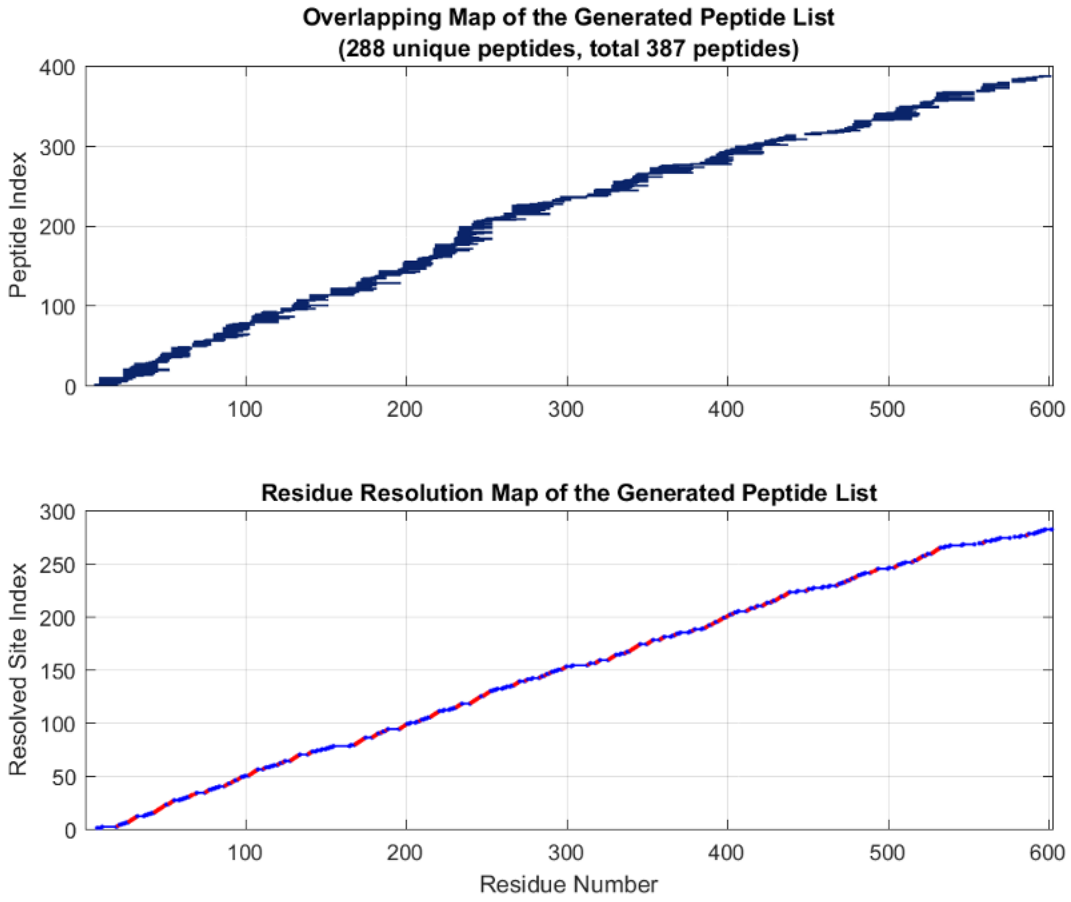

Figure 2.13: **Peptide and resolution maps of BtuB in 8M urea** BtuB was prepared as a concentrated stock in 8M urea according to a protocol published by the Fleming lab for spontaneous refolding studies [214]. Briefly, inclusion bodies were resolubilized in 8M urea, run over a Q Sepharose FastFlow anion exchange column on a gradient from 150 to 500 mM NaCl in 8.0 M urea, 20 mM borate pH 8.0, and desalted by concentration in a 10,000 MWCO Amicon spin column.

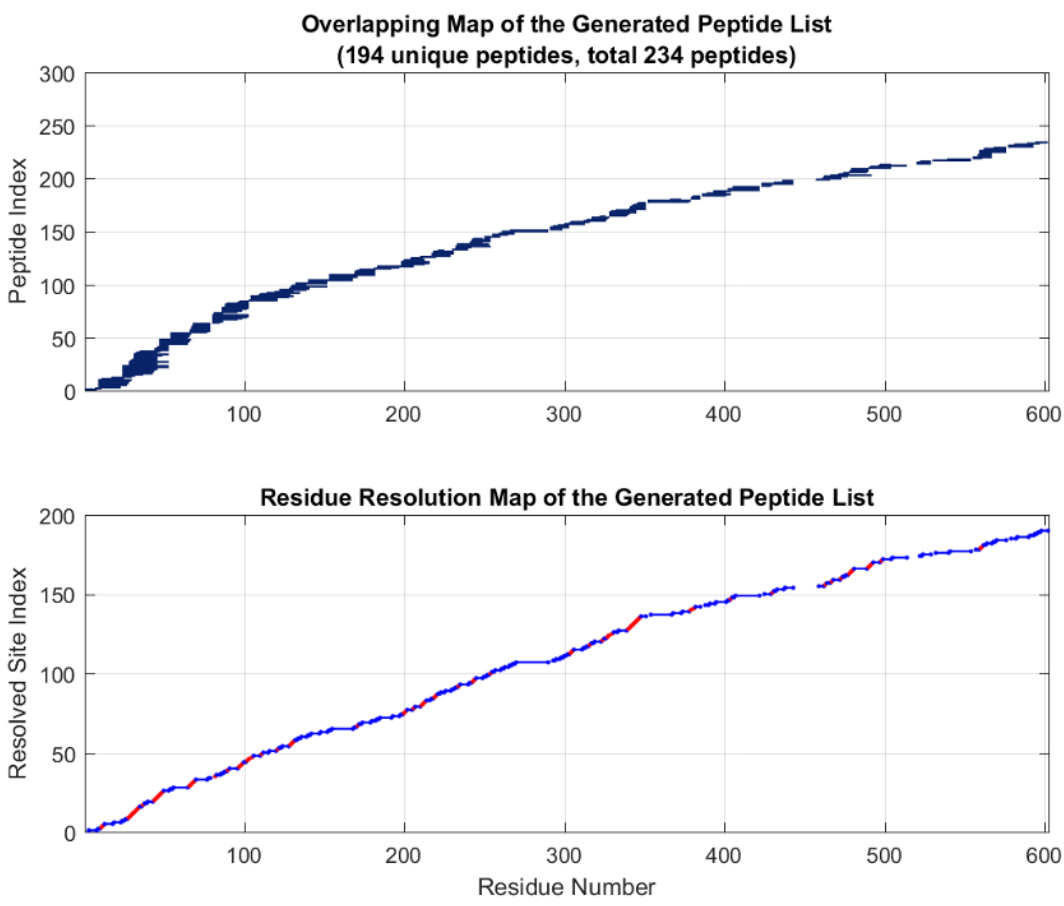

Figure 2.14: **Peptide and resolution maps of BtuB in azolectin liposomes** BtuB was prepared in azolectin liposomes by extensively dialyzing a mixture of protein, lipid, and detergent against a large volume of solution lacking detergent, with daily buffer changes. For details, see [136].

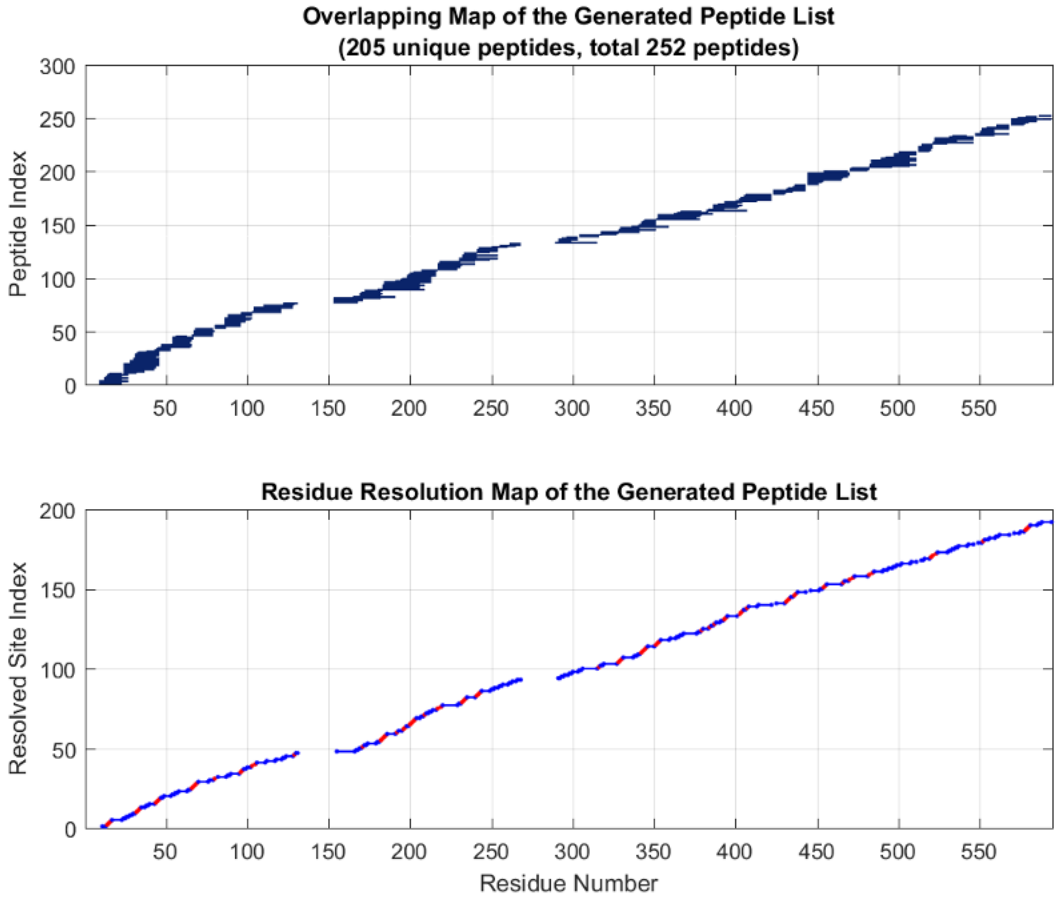

Figure 2.15: **Peptide and resolution maps of BtuB in DDM detergent** BtuB LH4 was extracted with C_8E_4 detergent and purified by a 50-900 mM LiCl gradient in BisTris pH 6.9 on a DEAE FastFlow Sepharose anion exchange column. Protein-containing fractions were concentrated and desalted by spin column concentration, supplemented with 20x CMC LMNG, incubated for 1 hour, and injected on a BioRad Enrich 650 SEC column with no detergent in the running buffer, only 20 mM BisTris pH 6.9. This allowed for separation of protein-laden from empty detergent micelles, as the demicellization time of LMNG exceeds the time required to complete the SEC run. Eluting protein was immediately supplemented with 2x CMC DDM, briefly concentrated to 1 μM, and was proteolyzed with soluble pepsin according to the same protocol as was used for OMs and assignment run data were searched against the sequence of BtuB.

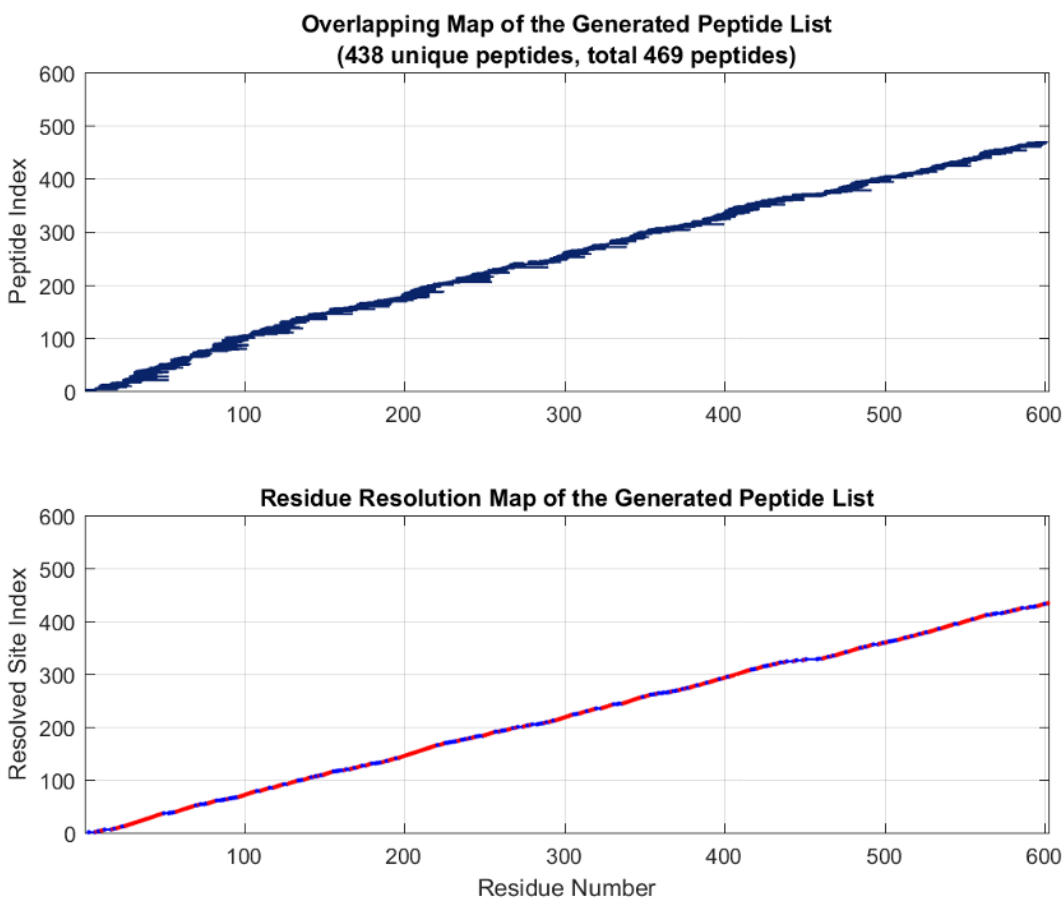

Figure 2.16: **Peptide and resolution maps of BtuB in native-like OMs** Several assignment runs under the conditions described in section 2.7.4 were searched against the LH4 sequence (BtuB with a his_6tag+GSS insertion on an extracellular loop).

Figure 2.17: **Peptide and resolution maps of TonB** Assignment data from the same runs as described in **Figure 2.16** were searched against the sequence of $\text{TonB}_{\Delta\text{N}}$.

2.6.3 Offline proteolysis of BtuB assayed by SDS-PAGE

To assess and optimize the cleavage of BtuB for generating peptides for HDX-MS, "offline" digestions were performed using soluble pepsin. Different temperatures, urea concentrations, and choices of detergent were explored.

The 2M urea series presented on the left half of **Figure 2.23** was deemed most likely to provide the optimal cleavage results, with near-complete digestion of a mass corresponding to the BtuB plug domain occurring within 3 minutes, and the greatest number of intermediate cleavage products visible at shorter times. Intermediates present at the shorter times were inferred to represent partial cleavages at more amino-terminal sites within the plug domain, and therefore a cleavage course proceeding through the greatest number of intermediates in the shortest time was seen as desirable.

To perform the offline proteolysis assays in **Figures 2.18-2.23**, 50 μM of detergent-extracted BtuB LH4 construct (or a 2 μL aliquot of resuspended OMs) was subjected to pepsinization in a 600mM glycine, pH 2.5 buffer, with various additives (detergents, urea, ZrO_2). Proteolysis was initiated by adding 10% reaction volume pepsin from a stock of 10x the working concentration to a mixture of the remaining components. Pepsin concentrations in the proteolysis reactions were 2.5 μM unless specified otherwise. The proteolysis was terminated by aliquoting samples into an equal volume of 2 M tris(hydroxymethyl)aminomethane (Tris) buffer, pH 9.8, pre-mixed with SDS-PAGE loading buffer. Electrophoresis was carried out for 80 minutes at 180 V in 4-20% Mini-PROTEAN TGX precast gels. 16 μL loaded of quenched pepsinization reaction were loaded per lane, plus 4 μL of 5x SDS-PAGE loading buffer.

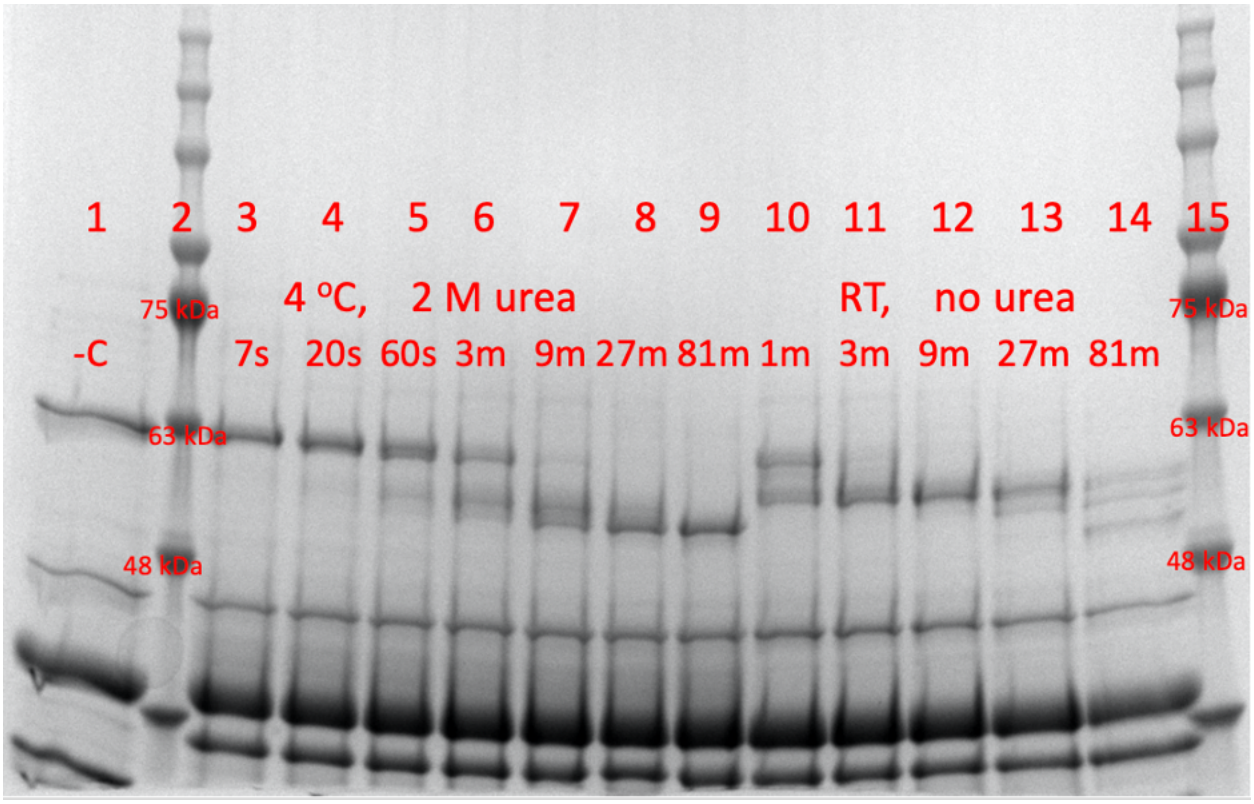

Figure 2.18: **Offline SDS-PAGE assay measuring urea- and temperature- dependence of BtuB proteolysis, part 1** Lane 1: undigested input protein (negative control). Lanes 2 and 15: 3.5 μL of GoldBio bluestain protein ladder. 48, 63, and 75 kDa masses labeled for reference. Lanes 3-9: 7, 20, 60, 180, 540, 1620, 4860 sec. time points respectively, of a protease reaction carried out in 2 M urea at 0 ^{o}C (tube kept on ice). Lanes 10-14: 60, 180, 540, 1620, 4860 sec. time points, respectively, of a proteolysis reaction carried out at room temperature with no denaturant added.

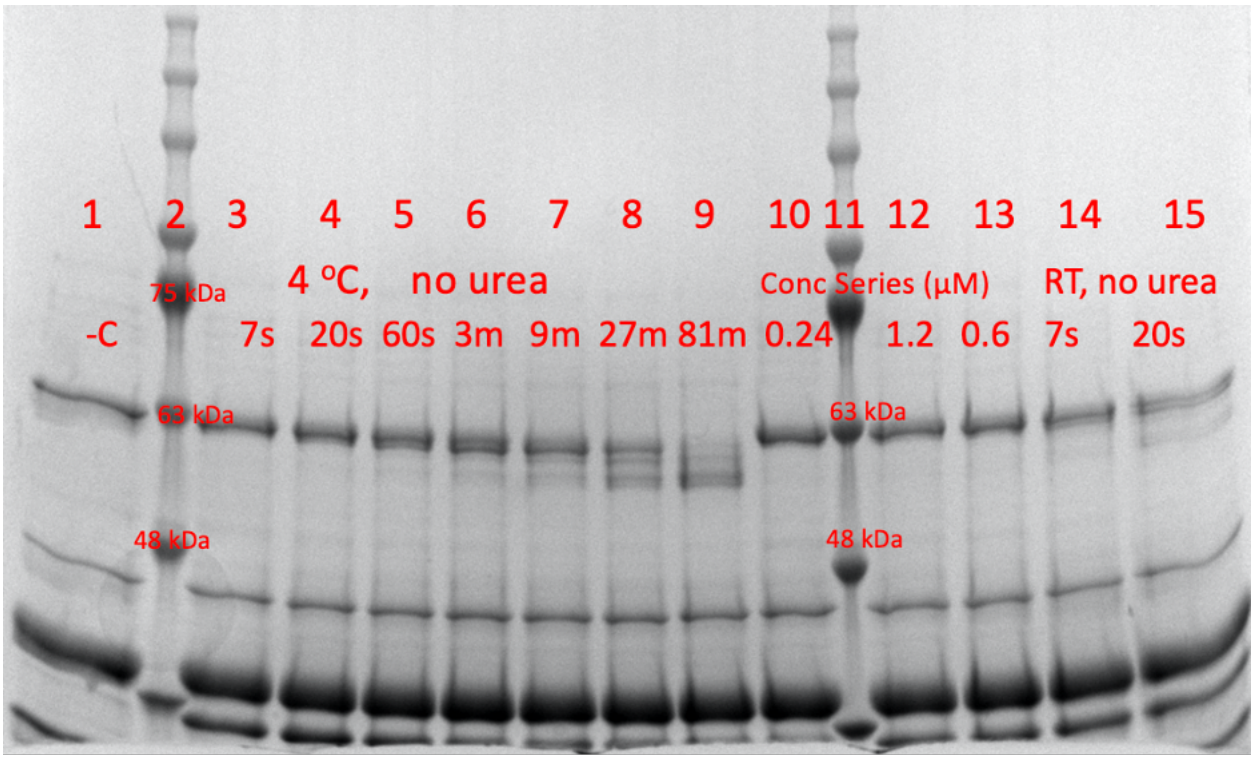

Figure 2.19: **Offline SDS-PAGE assay measuring urea- and temperature- dependence of BtuB proteolysis, part 2** Lane 1: undigested input protein (negative control). Lanes 2 and 11: 3.5 μL of GoldBio bluestain protein ladder. 48, 63, and 75 kDa masses labeled for reference. Lanes 3-9: 7, 20, 60, 180, 540, 1620, 4860 sec. time points respectively, of a protease reaction carried out at 0 ^{o}C (tube kept on ice) with no denaturant added. Lanes 10, 12, and 13: 540 second time points of a protease reaction carried out in 2 M urea at 0 ^{o}C using 0.24, 1.2, 0.6 μM pepsin, respectively. Lanes 14 and 15: 7 and 20 second time points, respectively, of a protease reaction carried out at room temperature with no added urea.

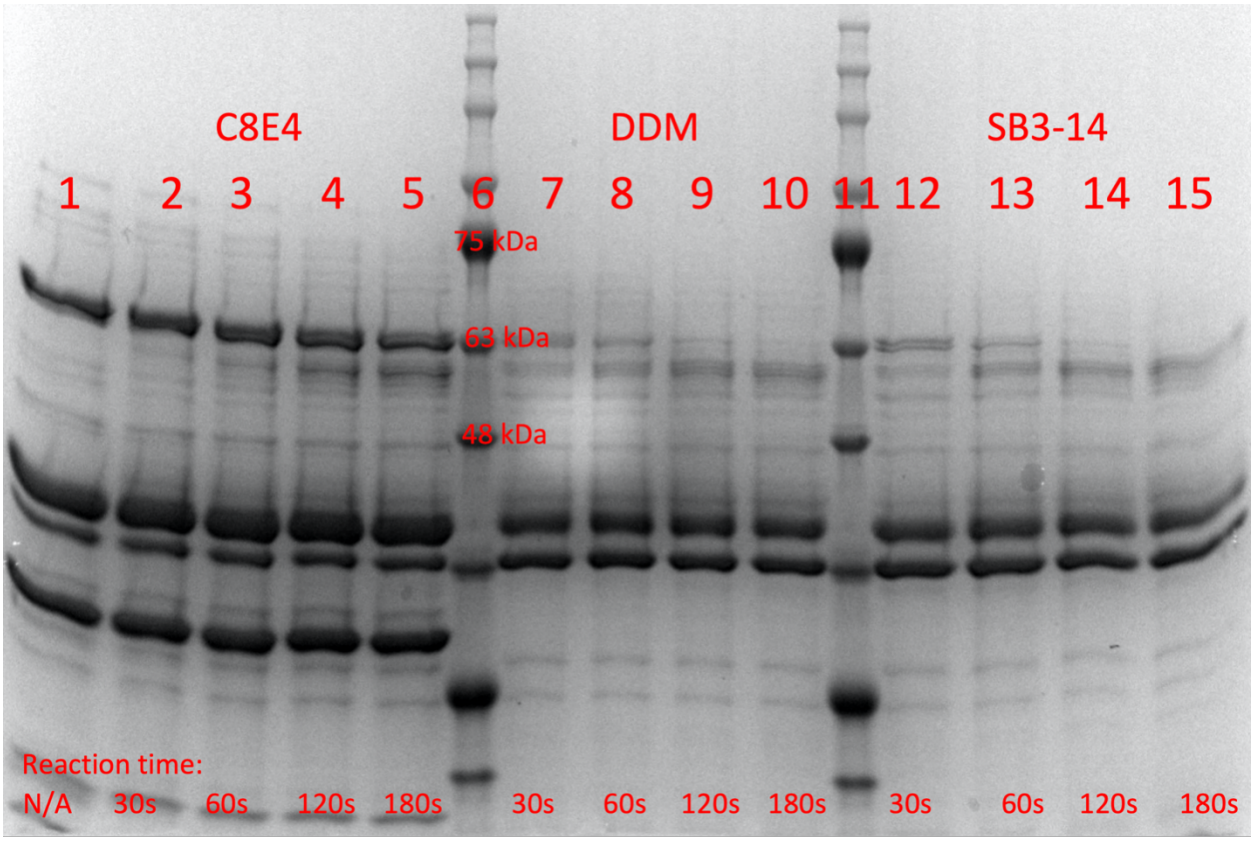

Figure 2.20: **Offline SDS-PAGE assay measuring detergent dependence of BtuB proteolysis, part 1** Lane 1: undigested input protein (negative control). Lanes 6 and 11: 3.5 μL of GoldBio bluestain protein ladder. 48, 63, and 75 kDa masses labeled for reference. Lanes 2-5: 30, 60, 120, and 180 sec. time points, respectively, of a protease reaction carried out at room temperature with no denaturant added. Lanes 7-10 and 12-15: Same as lanes 2-5, except with DDM and 3-(N,N-Dimethyltetradecylammonio)propanesulfonate (SB3-14) detergents, respectively. Each detergent was used at 5x CMC (protein was extracted at 20x CMC and after ultracentrifugation extracted protein fractions were diluted 4x for proteolysis).

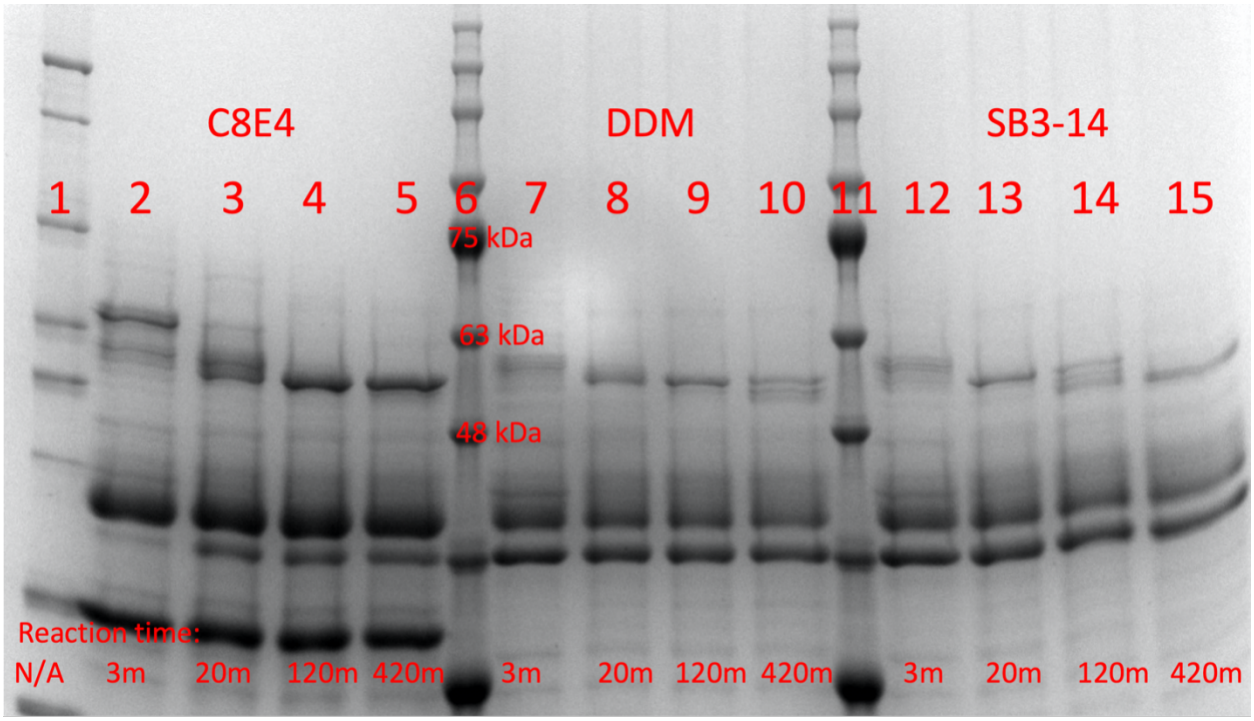

Figure 2.21: **Offline SDS-PAGE assay measuring detergent dependence of BtuB proteolysis, part 2** Lane 1: undigested input protein (negative control). Lanes 6 and 11: 3.5 μL of GoldBio bluestain protein ladder. 48, 63, and 75 kDa masses labeled for reference. Lanes 2-5: 180, 120, 7200, and 25200 sec. time points, respectively, of a protease reaction carried out at room temperature with no denaturant added. Lanes 7-10 and 12-15: Same as lanes 2-5, except with DDM and SB3-14 detergents, respectively. Each detergent was used at 5x CMC (protein was extracted at 20x CMC and after ultracentrifugation extracted protein fractions were diluted 4x for proteolysis).

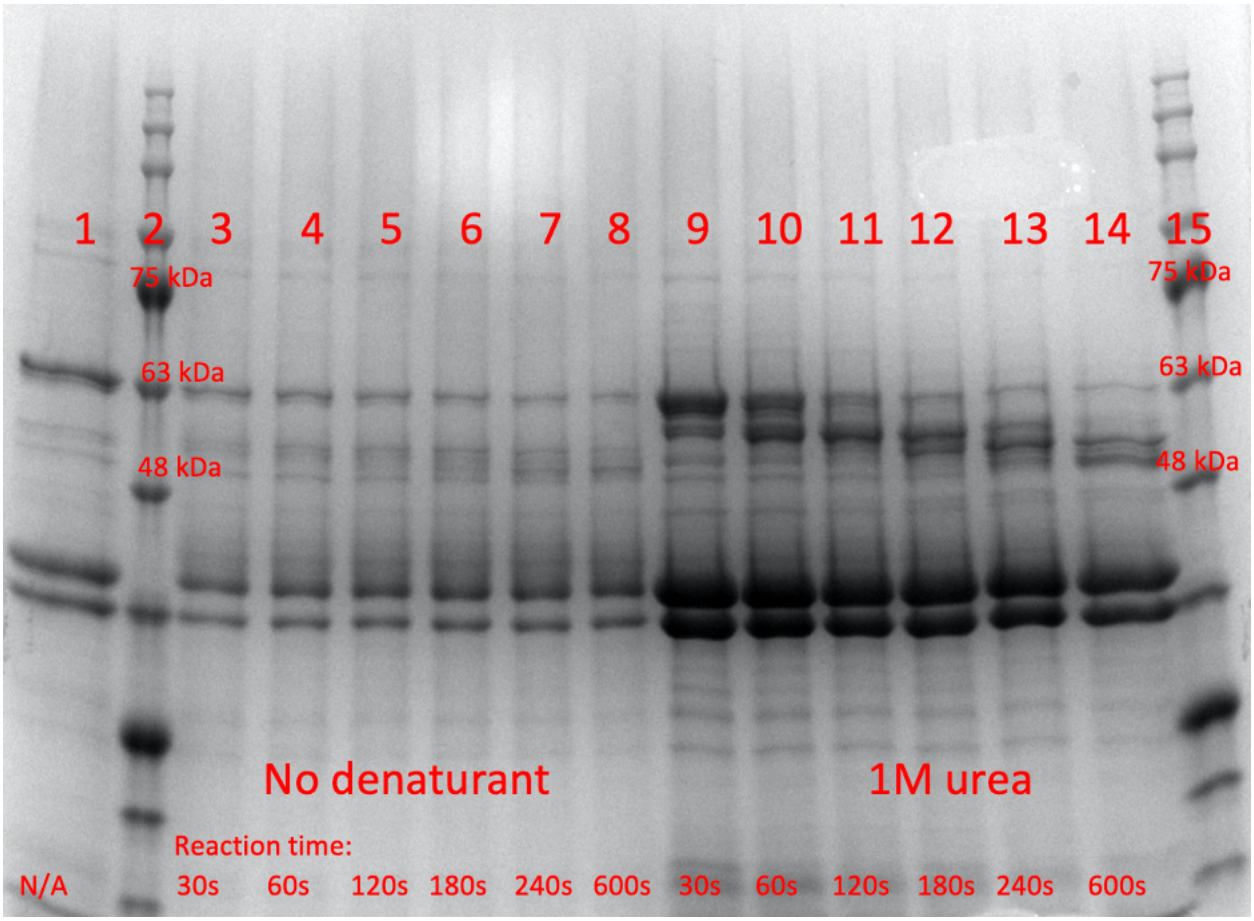

Figure 2.22: **SDS-PAGE assay optimizing urea concentration for HDX proteolysis, part 1** Lane 1: undigested input protein (negative control). Lanes 2 and 15: 3.5 μL of GoldBio bluestain protein ladder. 48, 63, and 75 kDa masses labeled for reference. Lanes 3-8: 30, 60, 120, 180, 240, and 600 sec. time points, respectively, of a protease reaction carried out at 0 ^{o}C (tube kept on ice) with no denaturant added. Lanes 9-14: Same as lanes 3-8 but with 1 M urea present in the digestion reaction.

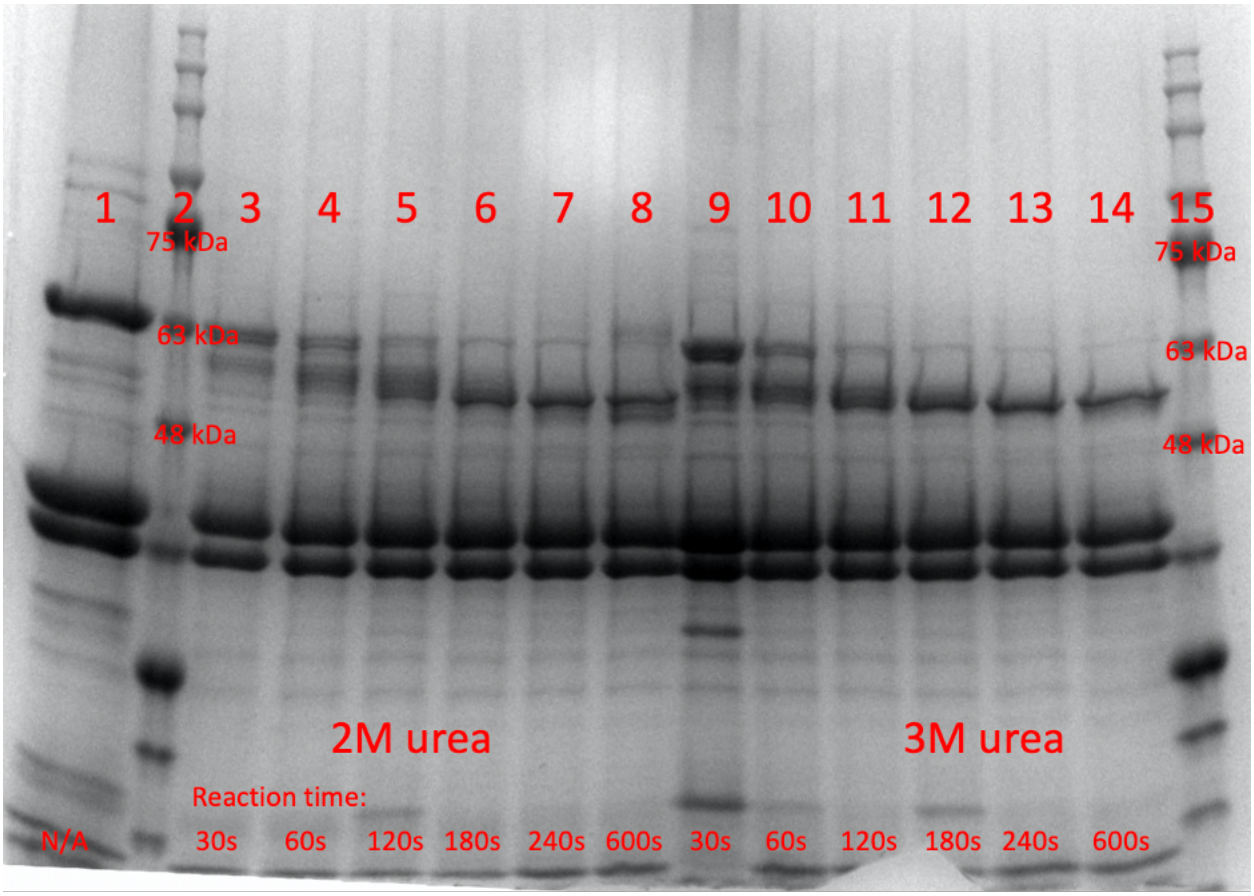

Figure 2.23: **Optimization of urea concentration for HDX proteolysis, part 2** Lane 1: undigested input protein (negative control). Lanes 2 and 15: 3.5 μL of GoldBio bluestain protein ladder. 48, 63, and 75 kDa masses labeled for reference. Lanes 3-8: 30, 60, 120, 180, 240, and 600 sec. time points, respectively, of a protease reaction carried out at 0 ^{o}C (tube kept on ice) with 2 M urea in the digestion reaction. Lanes 9-14: Same as lanes 3-8 but with 3 M urea present in the digestion reaction.

2.6.4 Sequence analysis of BtuB

To investigate the conservation of the Ionic Lock in BtuB, a multiple sequence alignment of BtuB genes was carried out. The Ionic Lock was found to be strongly, but not absolutely conserved, raising questions about the interplay between B12 and TonB binding events in BtuB variants lacking the Ionic Lock.

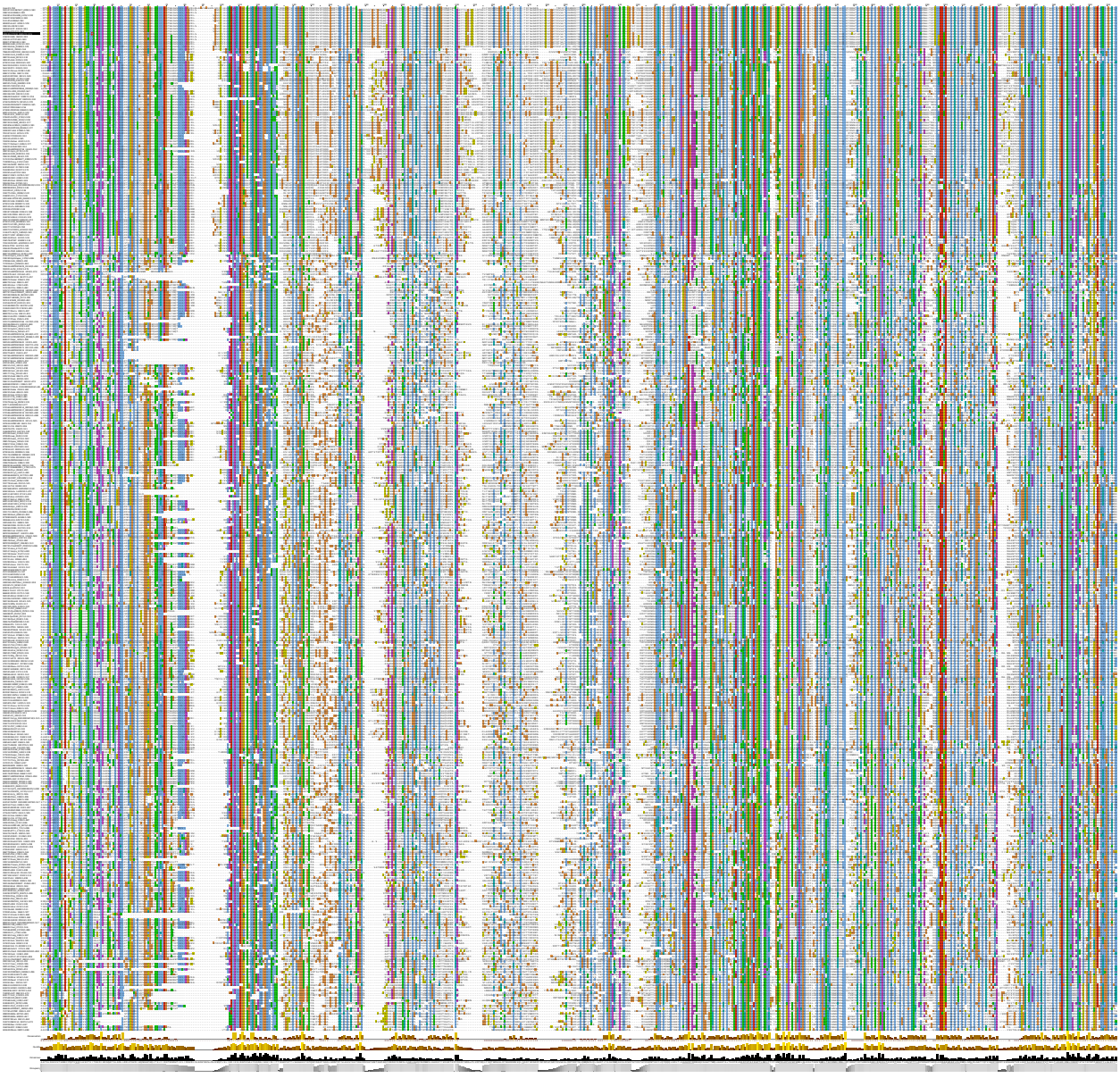

Figure 2.24: **Multiple sequence alignment of BtuB Top)** 392 BtuB genes retrieved from the EggNOG 5.0 database (Query 4105CHI [215]). 456 protein sequences were aligned using MUSCLE [216, 217]. Alignments were manually de-gapped by iterative deletion of columns (other than *E. coli* BtuB) containing mostly gaps and re-alignment, with a final round of alignment to *E. coli* BtuB (top row) to preserve the residue indexing. Sequences were discarded if they did not contain an alignable plug domain or had large missing segments. Clustalx coloring was used in the Jalview program (www.jalview.org) to plot the alignment.

2.7 Materials and Methods

Chemicals were purchased from Sigma-Aldrich (St Louis, MO) unless otherwise noted.

2.7.1 Bacterial strains and plasmids

TonB 32-239 in pHis Parallel and full length BtuB in pAG1 were received as a generous gift from Professor Robert Nakamoto at the University of Virginia. pHis is derived from pET22b and contains a 0.7kb insertion of TonB except for the amino terminal transmembrane helix, described further in [218]. pAG1 is derived from pUC8 and contains a 2.4kb insertion of the BtuB gene from E. coli [219]. For construction of the LH4 plasmid, QuikChange II mutagenesis was used to insert a five additional histidines, a glycine, and two serines to form a hexahistidine tag and GSS spacer between residues Asp448 and Thr450 using the following primers: (Position 449 is already a histidine in the wild-type sequence) forward 5'-CATCATCATCATCACGGCAGCAGCACCCTGAAATATTACAACGAAGGG-3' and reverse 5'- CCGTGATGATGATGATGGTGATCATCATAATCGATCAAATCAC-3'.

2.7.2 Protein expression and purification

$TonB_{\Delta N}$ (residues 32-239) containing an amino terminal HisTag and proTEV cleavage site was transformed into BL21 (DE3) *E. coli* on LB plates supplemented with 100 μM ampicillin (LB/AMP). A single colony was picked to inoculate an overnight culture of 10 mL of 2 x YT medium. This culture was used to inoculate 1L of 2 x YT medium and grown to 0.7-0.8 OD at 37 ^{o}C before induction with 0.5 mM IPTG at 20 ^{o}C for 5 hours. Cells were harvested by centrifugation at 6500 RPM for 12 minutes at 4 ^{o}C, and frozen or resuspended in 25 mM Tris-HCl, 100 mM NaCl, 1 mM PMSF, pH 7.5 and lysed immediately by 5 passes through a French press at 0 ^{o}C (solutions kept on ice). The lysate was clarified by centrifugation for 30 min at 12,500 RPM at 4 ^{o}C in a Sorvall Legend X1R centrifuge fitted with a FiberLite F15-8x50c and applied to a 5 mL column of equilibrated nickel-NTA resin. The column

was washed with 20 column volumes (100 mL) of wash buffer: 50 mM Tris-HCl, 100 mM NaCl, 20 mM imidazole, pH 7.5 and eluted 6 times with 5 mL each of elution buffer, which was the same as wash buffer, except that the imidazole concentration was increased to 300 mM. Protein containing fractions were pooled and dialyzed in a length of 3.5 kDa molecular weight cutoff tubing against 2 L of dialysis buffer: 50 mM Tris-HCl, 100 mM NaCl, pH 7.6 for 2 hours before addition of 1 mg of homemade TEV protease in 1 mL of TEV protease storage buffer: 50 mM Tris-HCl, 1 mM EDTA, 5 mM DTT, 50% glycerol, 0.01% Trion, pH 7.6. TEV cleavage was allowed to proceed under dialysis for 16 hours at 4 ^{o}C. Cleavage was assessed by SDS-PAGE electrophoresis and a subsequent round of subtractive Ni-IMAC performed to remove uncleaved protein. The flowthrough from this substractive Ni-IMAC round was concentrated and injected onto a 5 mL pre-packed HiTrap SP HP anion exchange column (Cytiva, Washington D.C., Cat# 17115201) for purification by a 20 min gradient from 100% buffer A (25 mM Tris, 50 mM NaCl, pH 7.5) to 100% buffer B (25 mM Tris, 1 M NaCl, pH 7.5). Protein-containing fractions were checked by SDS-PAGE and concentrated to 30-70 μM in 25mM Tris 50 mM NaCl pH 7.5 using spin filtration before addition to pelleted outer membrane stocks to obtain BtuB:TonB$_{\Delta N}$ or BtuB:B12:TonB$_{\Delta N}$ complex samples (with B12 addition as above) with a final TonB concentration of 26 μM.

BtuB wild-type or LH in pAG1 was transformed into either BL21 *E. coli* or a specialized strain with four abundant OMPs deleted, termed ΔABCF [208]. A single colony was picked to inoculate 5mL of LB/AMP and grown overnight at 30 ^{o}C with shaking at 225 RPM. The next day, 1 mL of this culture was taken to inoculate 50 mL of LB/AMP medium and grown at 30 ^{o}C for 6 – 8 hours, before seeding 1 L of cell culture. This 1 L of culture was either grown to OD$_{600}$ = 0.6 – 0.8 and induced or split into up to 10 L of LB/AMP medium for large-scale expression. Protein was induced at 30 ^{o}C for 4 hours with 1 mM IPTG. Cells were harvested by centrifugation in a Sorvall RC6+ centrifuge equipped with F10s 6x500y rotor for 30 minutes at 6000 RPM (6340 x g) at 4 ^{o}C and frozen at -80 ^{o}C until purification.

Frozen cells were thawed on ice and resuspended in 40 mL of resuspension buffer per

liter of cell culture. The resuspension buffer composition was: 50 mM Tris, 100 mM NaCl, pH 8.0, supplemented before lysis with 10 mM $MgCl_2$, 0.1 mg/mL lysozyme (Sigma ref# 6876), 0.05 mg/mL DNAse I (Goldbio, St. Louis, MO, cat# D-300-1). For cell pellets grown in ΔABCF *E. coli*, $MgCl_2$ was omitted from the resuspension buffer as it causes clumping of cells and outer membranes [208]. Resuspended cells were kept on ice and homogenized by at least 5 passes through an Emulsiflex-C5 French press set to 40 psi. The cell lysate was clarified by centrifugation in a Sorvall Legend-X1R centrifuge equipped with F15-8x50cy rotor for 30 minutes at 7000 RPM at 4 ^{o}C. The clarified lysate was ultracentrifuged in 70 mL polycarbonate (Beckman Coulter, Brea, CA, part # 355655) bottles for 60 minutes at 40,000 RPM (∼100,000 x g) at 4 ^{o}C in a Beckman Coulter Optima L-100 XP ultracentrifuge equipped with 45 Ti rotor. The resulting total membrane pellets were washed by resuspension with a number 10 round tipped paint brush in ∼6 mL per gram of cell membrane mass of resuspension buffer and Dounce homogenization before ultracentrifugation, performed as before. Washed total membranes were resuspended and Dounce homogenized as before prior to addition of 0.5% sodium N-lauroyl sarcosinate ("sarkosyl", from a 10% w/v stock in water) and incubation on a rotisserie for 30 minutes to 1 hour at room temperature or overnight at 4 ^{o}C to solubilize the inner membranes. Following another ultracentrifugation step as described above, outer membranes were again homogenized and ultracentrifuged as described above to wash out residual sarkosyl. This step was repeated once more prior to final resuspension of the washed outer membrane pellet in 5 mL of resuspension buffer. Resuspended washed outer membranes were aliquoted and stored at 4 ^{o}C for use in native-like outer membrane hydrogen exchange experiments, or frozen at -20^{o}C until extraction for use in detergent hydrogen exchange experiments.

Extraction from outer membranes was performed by addition of concentrated n-octyl tetraoxyethylene (C_8E_4, BACHEM, Bubendorf, Switzerland, article # 4006356.0025) to a final concentration of 150 mM (4.6% w/v, or 19 x CMC) and incubation on a rotisserie at room temperature for 2 hours. Insoluble debris was removed by ultracentrifugation for 60

minutes at 100,000 x g (47,246 RPM) at 4 ^{o}C in a Beckman Coulter MAX-XP microultracentrifuge equipped with TLA-55 rotor. C_8E_4-extracted BtuB was either further purified by IMAC on a 5 mL Ni-NTA column (Goldbio, cat# H-320-100), with a 50-600 mM LiCl gradient on a DEAE FastFlow anion exchange column with 20mM BisTris pH 6.9 or taken directly for detergent exchange. Detergent exchange was carried out by incubation of BtuB aliquots with 50 x CMC of lauryl maltose neopentyl glycol (LMNG, Anatrace, Maumee, OH, ref# NG310, added from a concentrated stock in water) for 1 hour at room temperature before injection on a BioRad Enrich 650 SEC 10 x 300 mm column with 20 mM BisTris pH 6.9 as the running buffer. BtuB-containing fractions were supplemented with 1.5 x CMC of n-dodecyl-β-D-maltoside (DDM, Anatrace, D322S, added from concentrated stock in water) immediately upon elution and either concentrated or immediately taken for HXMS experiments.

2.7.3 Proteolysis Assay

BtuB used for proteolysis assays was either washed and resuspended unextracted outer membranes, C_8E_4 extraction reaction supernatants, or Ni-IMAC and/or SEC purified DDM-solubilized protein fractions. BtuB was diluted to 1 μM on ice in HX quench buffer: 600 mM glycine pH 2.5 buffer, with 0 - 3 M urea, and the reactions were started by adding 0.5 mg/mL pepsin from a concentrated stock. At times ranging from 7 seconds to 243 minutes aliquots of the reaction were diluted with an equal volume of proteolysis quench buffer: 2 M Tris pH 9.8 and spun at 15,000 x g for 3 minutes before addition of Laemmli sample buffer and boiling prior to loading on SDS-PAGE. Electrophoresis was carried out in Novex Wedgewell 4-20% acrylamide gradient Tris-Glycine mini gels (Thermo Fisher Scientific, Waltham, MA), run in an Invitrogen Mini Gel tank at 180 V for 80 minutes at 4 ^{o}C with ice packed around the cell. Gels were stained with AcquaStain protein stain (Bulldog Bio), Coomassie R-250, Invitrogen His-Tag In-Gel Stain, or transferred to western blots, and either imaged or selected bands were cut out for downstream applications such as Edman

degradation or trypsin/endopeptidase LysC digestion followed by LC/MS/MS identification of proteolysis products.

2.7.4 Hydrogen Exchange Labeling Experiments

Hydrogen exchange label, simultaneous quench/digestion, and injection steps were all performed manually for experiments performed on protein in native-like outer membranes. Labeling in a solution of ∼93% D at room temperature (22 ^{o}C) was initiated by addition of 2 μL of thoroughly agitated native-like outer membrane stock (in 20 mM BisTris pH 6.9) to 28 μL of deuteration buffer (50 mM NaPi, 150 mM NaCl, made with dibasic sodium hydrogen phosphate and adjusted to $pD_{read} = pD_{desired} - 0.4$ using DCl). For labeling reactions involving B12 liganded samples, 1% v/v of 100x concentrated stocks (2 mM B12 and 100 mM $CaCl_2$) were added to aliquots both protein stock and label solutions to obtain a final concentration of 20 μM B12 and 1 mM $CaCl_2$. For labeling reactions involving TonB CTD, aliquots of BtuB samples were allowed to settle and half of the volume was aspirated and replaced with a solution of $TonB_{\Delta N}$ concentrated to 50 μM in 20 mM BisTris pH 6.9. Immediately after addition of outer membrane suspensions to label buffer, samples were triturated 5 or more times to ensure complete mixing. Quenching of the HX label reaction and digestion was performed by repeated trituration of the HX label reaction with a 200 μL pipette and aspiration of the entire volume and transfer into an Eppendorf tube containing 37 μL freshly prepared quench mix sitting inside an ice-chilled heat transfer block: 30 μL of 600 mM glycine, 4 M urea, pH 2.5, 2.0 μL of thrice-desalted 10 mg/mL porcine pepsin (Sigma-Aldrich, ref# P6887) in 100 mM sodium citrate, pH 4.4, 2.5 μL of 2.5 mM DDM in water, and 2.5 μL of a 300 mg/mL aqueous suspension of ZrO_2 coated silica (beads extracted from Supelco brand cartridges, Sigma-Alrich, ref# 55261-U). Digestion was carried out for 3 minutes before resuspension by repeated trituration and aspiration of the whole ∼67 μL volume onto a cellulose acetate spin cup (Thermo Pierce, Waltham, MA ref# 69702) held in a 1.5 mL polypropylene Eppendorf tube. The quenched digestion mix was filtered

by spinning for 30 seconds at 16,000 RCF in an Eppendorf 5415 R centrifuge fitted with a FA-45-24-11 rotor pre-chilled to 4 ^{o}C. Filtered peptide-containing solutions were aspirated with a glass ice-chilled 50 μL glass Hamilton syringe and immediately injected into the LC sample loading loop.

For peptide assignment MS/MS runs, the protocol above was repeated, except for a brief incubation in an undeuterated "mock HX" buffer using the same samples as the HX experiments and with 8M urea solubilized BtuB derived from inclusion bodies instead of native membranes. For these, the "mock HX" and quench buffers' urea concentrations were varied from 0 to 4 M to optimize peptide coverage and signal intensity. Additionally, in-exchange controls to account for deuteration towards the 41.5% D level present in the quench solution were performed by mixing HX and quench buffers prior to addition of BtuB. Similarly, full-exchange ("All D") controls were performed by incubating 8 M-urea solubilized unfolded BtuB with pD_{corr} 7.2 label buffer for 600 – 64500 seconds at room temperature. In-exchange controls measured deuteration levels between 0 – 5% D, and All D controls measured deuteration levels of 70-75%D. The mean level of back exchange in peptides used in our analysis was 27%, with 73% of the label remaining on the longest urea control. There was a weak correlation of back exchange levels with sequence position, with peptides covering residues 1-79 having an average back exchange level of 25 and peptides covering residues 80-137 having an average back exchange level of 30%.

Fluid handling operations for HXMS experiments in detergents were carried out with a Trajan LEAP HDX PAL workstation. 25 to 30 μM of DDM-solubilized BtuB wild-type or "LH4" samples ("LH4" is a construct of BtuB with a hexahistidine tag inserted after position 449) were diluted into >99%D 25 mM NaPi, 25 mM NaOAc, 100 mM NaCl, pH 5.0 – 7.0 labeling buffer for 0.25 - 900 minutes at 22 ^{o}C before 2-fold dilution into a 4 ^{o}C-chilled vial containing HX quench buffer: 600 mM glycine pH 2.5, 2 M urea, with the quench vials being manually supplemented with 2 μL of 10 mg/mL pepsin at the start of each time course. The quench reaction time was set to 1 minute, and each fluid transfer operation involving BtuB

was followed with two cycles of aspiration and dispensing to ensure proper mixing.

2.7.5 Mass Spectrometry

For labeling experiments, upon injection peptides were trapped and desalted by flowing across a 5x1 mm C8 5 μm particle column (TARGA brand, Higgins Analytical, Mountain View, CA, TP-M501-C085) for 3 minutes at 100 μL/min. After desalting, the trap was diverted to be in line with a Dionex Ultimate-3000 gradient pump flowing at 20 μL/min, with a 50 x 0.5 μm C18 3 μm particle column (TARGA brand, Higgins Analytical, TS-05M5-C183) in line for peak refocusing upstream of the HESI-II (Thermo Fisher Scientific, cat# IQLAAEGABBFACNMAGY) probe attached to a Thermo Q Exactive mass spectrometer, and a 14-minute gradient from 10% to 60% buffer B was immediately started. MS data were collected from 2 to 13 minutes into the gradient, and the flow diverted to waste otherwise. Buffer A was 0.1% formic acid in water, and buffer B was 0.1% formic acid in acetonitrile. After the main gradient, the pump was set to 90%B for 2 minutes, then down to 10%B for a minute, and two trapezoid washes up to 90%B were performed to clean the columns before the next injection. Electrospray ionization was performed at 180 ^{o}C, with the following parameters: spray voltage set to 3.2 kV, 1 microscan per scan, resolution 140,000, AGC target 3e6, minimum IT 100ms, scan range 400-2000 m/z, dynamic exclusion 10ppm, sheath gas flow rate 5, aux and sweep gas flow rates 0.

For assignment experiments, peptides were analyzed by performing unlabeled injections of outer membrane samples, or an 8 M urea solubilized concentrated stock of BtuB purified from inclusion bodies, after being expressed without a signal sequence. MS/MS data were acquired with the following parameters: data collected from 2 to 13 minutes of an identical gradient to HX runs detailed above, Full MS as detailed above, dd-MS2: resolution: 17,500, automatic gain correction target: 1e5, maximum integration time: 200 ms, loop count: 10, MSX count: 1, TopN: 10, isolation window: 1.9, m/z isolation offset: 0.00, scan range: 200 to 2000 m/z, fixed first mass: 100.0 m/z, NCE / stepped: NCE 27, spectrum data type:

profile.

2.7.6 Data Processing

Peptide signals were assigned by searching against a sequence database containing pepsin and BtuB sequences using the meta-search program SearchGUI version 3.3.21, (search settings: unspecific cleavage, precursor charge 1-8, isotopes 0-1, precursor m/z tolerance 10.0 ppm, fragment m/z tolerance 0.5 Da, no post-translational modifications, peptide length 5-30) incorporating X! Tandem, MS Amanda, and Comet algorithms. Data were inspected in PeptideShaker version 1.16.45, and results were imported into HDExaminer 3.1 (Sierra Analytics, Modesto, CA). HDExaminer was used to fit isotopic envelopes, enabling bimodal fits where separately exchanging subpopulations were present. Integration bounds of retention time as well as m/z were adjusted manually after an initial round of calculations performed by the program. While attempting to maintain consistency, isotopic envelope integration bounds were sometimes overridden to exclude obvious noise and carried over peptide signal near 0%D. Occasionally, integration bounds had to be manually chosen to achieve consistent extraction of heavily overlapped envelopes in cases where a peptide's independently exchanging subpopulations failed to diverge at early time points.

A subsequent round of manual adjustment was performed considering inter-peptide differences, to ensure that all overlapping peptides for a sequence fragment exhibited the same behavior. In cases where a peptide grossly disagreed with others covering the same sequence it was excluded from further analysis. In some instances, all time points from pairs of peptides with similar m/z signals and LC elution times were manually re-integrated multiple times to assess the contributions from overlapping envelopes.

CHAPTER 3

FOLDING STUDIES OF TBDT PLUG DOMAINS

The material presented in this chapter is unpublished work representing my early inquiries into the folding of independently expressed TBDT plug domains. Yi Zhang from the Royer lab performed high pressure NMR work described in **Figures 3.5 and 3.5**. Joseph Sachleben assisted with collection and analysis of NMR data. Isabelle Gagnon assisted in cloning, expression, and purification of protein constructs.

I designed all protein constructs, prepared all samples, performed all circular dichroism, stopped-flow fluorescence, mass spectrometry, and SAXS measurements. I performed all data analysis except for the chevron plot, which was made together with Michael Baxa, and SAXS analysis, which was done by Joshua Riback. Srinivas Chakravarthy at APS BioCAT assisted with SAXS measurements.

3.1 Summary

Authors: Adam M. Zmyslowski, Michael C. Baxa, Joshua A. Riback, Joseph R. Sachleben, Isabelle Gagnon, Yi Zhang, and Catherine A. Royer, and Tobin R. Sosnick.

In TBDT crystal structures, the interface between the plugs and the inside surface of the barrels is well hydrated and is composed primarily of H-bonded, charged, and polar contacts, despite being located inside the membrane plane. The detailed folding behavior of the plug during the transport cycle is unknown. CD, NMR, and SAXS results indicate that several separately expressed plug domains are unfolded in solution whereas those from BtuB and CirA adopt a partial globular fold consistent with their crystal structures. Thermodynamic and kinetic folding experiments were carried out to characterize the partially folded state and determine to what extent it might resemble a putative pore-forming transport intermediate in BtuB.

3.2 Introduction

This project was originally initiated based on a report that the plug domain of *E coli*. FepA retains residual structure and specific affinity for its substrate, enterobactin, when the domain is expressed alone [220]. A soluble construct of the first 150 residues, termed FepA150, was shown to have several dispersed peaks in two-dimensional NMR spectra, and its circular dichroism spectrum indicated partial secondary structure. Iron-loaded enterobactin underwent fluorescence polarization changes in the presence of this FepA150 construct, and iron-loaded enterobactin caused paramagnetic relaxation enhancement signal decreases in only a subset of peaks, unlike iron-loaded ferrichrome which uniformly reduced peak intensity. Following the reasoning of the authors that it may be useful for the plug domain to retain a weaker affinity and partial fold when it unfolds into the periplasm during transport, we sought to perform a survey of other TBDTs to determine whether such features were general. Two of six tested TBDT plug domains (constructs indicated by appending "p" to their gene name, *e.g.* BtuBp) retained substantial structure in solution, and this chapter describes their thermodynamic characterization.

3.3 Results

Plug domains were expressed as fusions to NuG2, a redesigned version of protein G [221], with an intervening His_6-GSS-TEV sequence. This expression system, which allows for high expression levels of protein in inclusion bodies, is commonly used in the Sosnick lab and has been described elsewhere [222]. Proteins were purified by Ni-NTA immobilization metal affinity chromatography (IMAC) and reversed phase high performance liquid chromatography (RP-HPLC). Protein-containing fractions were checked by sodium dodecyl sulfate polyacrylamide gel electrophoresis (SDS-PAGE) and lyophilized for long term storage.

3.3.1 Identification and circular dichroism characterization of TBDTs with spontaneously folding plug domains

Lyophilized protein was resuspended in CD buffer: 10 mM NaPi, 100 mM NaF, pH 7.0. CD spectra were collected at 20 ^{o}C, at concentrations of 1-100 μM, with 0.01-1 cm path length cuvettes using a Jasco J715 spectropolarimeter. Raw data $[\theta]$ were converted to normalized units of mean residue ellipticity

$$[\theta] = \frac{100 \cdot \theta}{C \cdot N \cdot l} \tag{3.1}$$

where C is the concentration of protein in molar, N is the length of the protein in amino acids and l is the path length of the cuvette.

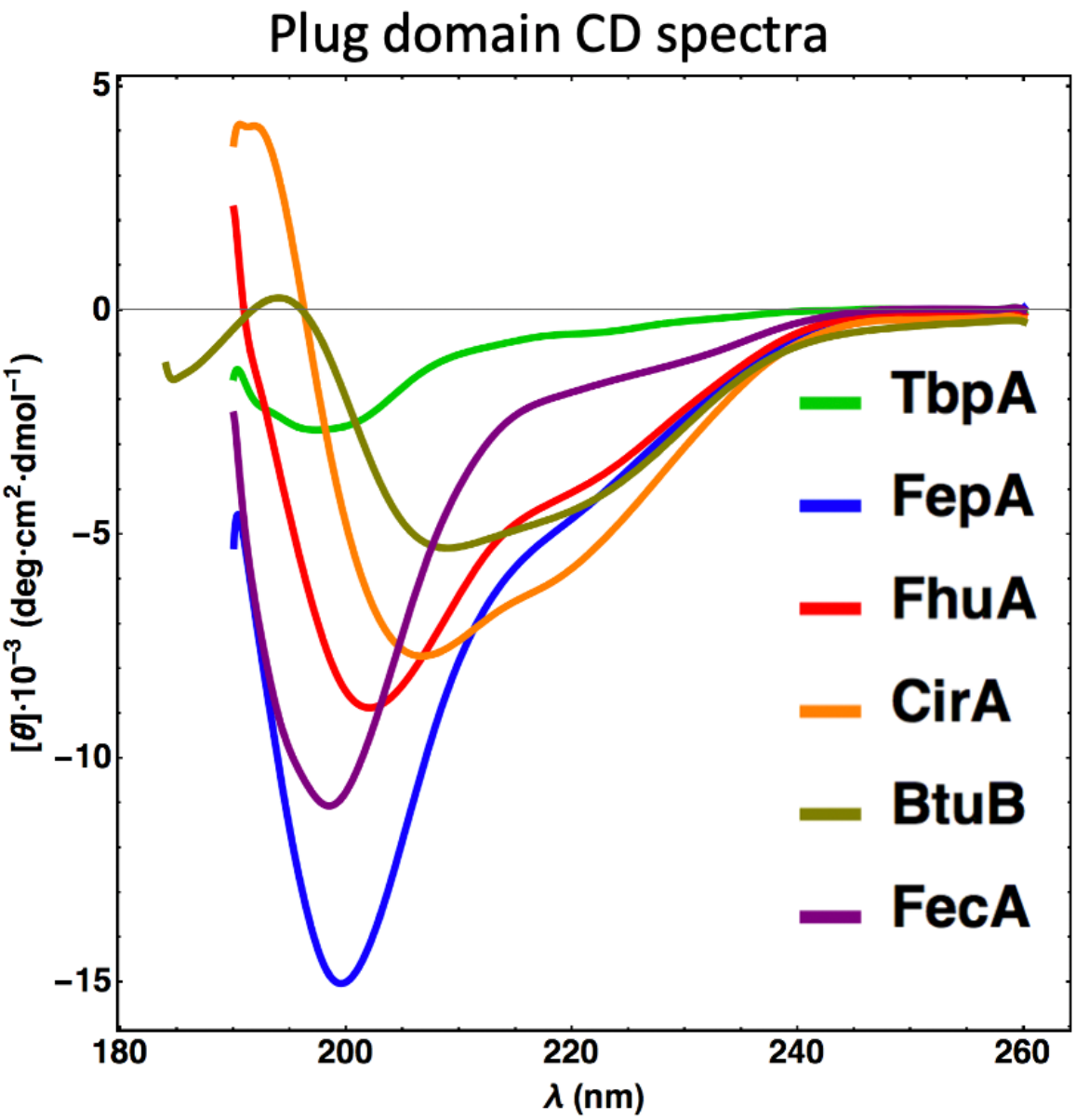

Figure 3.1: **Normalized circular dichroism spectra of six different TBDT plug domains** BtuB and CirA have spectra indicative of significant secondary structural content.

3.3.2 SAXS studies of plug domains

Small angle X-ray scattering was performed to assess the folding of several plug domains. CirAp and BtuBp were found to be partially folded, and the structured elements in CirAp were able to be diminished or augmented by addition of denaturant (guanidinium hydrochloride) and cosmotropic osmolyte (glycine betaine), respectively. BtuBp was not stable in solution above 150 μM, 4 ^{o}C. Raising temperature or concentration caused rapid precipitation of BtuBp, precluding measurements with osmolyte and making sample generation difficult. A dramatic precipitation of protein also happened for all plug domain constructs upon TEV cleavage, and thus the samples were centrifuged prior to subtractive Ni^{2+}-IMAC. FepAp, TbpAp, and FhuAp were readily soluble, but did not contain detectable structure in any condition measured.

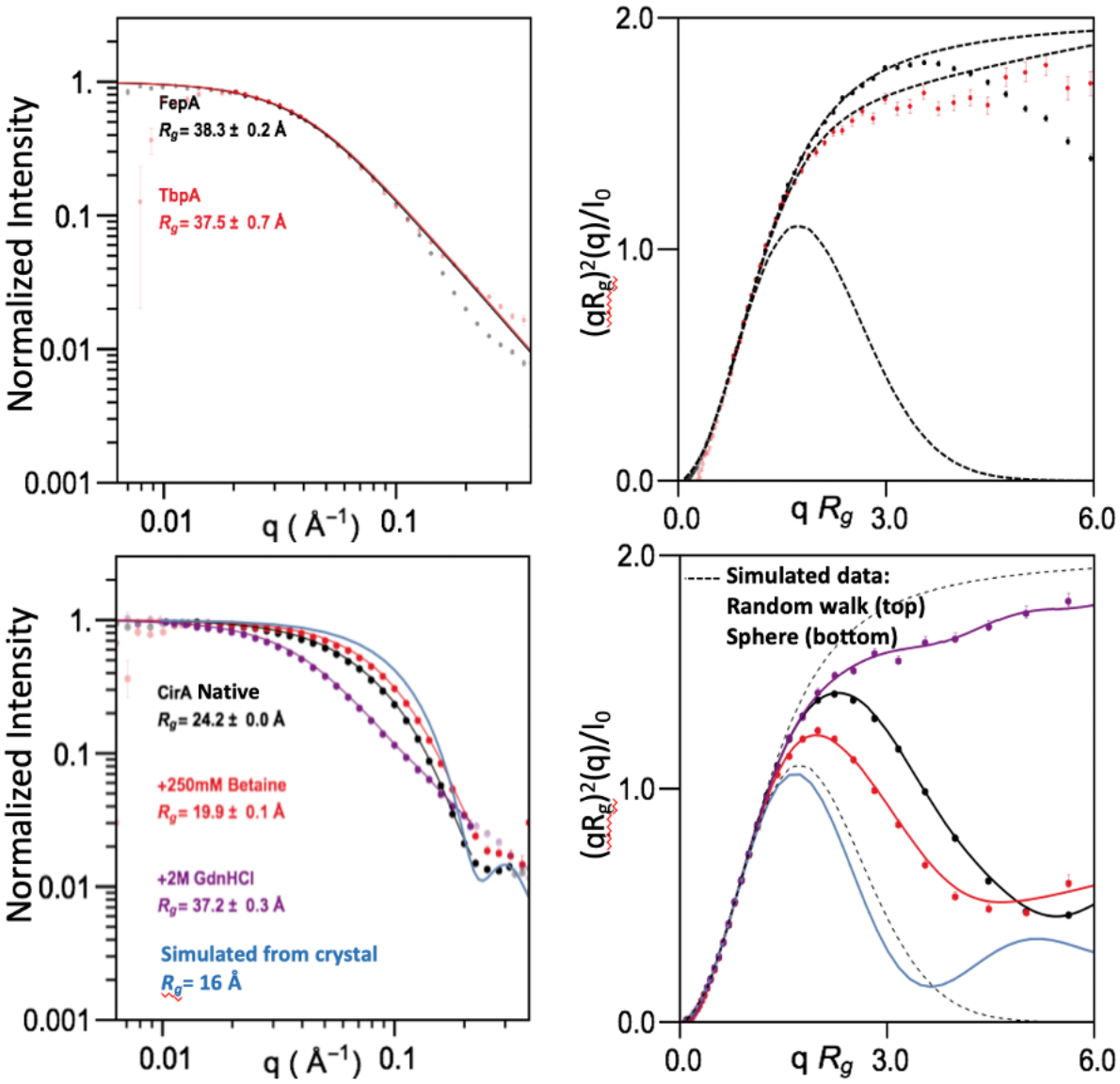

Figure 3.2: **SAXS studies of plug domains** **A)** Log-Log normalized scattering intensity curves for FepA and TbpA proteins with calculated radii of gyration (R_g), which match those for an unfolded polypeptide chain of the construct length. **B)** Dimensionless Kratky plots for the data in **A)**. Also shown is a simulated dimensionless Kratky plot for a simulated sphere of protein-like density and mass matching the plug domains. **C)** Log-Log normalized scattering intensity curves for CirAp under three conditions: native-like buffer (20 mM HEPES pH 7.4, 150 mM KCl, black), native-like buffer + 250 mM glycine betaine (red), native-like buffer +2 M guanidinium hydrochloride (purple). In blue is simulated data from the conformation observed in the crystal structure (PDBID: 2HDF). **D)** Dimensionless Kratky plots for the data in **C)**, along with simulated scattering curves for a sphere and self-avoiding random walk (dashed, bottom and top, respectively).

3.3.3 Kinetic folding studies of BtuB plug domain

A kinetic folding analysis was carried out for BtuB plug domain. Protein was rapidly diluted into or out of high denaturant concentrations and the change in tryptophan fluorescence over time was fit to a double exponential function. The major logarithm of the major exponential phase (containing the larger amplitude) reflects the logarithm of the folding (or unfolding rate). The extrapolation of these rates to the vertical axis reflects the rates of folding and unfolding at no denaturant. Multiplication of the ratio of the folding rate to the unfolding rate (the difference in vertical axis intercepts on a log plot) by RT (the ideal gas constant and temperature) gives the free energy of folding. The minimum of the fitted curve, around 1.6-1.8 M guanidinium-HCl, represents the folding midpoint of the protein, or the concentration of denaturant at which the stability is zero, and the protein equally populates the folded and unfolded states.

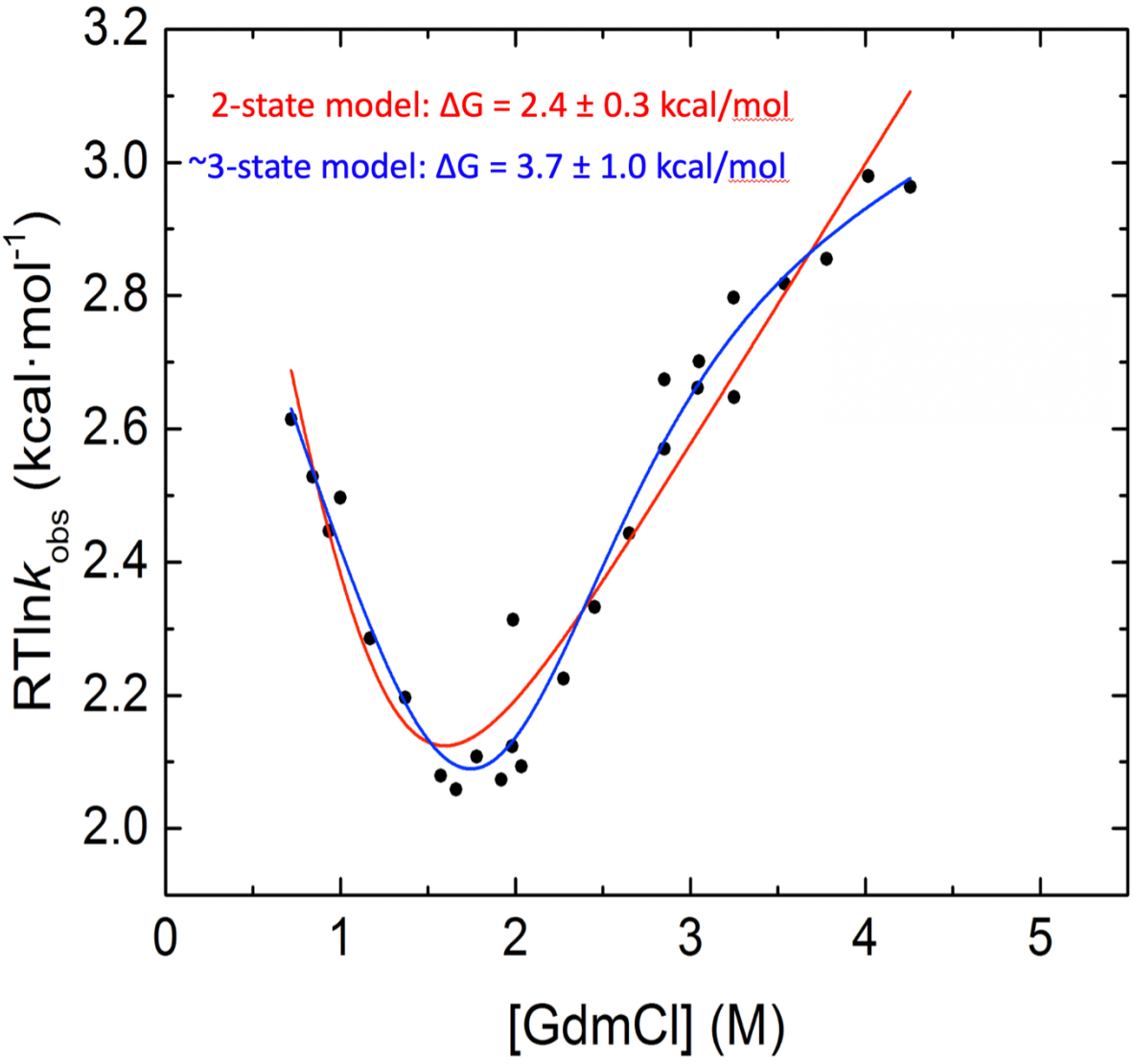

Figure 3.3: **Chevron plot for BtuB plug domain** Data were fitted to two-state (red) and three-state (blue) models, as the data above 3 M GdmCl appear to display evidence of a folding intermediate (reduction in slope above 3M).

3.3.4 NMR studies of TBDT plug domains

Plug domain folding was also assessed by collecting two-dimensional NMR spectra for several TBDT plug domain constructs. BtuB and CirA plugs were found to contain dozens of well-dispersed peaks, indicating a large fraction of their residues were folded in solution. Sample buffer compositions used were 18 mM NaPi, pH 5.5-6.5, 0.45 mM EDTA, 10% D_2O, 0.018% NaN_3, 45-180 mM NaCl. Temperatures were optimized for each sample, as the different plug domains had very different temperature-solubility profiles. BtuB plug was not soluble for more than a day above 15 ^{o}C and 250 μM, whereas CirA plug was able to be concentrated to 1 mM and was stable for several weeks at 35 ^{o}C. Unfolded plug domains generally had good solubility properties, and were measured at 25 ^{o}C, and 300-600 μM.

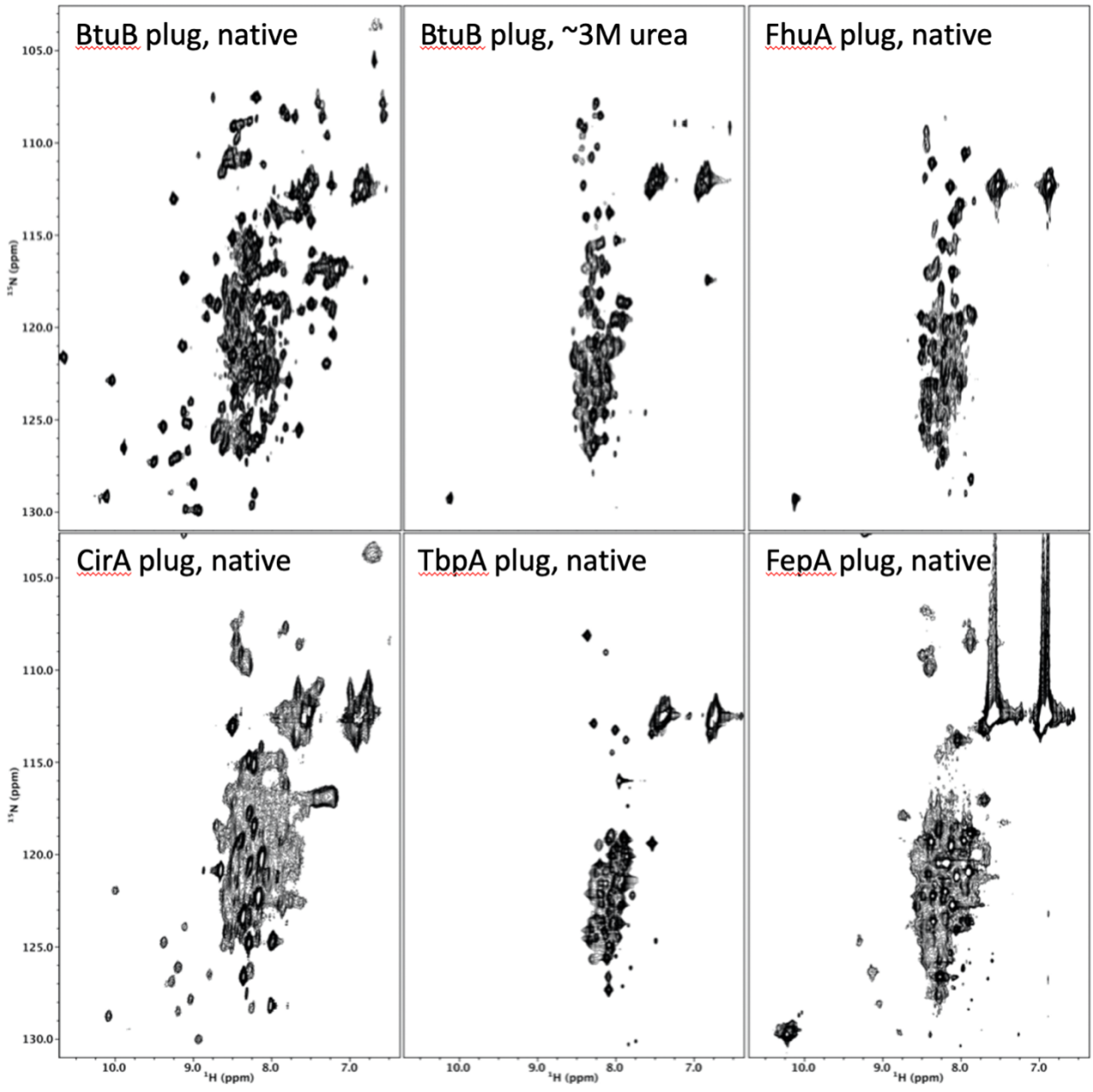

Figure 3.4: **^{1}H-^{15}N HSQC NMR spectra of plug domains** BtuB and CirA plug domains display chemical shift dispersion for several peaks each under native (non-denaturing) conditions. The dispersed peaks disappear for BtuB plug upon denaturation of the structure with 3 M urea. A similar effect was also observed for CirA plug.

3.3.5 Pressure denaturation NMR

To reversibly investigate folding and provide an independent measure of the folding stability, the BtuB plug domain was subjected to pressure denaturation by collaborators in the Royer lab at Rensselear Polytechnic Institute. Yi Zhang collected the pressure denaturation NMR spectra and and returned the data for analysis. Data were collected on a Bruker Avance III 600 MHz/14 T widebore NMR spectrometer equipped with a 5 mm TBI probe, at 15 ^{o}C, using 450 μL of shipped sample + 50 μL of D_2O. Peaks were picked for each spectrum, volumes integrated, and fit to a sigmoidal profile of sign corresponding to peak appearance or disappearance under increasing pressure. All NMR spectra were collected with 16 direct dimension scans. Sample composition was 300 μM BtuBp, 200 mM NaCl, 20mM NaPi pH 5.57, 50 μM EDTA, and approximately 20mM GdmCl (left over from sample solubilization, lowered by spin filter concentration).

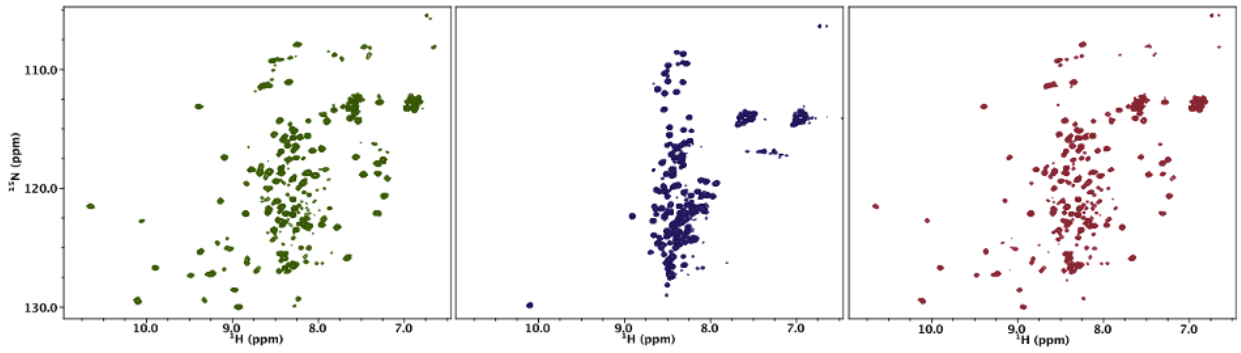

Figure 3.5: **Endpoint spectra of BtuB pressure ramp NMR experiments Left, right:** HSQC spectra collected at a pressure of 10 bar, before and after the pressure ramps, respectively. **Middle:** HSQC spectrum collected at 2000 bar, the highest pressure applied.

3.3.6 Analysis of pressure denaturation NMR data

Three well-dispersed peaks are indicated by red squares in the top right panel of **Figure 3.6**, but integrations were attempted for every peak. Because many peaks overlapped and changed chemical shifts as a function of pressure, integration bounds had to be manually adjusted for each peak in each spectrum. Fits were attempted for every peak in the spectrum of BtuBp domain, but several outliers were discarded due to implausibly high or low ΔG and $P_{midpoint}$ values. Data were fit to the equation:

$$A(P) = \frac{A_{max}}{1 + e^{(\frac{P \cdot \Delta V - \Delta G}{RT})}} \tag{3.2}$$

Where A(P) is the signal amplitude (integrated peak volume) as a function of pressure, A_{max} is the maximum signal amplitude, P is the pressure, ΔV is the volume change upon unfolding, ΔG is the free energy of unfolding, R is the ideal gas constant, and T is the temperature, 15 ^{o}C.

3.3.7 T2 relaxation rate measurements of BtuB plug domain

The transverse relaxation rate was measured in a series of specialized experiments. Peaks were picked for each spectrum and their integrated volumes fitted using a specialized module in the program NMRViewJ to obtain an average decay rate of 14.5 ms^{-1}. This T2 decay rate corresponds to a rotational correlation time of 10.7 ns, or an estimated molecular weight of 17.5 kDa, 18% larger than the molecular weight of the BtuB plug domain.

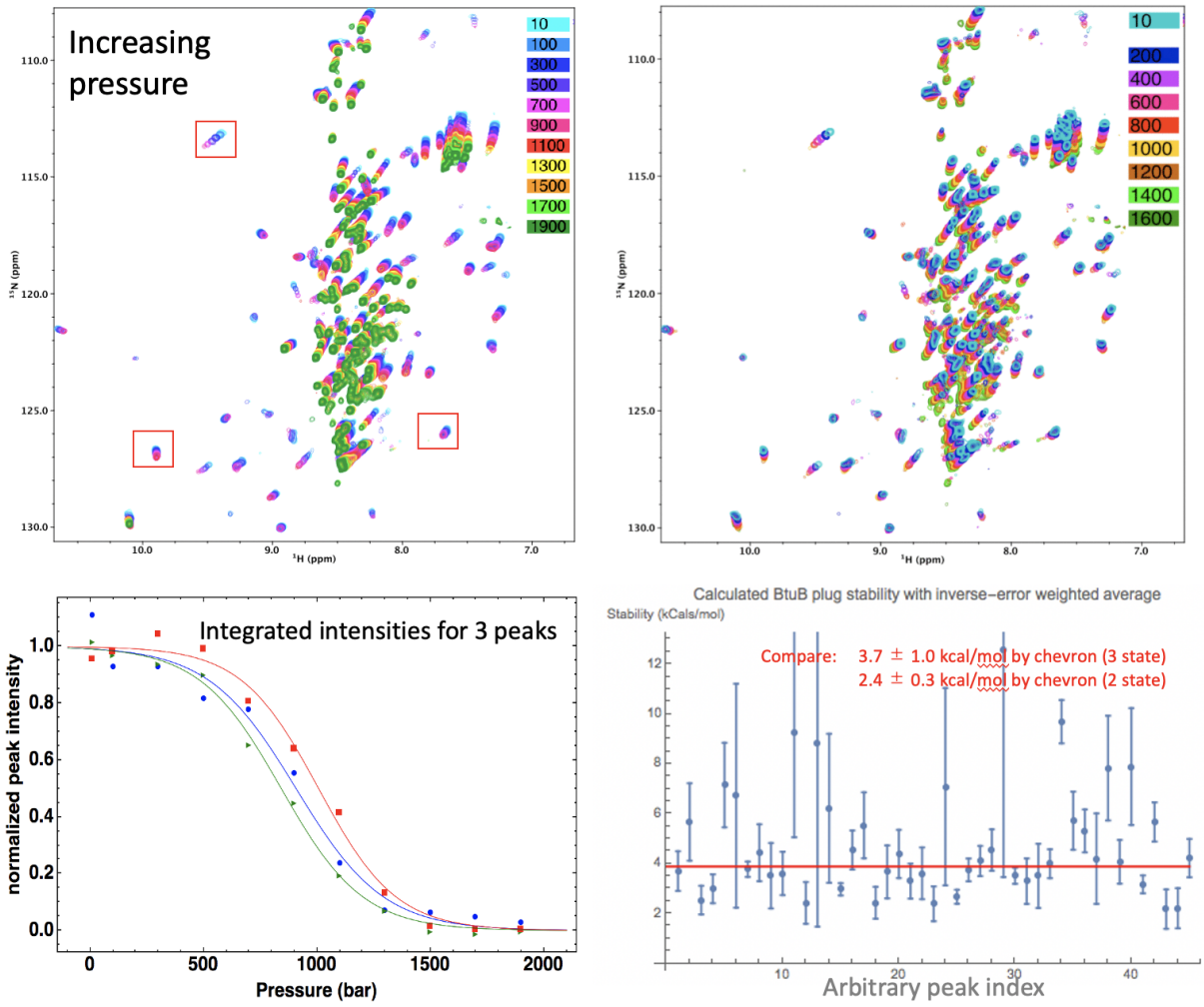

Figure 3.6: **Pressure denaturation NMR data analysis Top left:** Overlay of NMR spectra collected with increasing pressure. Three well-dispersed peak series are indicated with red rectangles to show chemical shift changes with pressure. **Top right:** Overlay of NMR spectra collected with decreasing pressure. **Bottom left**: Integrated peak intensities for three selected peaks. **Bottom right:** Stability vs. arbitrary peak index for 45 well-fitted peaks, with a red line placed at the inverse-error weighted average value of 3.9 kcal/mol.

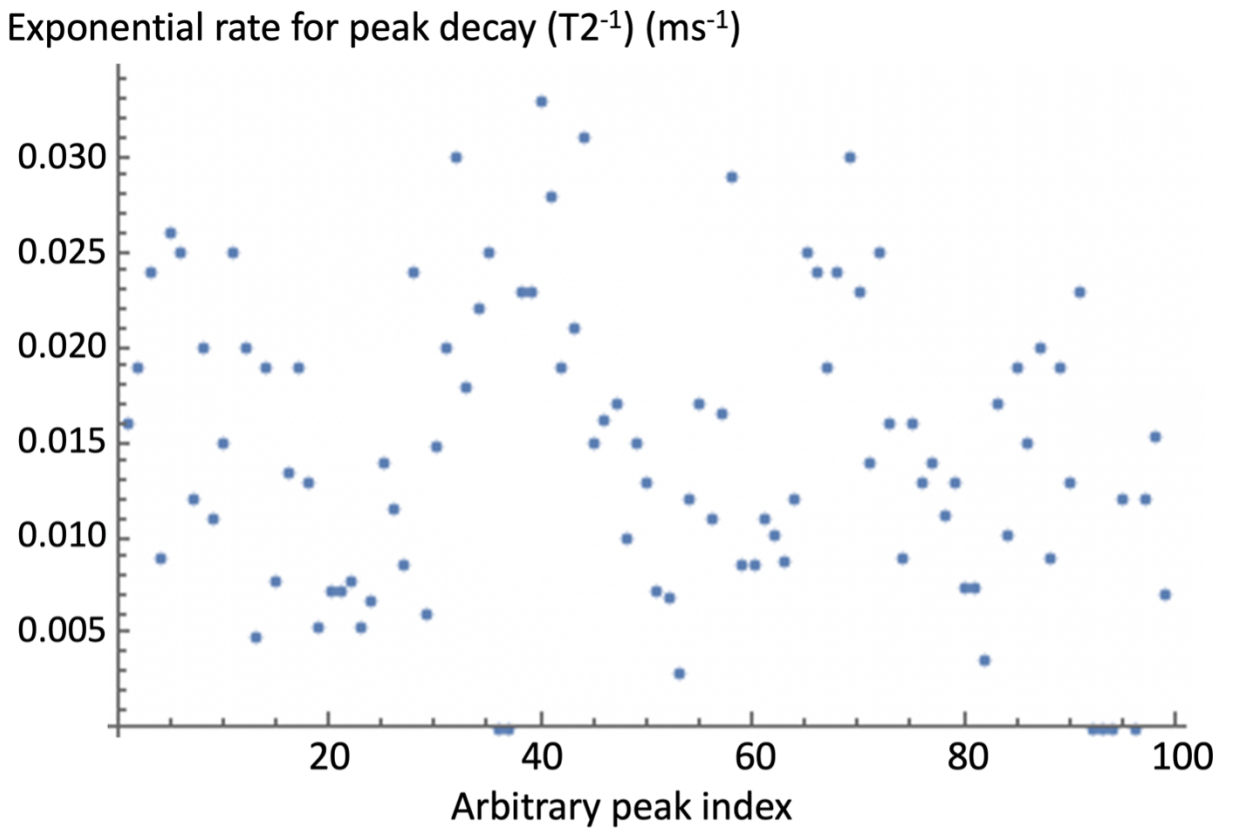

Figure 3.7: **Fitted transverse relaxation rates for BtuB plug domain** measured at 15 ^{o}C.

3.4 Discussion

The BtuB and CirA plug domains were found to have a stably folded structure, for approximately half of their sequence, each, with a free energy of unfolding of 2-3 kcal/mol. Prior to re-orienting the project to study BtuB in the context of the β-barrel, assignments were attempted on these BtuBp and CirAp, but during the process of collecting three-dimensional data for peak assignment of BtuB plug domain it became apparent that signals from experiments with long transfer times (e.g., HNCACB, CBCACONH) were significantly weaker than expected given the relatively strong data for initial three-dimensional experiments such as the HNCO and HNCA. Together with the poor solubility behavior of the BtuB plug, this led us to suspect that the protein was not tumbling rapidly enough in solution to give good NMR signals. CirAp had better solubility and sample stability properties, but many resonances were also missing from long transfer time experiments necessary to unambiguously assign the full sequence. Consequently, with the use of ^{15}N-edited TOCSY experiments to aid in identification of an amide resonance's sidechain, only certain di- and tri-peptides within the sequence were assigned to peaks in the HSQC spectrum. These short segments were concentrated within the amino-terminal half, where resonances were stronger and better dispersed.

3.5 Supplemental Figures

The structural similarities between plug domains have been the object of some prior study [220, 223], and early in the project I conducted bioinformatic analyses and comparisons of published structures of the plug domains, as more structures and sequences had become available since the early publications examining them.

3.5.1 Structural analysis and sequence comparison of TBDT plug domains

Of the TBDT structures that have been solved, most or all appear to have a similar plug domain topology. The central four-stranded β-sheet is an invariant feature, as is the connection between the plug & barrel domains. Besides the amino-terminal features involved in regulation and TonB interactions, the most variable parts of the structures are the secondary structural elements on the periphery of the plug domain, particularly near the substrate binding site (top left region of **Figure 3.8**) and extracellular loops. This is expected, as ligands seen in crystal structures generally contact both the plug domain and extracellular loops, and the loose packing of the periphery of the plug domain allows for accommodation of differently sized secondary structural elements..

3.5.2 Plug domain contact map analysis

The similar orientation of the plug domain within the β-barrel of all TBDTs crystallized so suggests that the plug is seated within the barrel by a similar set of contacts. I performed a structure-based sequence alignment using the RaptorX webserver [224]. Structures corresponding to the following 19 PDB codes were submitted: 1BY3, 1FEP, 1FI1, 1KMP, 1NQE, 1PO0, 1XKW, 2HDF, 2W75 (Chain A), 3CSN, 3FHH, 3QLB, 3V89, 4AIQ, 4B7O, 4EPA, 4RDT, 4ZGV, and 5FQ6. The contact maps of each structure were mapped onto this alignment for the purpose of determining which TBDT structural features are conserved among the crystallized subset, and which are idiosyncratic.

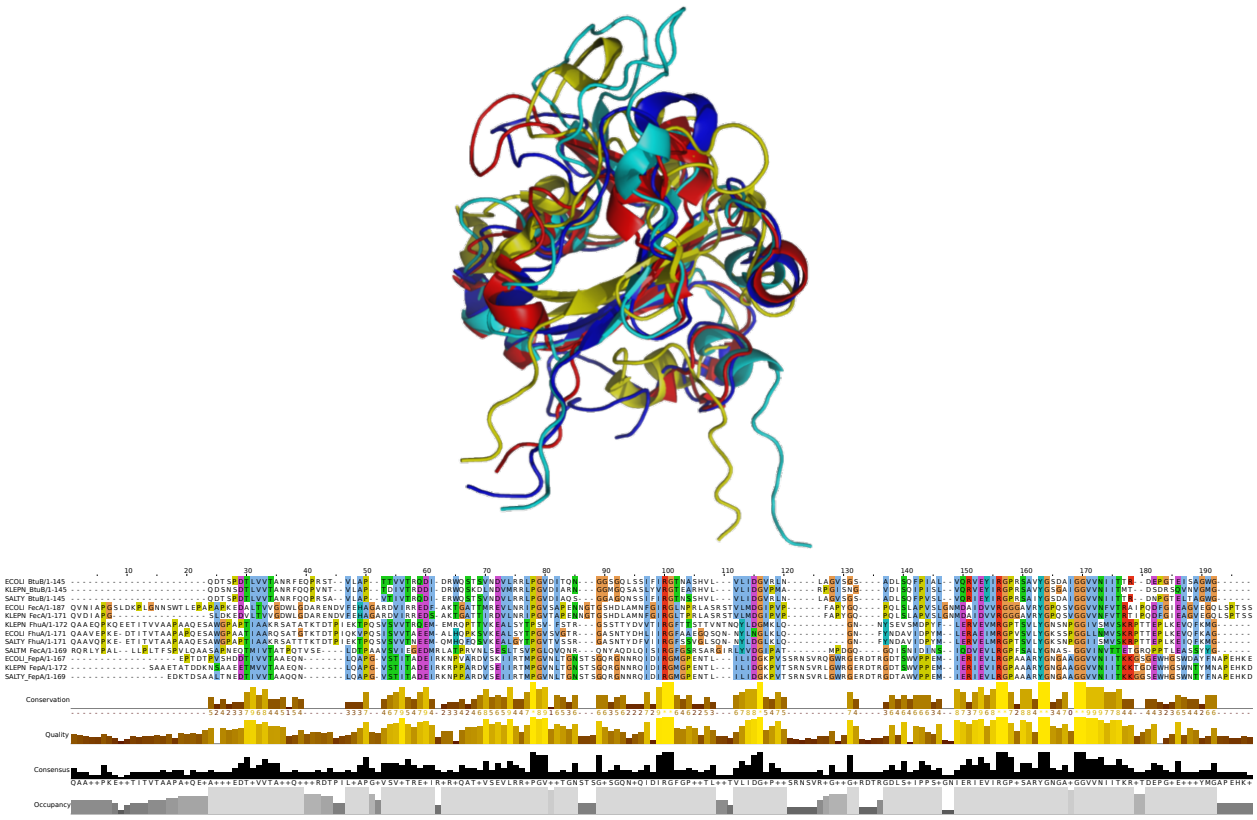

Figure 3.8: **Cross-species sequence comparison of TBDTs Top)** An overlay of plug domains from *E. coli* BtuB (red), FecA (yellow), FepA (teal), and FhuA (blue). The carboxy termini of the plug domains, connecting them to the β-barrel, are on the bottom left, and the amino termini are on the bottom right. The amino termini are often disordered, with the position of the Ton box not resolved for many TBDT crystal structures. **Bottom)** A sequence alignment of the plug domains from the above four TBDTs, from the three following organisms: *Escherichia coli* (ECOLI), *Klebsiella pneumoniae* (KLEPN), and *Salmonella typhimorium* (SALTY). Note that the sequences of the same TBDTs from different species are more similar to each other than the different TBDTs from the same species.

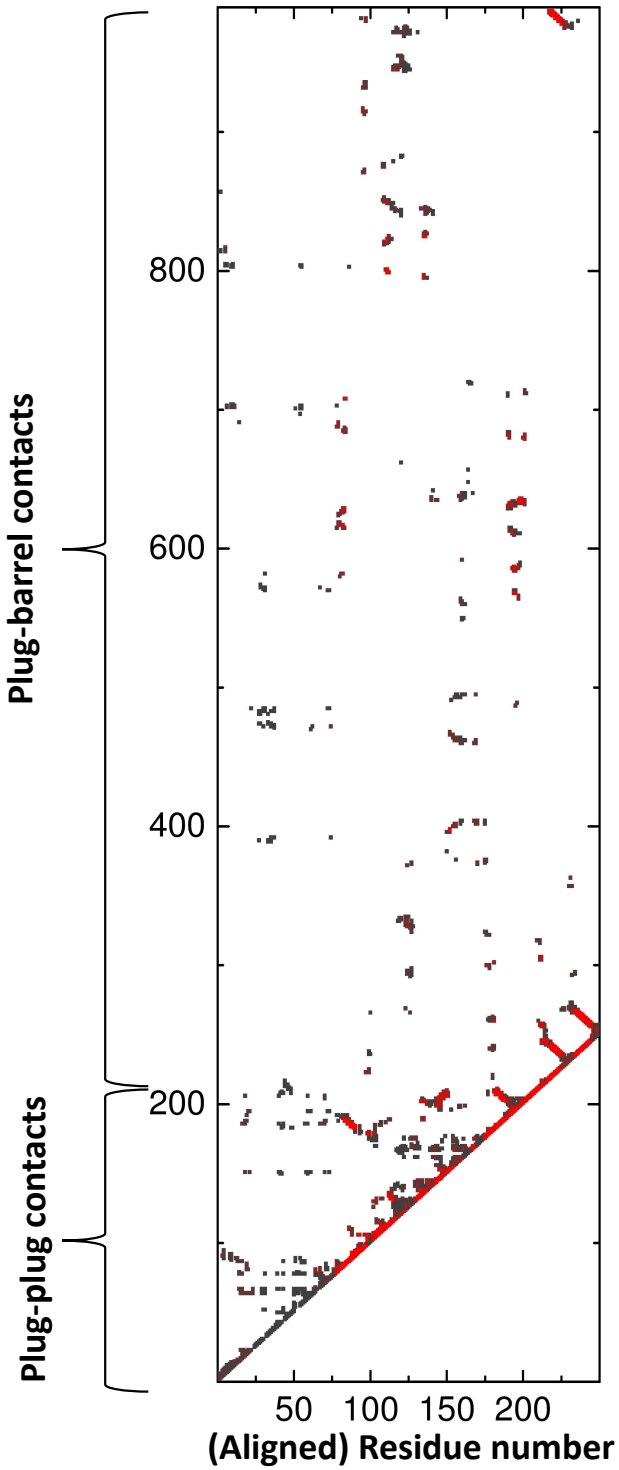

Figure 3.9: **Contact map analysis of TBDTs** Individual C_α-C_α distances shorter than 5 Å, found only in a single TBDT's plug domain, are drawn as a black pixel. As the same contact is counted in more structures, the color of the pixel lightens to shades of red, with the brightest red corresponding to a contact shared among 8 structures.

3.6 Methods

Plug domain constructs were cloned into a pET21 construct containing an amino terminal NuG2 HisTag and proTEV cleavage site was. Plug domain constructs were transformed into BL21 (DE3) *E. coli* on LB plates supplemented with 100 μM ampicillin (LB/AMP). A single colony was picked to inoculate an overnight culture of 10 mL of 2 x YT medium. This culture was used to inoculate 1L of 2 x YT medium and grown to 0.7-0.8 OD at 37 ^{o}C before induction with 0.5 mM IPTG at 20 ^{o}C for 5 hours. Cells were harvested by centrifugation at 6500 RPM for 12 minutes at 4 ^{o}C, and frozen or resuspended in 50 mM Tris-HCl, 150 mM NaCl, 1 mM PMSF, pH 7.4 and lysed immediately by 5 passes through a French press. The lysate was clarified by centrifugation for 30 min at 12,5000 RPM at 4 ^{o}C in a Sorvall Legend X1R centrifuge fitted with a FiberLite F15-8x50c and applied to a 5 mL column of equilibrated nickel-NTA resin. The column was washed with 20 column volumes (100 mL) of wash buffer: 50 mM Tris-HCl, 100 mM NaCl, 20 mM imidazole, pH 7.4 and eluted 6 times with 5 mL each of elution buffer, which was the same as wash buffer, except that the imidazole concentration was increased to 300 mM. Protein containing fractions were pooled and dialyzed in a length of 3.5 kDa molecular weight cutoff tubing against 2 L of dialysis buffer: 50 mM Tris-HCl, 100 mM NaCl, pH 7.6 for 2 hours before addition of 1 mg of homemade TEV protease in 1 mL of TEV protease storage buffer: 50 mM Tris-HCl, 1 mM EDTA, 5 mM DTT, 50% glycerol, 0.01% Triton, pH 7.6. TEV cleavage was allowed to proceed under dialysis for 16 hours at 4 ^{o}C. Cleavage was assessed by SDS-PAGE electrophoresis and a subsequent round of subtractive Ni-IMAC performed to remove uncleaved protein. The flowthrough from this was concentrated and injected onto BIO-RAD NGC chromatography system equipped with a Zorbax 300-SB C18 5 μm bead size, 9.4x250 mm reversed phase column (Agilent Technologies, Santa Clara, CA, P/N 880995-202). Reversed phase purification was carried out by running a gradient from 5% (buffer A) to 95% (buffer B) acetonitrile in water with 0.1% TFA in both buffers. Protein-containing fractions were checked by SDS-PAGE and frozen at -80 ^{o}C before cryodesiccation to obtain

pure protein powder for long term storage. For sample generation, protein powder stocks were dissolved into the appropriate buffer with the aid of up 4 M guanidinium hydrochloride, with the sample concentration and removal of the solubilization-aiding denaturant occurring by spin filtration. For BtuB samples approaching the concentration ceiling, spin column concentration was stopped every 10-15 minutes with trituration of the samples using a 200 μL pipette to prevent sample loss from formation of zones of high local protein concentration.

CHAPTER 4

CONCLUSIONS AND FUTURE DIRECTIONS

The previous chapters describe work probing early stages of the BtuB transport cycle, specifically the responses to B12 ligand and TonB CTD binding, and characterizing the folding of the BtuB and other plug domains. This chapter will discuss the impact of the findings described on the existing models of pore formation in BtuB and consider how future work might address the outstanding questions about the transport mechanism, as well as newly raised technical issues regarding HDX in OMs.

4.1 Conclusions

4.1.1 B12 binding allosterically unfolds the amino terminus of BtuB

Different aspects of our experimental results lend support to both the force-dependent and the force-independent models of pore formation in BtuB. Mutations to the Ionic Lock have recently been shown to induce changes in EPR spectra consistent with motions in the loops of SB3. In the force-independent model [133], TonB binding breaks the Ionic Lock and causes motions of SB3 when B12 is present. We have found that the Ionic Lock must be broken before TonB binding, and that SB3 displays heterogeneous exchange behavior in the presence of B12 alone, with SB3 data becoming difficult to interpret in the presence of $TonB_{\Delta N}$. Surprisingly, we did not observe any evidence of pore formation, or even global plug domain destabilization. This might be expected under the force-dependent model of pore formation, but the high stability measured for even the first pair of helices of BtuB, which comprise residues 31-47, implies that if pore formation does depend on force, the transporter has not evolved to lower the force required for gating of the pore in response to binding of either B12 or TonB.

4.1.2 The unfolded state of BtuB's plug domain experiences significant nonstructural environmental protection

In Chapter 2, we hypothesized that local environmental effects, as well as weak binding to the peptidoglycan to be together responsible (at least in part) for the slowed exchange in the nonnative control as well as unfolded peptides in the B12-bound condition (Peptide_{1-8} and the series including Peptide_{9-23} through Peptide_{9-30}). Factors such as local electrostatic fields and solvent accessibility have been proposed to influence protection factors [225, 226, 227, 228]. However, it is unclear how significant these effect are, as solvent exposed amides can have measured protection factors of up to 40 if they are on an ordered secondary structural element such as a β-sheet [229]. Conversely, molecular dynamics has been employed specifically to investigate these factors in the context of a small soluble protein, ubiquitin [230], where the authors found that there was no difference in the solvation properties of protected versus unprotected amides. This surprising result was interpreted to suggest that water restriction near the protein surface does not play a role in measured HDX. Hydrogen bonding is therefore likely to be the dominant effect in protection of surface exposed residues on soluble proteins, but the relative contributions of other effects are not settled. Furthermore, these trends may not hold for membranes proteins.

4.2 Future directions

The mechanism of pore formation for BtuB remains an open question. Likewise, the proposed environmental-induced residual HDX protection from interactions with PG or altered pH should be considered in future studies on OMPs. Besides these issues, the physiological relevance of certain plug domains' capacity for independent folding remains unclear. Below I explore the importance of these matters and suggest approaches to address questions they raise.

4.2.1 BtuB transport mechanism

The experiments presented above have clarified an important step along the pathway of pore formation in BtuB and opened future avenues for exploration. Important next steps include characterization of BtuB Ionic Lock mutants, optimization of the technique for probing the SB3 loop, measurement of the denaturant dependence of HDX for the plug domain, and comparison to other TBDTs. The Ionic Lock mutants will allow for direct comparison to the studies already performed on these mutants. Measurement of the denaturant dependence will allow for identification of concerted unfolding events, which can be compared across ligand states to understand the dynamics of BtuB in the states preceding pore formation. Finally, comparison of BtuB's HDX data to that of other TBDTs can aid in understanding which features of the mechanism are specific to BtuB and which are general to other TBDTs, or if they are incidental features produced by the protein family's shared topology.

To address the differences in inferred causality of Ionic Lock breakage and TonB binding between our results and those reported by the Cafiso laboratory [133], HDX measurements should be performed on at least one of the single Arg14Ala, AspD316Ala, and double Arg14Ala/AspD316Ala mutants, as any of these will break the Ionic Lock and allow for TonB binding in our model as well. I expect similar exchange behavior to be found in the apo and B12-liganded states for all three of these mutants, each of them exchanging as rapidly as the B12-liganded wild-type protein. Furthermore, TonB binding should no longer depend on the presence of B12 for any of the mutants. The situation is likely to be very different in BtuB variants that lack an Ionic Lock. A sequence alignment performed on 392 BtuB sequences **(Figure 2.24)** [215] finds that the Ionic Lock is strongly conserved but is not maintained in all BtuB genes. Arg14 is present in 80% of the sequences, and Asp316 in just 51%, although 35 of the remaining 49% of residues at site 316 are Glu, suggesting that the salt bridge is largely conserved. Additionally, glycines appear to be conserved at positions two and four residues amino terminal to the Asp316 position, possibly reflecting a requirement for space to allow local structural rearrangements. Do any of the BtuB variants naturally lacking an

Ionic Lock also regulate TonB binding in a B12-dependent manner? If so, how stably are their amino termini folded? Both questions are can be answered by repeating our analysis on mutants and variants of interest.

The binding of TonB and B12 can also be decoupled by using a linker insertion, which will probably not accelerate the exchange behavior of residues carboxy terminal to Arg14. For a construct with a linker inserted in between the Ton box and the Ionic Lock, the Ton box should become more solution exposed. Hence, with a linker of sufficient length, the Ton box should be able to extend into solution where it is able to be bound by TonB without the Ionic Lock being broken. For a linker sequence, either the flexible sequence $(GSS)_n$ [231], or a double repeat of the natural sequence of residues 13-23 $(NRFEQPRSTVL)_2$ could be used, though it may be necessary to perform the Arg->Ala mutation in the doubled sequence to prevent interference with proper formation of the Ionic Lock. Additionally, the repeat should be inserted between positions 12 and 13 or positions 13 and 14, as residue A12 is the last residue in the Ton box, and residue Arg14 is the cationic half of the Ionic Lock, and neither of these residues should be perturbed to minimize unwanted effects on BtuB function.

The linker-insertion constructs should also have predictable behavior in atomic force microscopy (AFM) experiments as performed by the Brockwell lab [136]. Specifically, for linkers of sufficient length to allow TonB binding in the presence of an unbroken Ionic Lock, the AFM experiments should become possible in the absence of B12, which was present in all BtuB puling experiments reported in that study. Furthermore, an additional rupture event should be seen reflecting the breaking of the Ionic Lock, occurring before the others, which are expected to remain approximately the same in terms of force required for the rest of the pulling profile. A minor increase in force is expected due to the additional sequence linking the AFM probe with the folded domains, which is also expected to increase the contour length of all rupture events. The additional rupture event would correspond to the breakage of the Ionic Lock, which was presumably not originally observed because TonB cannot bind when the Ionic Lock is unbroken. Such observations would bolster the model set forth in

Chapter 2, whereas observations consistent with a folded amino terminus in mutants with a broken Ionic Lock would argue against it.

Future work should not be restricted to the amino terminus of BtuB. The recently proposed motions of SB3 [133] are partially reflected in our data, and merit further experimental investigation. MS signals for these peptides are among the most heterogeneous and weakest in our dataset. This complexity presents an opportunity as well as a challenge. The presence of three differently exchanging populations suggests that this region of BtuB has at least two structurally or dynamically distinct populations in the folded state, which do not interconvert on the experimental time scale of multiple hours. Little is known about the significance of these populations, or how one might separate them for individual characterization. Use of proteases other than pepsin, as reviewed in the introduction, can help to produce more peptides from this region, and use of combinations of proteases may produce shorter peptides. Shorter peptides aid in interpretation by narrowing the sequence to which an exchanging amide contributes signal, and more peptides can help in a similar manner by comparison of their data, as outlined above. Another option to study SB3 behavior would be to re-analyze existing data more completely by employing a more sophisticated analysis technique. The Sosnick lab presently analyzes data with a program which reports at most two independently exchanging populations. Extracting the isotopic envelope profiles and fitting them manually for a single scan is not difficult, but iteration the process as needed for a full analysis is intractable. The HDExaminer [232] program allows for convenient averaging of data over a chosen range of scans, comparing these averages for different time points and conditions, and performing constrained fits to extract deuterium uptake estimates. These features greatly reduce the time needed for analysis for an HDX set. Until the HDExaminer software is updated to support multi-modal fitting, such analysis would depend on the acquisition of new analysis software.

Measuring the denaturant dependence of the preparations described in Chapter 2 is another way to gain understanding of the folding properties of BtuB. The technique, termed

"native state hydrogen exchange" (NSHX) [233], has been used to study subglobal unfolding events in proteins that lead to partially unfolded intermediates [234]. Under the force-dependent model of pore formation, we expect to see no decrease in the concentrations of urea required for destabilization or unfolding of the plug domain past residues 25-30. In our interpretation of the force-dependent model, the Ionic Lock exists solely to regulate binding of TonB. Once TonB is engaged, force must be applied to form the pore, and the binding of TonB alone does not exert a substantial force. If TonB binding can trigger pore formation, however, then we expect exchange for certain elements of BtuB's plug domain to be accelerated, at least for some concentration of denaturant.

The experimental approach developed in Chapter 2 is likely to be applicable to different TBDTs from *E. coli* as well as other Gram-negatives. The crystallized members of the TBDT family generally share a common topology not only in the plug as well as β-barrel domains, with the former containing insertions and deletions at the periphery but usually keeping the same secondary structural elements in the same arrangement relative to the β-barrel. However, substrate-induced motions and signaling are not universally conserved among TBDTs even from the same species. For example, FhuA posseses a constitutively unfolded Ton box, while FecA undergoes a similar Ton box unfolding event as BtuB [235]. Additionally, some [236, 237] but not all [203, 238] measurements of TBDTs have found that they bind substrates in an induced fit mechanism [198], closing their extracellular loops behind substrates to trap them in a bound state. The generality of this phenomenon is unknown, as results depend on whether the experiments are performed in an environment containing LPS. It will be interesting to investigate whether these loops undergo slowed HDX in OM preparations compared to BtuB solubilized in detergents or vesicles. The existence of organisms with multiple TonB genes also raises questions about crosstalk and specificity between TonB and TBDT pairs within a single cell, and our technique may be used for investigating these in a native-like OM context.

Relatedly, FepA has long been hypothesized to contain two extracellular binding sites

for its substrate, enterobactin [239, 240], and an enterobactin transporter in *P. aeruginosa* has recently been shown to have two binding sites with different affinities [241]. Other transporters such as CirA [242] and PirA [243] also have long extracellular loops like these two enterobactin transporters, suggesting that the double binding site feature might be widespread [241]. Investigation of the HDX behavior at different ligand concentrations can reveal the differences in plug domain dynamics, as well as those in the loops themselves, which are induced by binding of substrate to one or both sites.

How feasible is measurement of in-OM HDX on disulfide-crosslinked mutants and the extracellular loops of TBDTs? To handle the former, it will suffice to add reductant to the quench solution. Tris(2-carboxyethyl)phosphine (TCEP) has been used in this manner, and is well tolerated by the protease, only mildly decreasing peptide coverage in certain cases, and sometimes increasing it in others [244]. Regarding the extracellular loops, preliminary peptide coverage maps of BtuB **(Figures 2.14-2.16)** indicate that our proteolysis conditions result in good digestion of the loops when BtuB is embedded in OMs, and near-complete coverage of the β-barrel. Signal levels are weaker than for the amino terminus, however, and the digestion gel assay shows that large quantities of β-barrel remain intact under our standard conditions **(Figures 2.5B, 2.18-2.23)**. The presence of an unfolded or misfolded subpopulation may be disproportionately responsible for these signals, and care should be taken to ensure that the results are not biased by such selective proteolysis. Proper interpretation of extracellular loop HDX may require additional controls such as runs where proteins are chemically separated from LPS after labeling (ideally using aprotic solvents to mitigate back exchange) and measured after resuspension in denaturant. Fortunately, the digestion of full length BtuB resolubilized with denaturants from an insoluble pellet is very efficient **(Figure 2.13)** and should not require much optimization for most TBDTs. To increase signal strength from difficult-to-digest extracellular loops and transmembrane β-strands, it may be useful to employ longer digestion times, or different and possibly mixed, proteases.

Mutagenesis studies should not be restricted to investigation of the Ionic Lock. Within

the plug domain, cysteine crosslinks between the inner barrel surfaces and amino termini of FhuA [245] and FepA [246] prevented transport in the oxidized state, but such tethering deeper inside the plug domain still permitted transport at a slowed rate [247]. More recently, crosslinks within the plug domain of FepA were found to abolish transport, while those between the plug and β-barrel generally permitted it [248]. It is unclear to what extent the disulfides were formed in those assays, however. Transport may have proceeded through a population of protein which did not form disulfides. A technique such as HDX which can independently measure different populations co-existing within the same sample is well-suited for follow-up studies. Additionally, it is unclear to what degree the introduction of disulfides interferes with transmembrane signal transduction, Our technique can quantitatively measure release of the Ton box for binding by TonB CTD upon substrate binding, and is well poised to answer some of the questions opened by recent studies of FepA [248]. Similar mutations have also been made on BtuB [249], and collaboration with groups specializing designing such mutations may aid in identification of motions seen in BtuB as functionally significant.

Furthermore, investigating the dependence of HDX on denaturant concentration in these mutants may reveal which unfolding events are relevant to the pore formation pathway. Cysteine crosslinks which impair transport may perturb different dynamical modes of the protein, observed as exchange through as local or subglobal unfolding events, than those which restrain the protein in ways unaffecting transport. The use of cysteine mutants to irreversibly trap a desired conformational state is fully compatible with the HDX-MS, and the technique does not suffer from incomplete disulfide formation.

4.2.2 Towards more native HDX measurements in outer membranes

As recent work from the Cafiso laboratory has shown [27, 133, 213, 250], the function of BtuB is somewhat perturbed even in outer membranes, relative to live cells. Sarkosyl treatment has been identified as modifying the results of EPR experiments conducted on BtuB in outer

membranes [133]. The potentially perturbative effects of sarkosyl in our experiments can be controlled for by repeating the measurements on OM samples prepared by sucrose gradient centrifugation [251, 252] instead of sarkosyl extraction. Alternatively, our approach can be adapted to experiments where labeling is performed *in vivo*, if the matter of back exchange during OM sample preparation is resolved. Two approaches are worth considering: either the rate of back exchange must be slowed, or a labeling technique which is insensitive to back exchange can be used.

Consideration of the second point is simpler, because a technique similar to HDX that can be applied to live cells already exists. Many HDX practices can be carried over to fast photochemical oxidation of proteins (FPOP), a technique which uses MS to detect peptides labeled by hydroxyl radicals. FPOP requires additional instrumentation, as the hydroxyl radicals are usually produced via Fenton chemistry consuming hydrogen peroxide [253], but this has been proven to work even *in vivo* [254]. Because the FPOP label is covalent, after labeling the workflow up to the peptide generation and measurement stages can remain the same, with the only major change required being accommodation of the different chromatographic and mass spectral properties of the hydroxylated peptides. As a final note, because FPOP labeling times are generally short, often in the microsecond range, the technique is best suited to report of fast dynamics of proteins rather than on thermodynamics or slowly interconverting populations, as HDX-MS does well. For this reason, it is complimentary to HDX, providing information which could corroborate our findings (e.g., about B12 causing unfolding in the amino terminus) but not recapitulate them exactly.

Due to the permeability of the outer membranes to small molecules, labeling of live cells can be accomplished by handling them as described for OM samples in Chapter 2. To perform an HDX study of OMPs labeled in live cells, however, an important rearrangement in the order of several steps would be required. This rearrangement would in turn necessitate further changes to mitigate the resulting increase in back exchange. Instead of obtaining

peptides immediately after labeling, peptides should be generated on the inner surface of the OMs after lysis and OM isolation. This is because pepsin is too large to diffuse into cells and applying pepsin to a total lysate would likely result in excessive unwanted signals from other proteins.

Can the deuterium label realistically be retained throughout preparation of *in vivo* HDX-MS samples? Under optimal quench conditions of 0 ^{o}C and pH 2.5, the time constant for back exchange of BtuB's amino terminal 23 residues is approximately 3 hours [255]. Theoretically, this time should allow for retention of detectable levels of label throughout the OM preparation process used in Chapter 2. Practically, however, even transient heating by a few degrees can dramatically shorten the window during which label is retained. For this reason, a more rapid protocol with fewer steps is desirable. Ideally, the time between the end of the labeling period and pepsinization should not exceed one hour, to keep over 60% of the label on the proteins during sample preparation. Back exchange in our protocol which has labeling followed by pepsinization of OMs is about 25%. For example, a sample labeled in 90% D solution, which has retained 60% of the label until this point, will still be 40% deuterated at the longest time points. Additionally, if the outer membrane confers protection to unfolded sequences, then even acid-denatured segments of labeled OMPs will have a reduced rate of back exchange.

Reproducibility will also become a larger concern, as incubation times at different stages will have different effects on label recovery, since back exchange will be allowed to proceed for different amounts of time. Whole cell samples should therefore be frozen after labeling. Once a batch filtered peptide samples is ready for injection, it can be re-frozen so that back exchange is not proceeding while the samples are sequentially analyzed. Serialized sample handling is acceptable when the steps are short, but to ensure good reproducibility as many steps as possible after the labeling should be parallelized.

A critical feature of any protocol for extraction of labeled OMP peptides from whole cells is that lysis should still be separated from pepsinization by at two ultracentrifugation steps

so that no peptides are produced from cytosolic or inner membrane proteins. If sarkosyl is added directly to the lysate, then inner membrane proteins will become dissolved and only cell debris and OMs will pellet. In this way, a low-speed spin (e.g., 10 minutes at 6000 x g) can be used to separate the cell debris (and acid-precipitated proteins), and then the supernatant would once again be centrifuged to pellet outer membranes (this time for 20-30 minnutes at 40,000 x g). Resuspension of this second pellet would give a solution to which pepsin could be added to generate the labeled peptides. We harvested total and outer membrane pellets by ultracentrifugation for two cycles 60 minutes each, but this long time (and the repetition of each harvesting step) was chosen to optimize for sample yield and purity, rather than minimizing back exchange. A single 30-minute step should be sufficient to give measurable signals and keep the total sample preparation protocol under an hour in length while allowing 15 minutes each for lysis and OM pellet resuspension. Additionally, lysis may be carried out by cryomilling to minimize the contribution of this step to back exchange [256].

4.2.3 Non-structural protection factors in outer membranes

OMPs embedded in the OM may serve as a novel system to test the relative contributions of the effects discussed above to measured protection factors. Solvent exposure and local electrostatic effects, which have not been strongly supported as contributing to protection factors in solution, may be especially pronounced in the OM. Hydrogen bonding to peptidoglycan, on the other hand, which we consider to likely be the dominant effect, may be manipulated according to established approaches.

A first step to test the issue involves examination of the HDX of BtuB's well-behaved amino terminal peptides in OM preparations that have altered or reduced peptidoglycan. *E. coli* has been shown to remodel its peptidoglycan by introducing additional crosslinks when biogenesis of the outer membrane is perturbed [257]. With a strong enough perturbation, the effects of altered peptidoglycan structure might be manifested as altered protection factors in

the amino terminal region of BtuB in the B12-liganded state, or even elsewhere. For example, a strain of *E. coli* displaying peptidoglycan on its extracellular surface has been identified [258], which might induce analogous environmental protection effects for peptides whose exchange proceeds via exposure to solvent on the extracellular side. Potential expression differences between the three biological replicates presented in Chapter 2 did not appear to cause differences in protection factors, but it is possible that deliberate and more extreme perturbations could. Our study employed a single treatment with lysozyme adapted from standard protocols used for soluble protein, though many other cell wall hydrolases are available [259]. The level of PG digestion in our experiments was unknown. Employing combinations of hydrolases to digest the peptidoglycan more completely might reduce the maximum observed environmental protection. Alternatively, deletion, mutation or altered expression of Braun's lipoprotein [260] can affect OM properties, and preparations from *E. coli* manipulated in this way may have different OM environmental protection factors. Our technique is largely agnostic to sample composition as long as the denatured plug domain sequence is accessible to soluble proteases. A simple approach would be to screen for altered sequestration of BtuB's plug domain. **Figures 2.18-2.23** show perturbed digestion as a function of different i) detergents used to solubilize the protein, ii) denaturant concentration, iii) and temperature. Because the sample preparation process is relative short and not labor intensive, conducting tests of digestion efficiency and preliminary uptake measurements in a variety of OM contexts is likely to be feasible. The expression density in our system was sufficient to allow for large dilution factors, enabling high %D fractions in labeling experiments, so signal strength should not be a hindrance even if expression levels drop several-fold due to genetic manipulations of the host organism.

Another way to investigate the environmental effects of the outer membrane on HDX would be to express constructs of BtuB which lack the plug domain and use them as a substrate to which reference peptides can be affixed. I have confirmed significant secondary structural content of such plugless BtuB constructs inspired by early work on FhuA [84].

Though the simplest approach would be to replace the plug sequence, the lack of native cysteines in BtuB offers another possibility. A single cysteine could be mutated into a residue on the inner surface of the barrel and used as a site for attachment of reference peptides or small molecules.

In summary, a variety of protein engineering approaches could be combined with HDX to investigate the chemical and steric effects imposed by the native OM environment, using BtuB as both a reference with a large, easily controllable response, and as a scaffold for attachment of new probes.

REFERENCES

[1] J. E. Posey and F. C. Gherardini. "Lack of a role for iron in the Lyme disease pathogen". In: *Science* 288.5471 (2000), pp. 1651–3. ISSN: 0036-8075. DOI: 10.1126/science.288.5471.1651.

[2] A. D. Ferguson and J. Deisenhofer. "TonB-dependent receptors-structural perspectives". In: *Biochim Biophys Acta* 1565.2 (2002), pp. 318–32. ISSN: 0006-3002. DOI: 10.1016/s0005-2736(02)00578-3.

[3] Merry Youle. *Bridges Across the Periplasmic Moat*. Blog. 2014.

[4] C. Goemans, K. Denoncin, and J. F. Collet. "Folding mechanisms of periplasmic proteins". In: *Biochim Biophys Acta* 1843.8 (2014), pp. 1517–28. ISSN: 0006-3002. DOI: 10.1016/j.bbamcr.2013.10.014.

[5] J. E. Van Wielink and J. A. Duine. "How big is the periplasmic space?" In: *Trends Biochem Sci* 15.4 (1990), pp. 136–7. ISSN: 0968-0004. DOI: 10.1016/0968-0004(90)90208-s.

[6] M. Depuydt et al. "A periplasmic reducing system protects single cysteine residues from oxidation". In: *Science* 326.5956 (2009), pp. 1109–11. ISSN: 1095-9203. DOI: 10.1126/science.1179557.

[7] D. G. Thanassi et al. "Protein secretion in the absence of ATP: the autotransporter, two-partner secretion and chaperone/usher pathways of gram-negative bacteria (review)". In: *Mol Membr Biol* 22.1-2 (2005), pp. 63–72. ISSN: 0968-7688. DOI: 10.1080/09687860500063290.

[8] R. E. Dalbey and A. Kuhn. "Protein traffic in Gram-negative bacteria–how exported and secreted proteins find their way". In: *FEMS Microbiol Rev* 36.6 (2012), pp. 1023–45. ISSN: 1574-6976. DOI: 10.1111/j.1574-6976.2012.00327.x.

[9] H. Nikaido. "Transport across the bacterial outer membrane". In: *J Bioenerg Biomembr* 25.6 (1993), pp. 581–9. ISSN: 0145-479X. DOI: 10.1007/BF00770245.

[10] J. E. Horne, D. J. Brockwell, and S. E. Radford. "Role of the lipid bilayer in outer membrane protein folding in Gram-negative bacteria". In: *J Biol Chem* 295.30 (2020), pp. 10340–10367. ISSN: 1083-351X. DOI: 10.1074/jbc.REV120.011473.

[11] W. Vollmer, D. Blanot, and M. A. de Pedro. "Peptidoglycan structure and architecture". In: *FEMS Microbiol Rev* 32.2 (2008), pp. 149–67. ISSN: 0168-6445. DOI: 10.1111/j.1574-6976.2007.00094.x.

[12] V. Braun. "Covalent lipoprotein from the outer membrane of Escherichia coli". In: *Biochim Biophys Acta* 415.3 (1975), pp. 335–77. ISSN: 0006-3002. DOI: 10.1016/0304-4157(75)90013-1.

[13] A. Kovacs-Simon, R. W. Titball, and S. L. Michell. "Lipoproteins of bacterial pathogens". In: *Infect Immun* 79.2 (2011), pp. 548–61. ISSN: 1098-5522. DOI: 10.1128/IAI.00682-10.

[14] A. Steimle, I. B. Autenrieth, and J. S. Frick. "Structure and function: Lipid A modifications in commensals and pathogens". In: *Int J Med Microbiol* 306.5 (2016), pp. 290–301. ISSN: 1618-0607. DOI: 10.1016/j.ijmm.2016.03.001.

[15] B. Liu et al. "Structure and genetics of Escherichia coli O antigens". In: *FEMS Microbiol Rev* 44.6 (2020), pp. 655–683. ISSN: 1574-6976. DOI: 10.1093/femsre/fuz028.

[16] D. Liu and P. R. Reeves. "Escherichia coli K12 regains its O antigen". In: *Microbiology (Reading)* 140 (Pt 1) (1994), pp. 49–57. ISSN: 1350-0872. DOI: 10.1099/13500872-140-1-49.

[17] L. Leive. "Release of lipopolysaccharide by EDTA treatment of E. coli". In: *Biochem Biophys Res Commun* 21.4 (1965), pp. 290–6. ISSN: 0006-291X. DOI: 10.1016/0006-291x(65)90191-9.

[18] P. Cao and D. Wall. "The Fluidity of the Bacterial Outer Membrane Is Species Specific: Bacterial Lifestyles and the Emergence of a Fluid Outer Membrane". In: *Bioessays* 42.8 (2020), e1900246. ISSN: 1521-1878. DOI: 10.1002/bies.201900246.

[19] Cooper GM. *The Cell: A Molecular Approach*. 2nd ed. Cell Membranes. Sderland, MA: Sinaeuer, 2000.

[20] C. Dong et al. "Wza the translocon for E. coli capsular polysaccharides defines a new class of membrane protein". In: *Nature* 444.7116 (2006), pp. 226–9. ISSN: 1476-4687. DOI: 10.1038/nature05267.

[21] R. Koebnik, K. P. Locher, and P. Van Gelder. "Structure and function of bacterial outer membrane proteins: barrels in a nutshell". In: *Mol Microbiol* 37.2 (2000), pp. 239–53. ISSN: 0950-382X. DOI: 10.1046/j.1365-2958.2000.01983.x.

[22] H. J. Lessen et al. "Building Blocks of the Outer Membrane: Calculating a General Elastic Energy Model for β-Barrel Membrane Proteins". In: *J Chem Theory Comput* 14.8 (2018), pp. 4487–4497. ISSN: 1549-9626. DOI: 10.1021/acs.jctc.8b00377.

[23] E. R. Rojas et al. "The outer membrane is an essential load-bearing element in Gram-negative bacteria". In: *Nature* 559.7715 (2018), pp. 617–621. ISSN: 1476-4687. DOI: 10.1038/s41586-018-0344-3.

[24] G. Meng et al. "Protein oligomerization in the bacterial outer membrane (Review)". In: *Mol Membr Biol* 26.3 (2009), pp. 136–45. ISSN: 1464-5203. DOI: 10.1080/09687680802712422.

[25] R. Solan et al. "Gram-negative outer-membrane proteins with multiple β-barrel domains". In: *Proc Natl Acad Sci U S A* 118.31 (2021). ISSN: 1091-6490. DOI: 10.1073/pnas.2104059118.

[26] M. Chavent et al. "How nanoscale protein interactions determine the mesoscale dynamic organisation of bacterial outer membrane proteins". In: *Nat Commun* 9.1 (2018), p. 2846. ISSN: 2041-1723. DOI: 10.1038/s41467-018-05255-9.

[27] D. A. Nyenhuis et al. "Evidence for the Supramolecular Organization of a Bacterial Outer-Membrane Protein from In Vivo Pulse Electron Paramagnetic Resonance Spectroscopy". In: *J Am Chem Soc* 142.24 (2020), pp. 10715–10722. ISSN: 1520-5126. DOI: 10.1021/jacs.0c01754.

[28] U.S. Centers for Disease Control. *Antibiotic/Antimicrobial Resistance: Biggest Threats and Data*. Generic. 2021.

[29] P. Cornelis and J. Bodilis. "A survey of TonB-dependent receptors in fluorescent pseudomonads". In: *Environ Microbiol Rep* 1.4 (2009), pp. 256–62. ISSN: 1758-2229. DOI: 10.1111/j.1758-2229.2009.00041.x.

[30] M. Furman et al. "Salmonella typhi iron uptake mutants are attenuated in mice". In: *Infect Immun* 62.9 (1994), pp. 4091–4. ISSN: 0019-9567. DOI: 10.1128/iai.62.9.4091-4094.1994.

[31] B. L. Mortensen and E. P. Skaar. "The contribution of nutrient metal acquisition and metabolism to Acinetobacter baumannii survival within the host". In: *Front Cell Infect Microbiol* 3 (2013), p. 95. ISSN: 2235-2988. DOI: 10.3389/fcimb.2013.00095.

[32] K. D. Smith. "Iron metabolism at the host pathogen interface: lipocalin 2 and the pathogen-associated iroA gene cluster". In: *Int J Biochem Cell Biol* 39.10 (2007), pp. 1776–80. ISSN: 1357-2725. DOI: 10.1016/j.biocel.2007.07.003.

[33] V. J. Torres et al. "Staphylococcus aureus IsdB is a hemoglobin receptor required for heme iron utilization". In: *J Bacteriol* 188.24 (2006), pp. 8421–9. ISSN: 0021-9193. DOI: 10.1128/JB.01335-06.

[34] J. Wang et al. "Application of TonB-Dependent Transporters in Vaccine Development of Gram-Negative Bacteria". In: *Front Cell Infect Microbiol* 10 (2020), p. 589115. ISSN: 2235-2988. DOI: 10.3389/fcimb.2020.589115.

[35] M. F. Barber and N. C. Elde. "Escape from bacterial iron piracy through rapid evolution of transferrin". In: *Science* 346.6215 (2014), pp. 1362–6. ISSN: 1095-9203. DOI: 10.1126/science.1259329.

[36] C. Calmettes et al. "The molecular mechanism of Zinc acquisition by the neisserial outer-membrane transporter ZnuD". In: *Nat Commun* 6 (2015), p. 7996. ISSN: 2041-1723. DOI: 10.1038/ncomms8996.

[37] I. J. Schalk, G. L. Mislin, and K. Brillet. "Structure, function and binding selectivity and stereoselectivity of siderophore-iron outer membrane transporters". In: *Curr Top Membr* 69 (2012), pp. 37–66. ISSN: 1063-5823. DOI: 10.1016/B978-0-12-394390-3.00002-1.

[38] N. Gómez-Santos et al. "A TonB-dependent transporter is required for secretion of protease PopC across the bacterial outer membrane". In: *Nat Commun* 10.1 (2019), p. 1360. ISSN: 2041-1723. DOI: 10.1038/s41467-019-09366-9.

[39] B. M. Hopkinson and F. M. Morel. "The role of siderophores in iron acquisition by photosynthetic marine microorganisms". In: *Biometals* 22.4 (2009), pp. 659–69. ISSN: 1572-8773. DOI: 10.1007/s10534-009-9235-2.

[40] J. P. Gratia. "André Gratia: a forerunner in microbial and viral genetics". In: *Genetics* 156.2 (2000), pp. 471–6. ISSN: 0016-6731. DOI: 10.1093/genetics/156.2.471.

[41] E. Cascales et al. "Colicin biology". In: *Microbiol Mol Biol Rev* 71.1 (2007), pp. 158–229. ISSN: 1092-2172. DOI: 10.1128/MMBR.00036-06.

[42] W. Rabsch et al. "FepA- and TonB-dependent bacteriophage H8: receptor binding and genomic sequence". In: *J Bacteriol* 189.15 (2007), pp. 5658–74. ISSN: 0021-9193. DOI: 10.1128/JB.00437-07.

[43] A. D. Ferguson et al. "Crystal structure of the antibiotic albomycin in complex with the outer membrane transporter FhuA". In: *Protein Sci* 9.5 (2000), pp. 956–63. ISSN: 0961-8368. DOI: 10.1110/ps.9.5.956.

[44] Y. M. Lin et al. "Synthetic sideromycins (skepticism and optimism): selective generation of either broad or narrow spectrum Gram-negative antibiotics". In: *Biometals* 32.3 (2019), pp. 425–451. ISSN: 1572-8773. DOI: 10.1007/s10534-019-00192-6.

[45] Z. Chen et al. "Discovery of Fur binding site clusters in Escherichia coli by information theory models". In: *Nucleic Acids Res* 35.20 (2007), pp. 6762–77. ISSN: 1362-4962. DOI: 10.1093/nar/gkm631.

[46] P. White et al. “Exploitation of an iron transporter for bacterial protein antibiotic import”. In: *Proc Natl Acad Sci U S A* 114.45 (2017), pp. 12051–12056. ISSN: 1091-6490. DOI: 10.1073/pnas.1713741114.

[47] R. Zscherp et al. “Biomimetic enterobactin analogue mediates iron-uptake and cargo transport into”. In: *Chem Sci* 12.30 (2021), pp. 10179–10190. ISSN: 2041-6520. DOI: 10.1039/d1sc02084f.

[48] Z. Lin et al. “Total synthesis and antimicrobial evaluation of natural albomycins against clinical pathogens”. In: *Nat Commun* 9.1 (2018), p. 3445. ISSN: 2041-1723. DOI: 10.1038/s41467-018-05821-1.

[49] G. S. Tillotson. “Trojan Horse Antibiotics-A Novel Way to Circumvent Gram-Negative Bacterial Resistance?” In: *Infect Dis (Auckl)* 9 (2016), pp. 45–52. ISSN: 1178-6337. DOI: 10.4137/IDRT.S31567.

[50] R. Cohen-Khait et al. “Colicin-Mediated Transport of DNA through the Iron Transporter FepA”. In: *mBio* (2021), e0178721. ISSN: 2150-7511. DOI: 10.1128/mBio.01787-21.

[51] M. Równicki et al. “Vitamin B”. In: *Sci Rep* 7.1 (2017), p. 7644. ISSN: 2045-2322. DOI: 10.1038/s41598-017-08032-8.

[52] U.S. Food Administration and Drug. *FDA News Release: FDA approves new antibacterial drug to treat complicated urinary tract infections as part of ongoing efforts to address antimicrobial resistance*. Web Page. 2019.

[53] Y. Y. Syed. “Cefiderocol: A Review in Serious Gram-Negative Bacterial Infections”. In: *Drugs* 81.13 (2021), pp. 1559–1571. ISSN: 1179-1950. DOI: 10.1007/s40265-021-01580-4.

[54] S. M. Baghal, S. L. Gargari, and I. Rasooli. “Production and immunogenicity of recombinant ferric enterobactin protein (FepA)”. In: *Int J Infect Dis* 14 Suppl 3 (2010), e166–70. ISSN: 1878-3511. DOI: 10.1016/j.ijid.2009.12.009.

[55] D. A. Ala'Aldeen, H. A. Davies, and S. P. Borriello. "Vaccine potential of meningococcal FrpB: studies on surface exposure and functional attributes of common epitopes". In: *Vaccine* 12.6 (1994), pp. 535–41. ISSN: 0264-410X. DOI: 10.1016/0264-410x(94)90314-x.

[56] R. Dhar and J. S. Slusky. "Outer membrane protein evolution". In: *Curr Opin Struct Biol* 68 (2021), pp. 122–128. ISSN: 1879-033X. DOI: 10.1016/j.sbi.2021.01.002.

[57] M. W. Franklin et al. "Evolutionary pathways of repeat protein topology in bacterial outer membrane proteins". In: *Elife* 7 (2018). ISSN: 2050-084X. DOI: 10.7554/eLife.40308.

[58] M. Bayrhuber et al. "Structure of the human voltage-dependent anion channel". In: *Proc Natl Acad Sci U S A* 105.40 (2008), pp. 15370–5. ISSN: 1091-6490. DOI: 10.1073/pnas.0808115105.

[59] J. Pereira and A. N. Lupas. "The Origin of Mitochondria-Specific Outer Membrane β-Barrels from an Ancestral Bacterial Fragment". In: *Genome Biol Evol* 10.10 (2018), pp. 2759–2765. ISSN: 1759-6653. DOI: 10.1093/gbe/evy216.

[60] Ahmed F. Roumia et al. "OMPdb: A Global Hub of Beta-Barrel Outer Membrane Proteins". In: *Frontiers in Bioinformatics* 1.9 (2021). ISSN: 2673-7647. DOI: 10.3389/fbinf.2021.646581.

[61] G. Heijne. "The distribution of positively charged residues in bacterial inner membrane proteins correlates with the trans-membrane topology". In: *EMBO J* 5.11 (1986), pp. 3021–7. ISSN: 0261-4189.

[62] R. Jackups and J. Liang. "Interstrand pairing patterns in beta-barrel membrane proteins: the positive-outside rule, aromatic rescue, and strand registration prediction". In: *J Mol Biol* 354.4 (2005), pp. 979–93. ISSN: 0022-2836. DOI: 10.1016/j.jmb.2005.09.094.

[63] J. M. Rutz et al. “Formation of a gated channel by a ligand-specific transport protein in the bacterial outer membrane”. In: *Science* 258.5081 (1992), pp. 471–5. ISSN: 0036-8075. DOI: 10.1126/science.1411544.

[64] N. Cadieux, C. Bradbeer, and R. J. Kadner. “Sequence changes in the ton box region of BtuB affect its transport activities and interaction with TonB protein”. In: *J Bacteriol* 182.21 (2000), pp. 5954–61. ISSN: 0021-9193. DOI: 10.1128/JB.182.21.5954-5961.2000.

[65] R. J. Kadner. “Vitamin B12 transport in Escherichia coli: energy coupling between membranes”. In: *Mol Microbiol* 4.12 (1990), pp. 2027–33. ISSN: 0950-382X. DOI: 10.1111/j.1365-2958.1990.tb00562.x.

[66] J. F. Ellena et al. “Membrane thickness varies around the circumference of the transmembrane protein BtuB”. In: *Biophys J* 100.5 (2011), pp. 1280–7. ISSN: 1542-0086. DOI: 10.1016/j.bpj.2011.01.055.

[67] B. Van den Berg et al. “X-ray structure of a protein-conducting channel”. In: *Nature* 427.6969 (2004), pp. 36–44. ISSN: 1476-4687. DOI: 10.1038/nature02218.

[68] J. G. Sklar et al. “Defining the roles of the periplasmic chaperones SurA, Skp, and DegP in Escherichia coli”. In: *Genes Dev* 21.19 (2007), pp. 2473–84. ISSN: 0890-9369. DOI: 10.1101/gad.1581007.

[69] W. He et al. “Chaperone Spy Protects Outer Membrane Proteins from Folding Stress via Dynamic Complex Formation”. In: *mBio* (2021), e0213021. ISSN: 2150-7511. DOI: 10.1128/mBio.02130-21.

[70] N. K. Burgess et al. “Beta-barrel proteins that reside in the Escherichia coli outer membrane in vivo demonstrate varied folding behavior in vitro”. In: *J Biol Chem* 283.39 (2008), pp. 26748–58. ISSN: 0021-9258. DOI: 10.1074/jbc.M802754200.

[71] V. Robert et al. "Assembly factor Omp85 recognizes its outer membrane protein substrates by a species-specific C-terminal motif". In: *PLoS Biol* 4.11 (2006), e377. ISSN: 1545-7885. DOI: 10.1371/journal.pbio.0040377.

[72] J. Bakelar, S. K. Buchanan, and N. Noinaj. "The structure of the β-barrel assembly machinery complex". In: *Science* 351.6269 (2016), pp. 180–6. ISSN: 1095-9203. DOI: 10.1126/science.aad3460.

[73] H. T. Bergal et al. "The Structure of a BamA-BamD Fusion Illuminates the Architecture of the β-Barrel Assembly Machine Core". In: *Structure* 24.2 (2016), pp. 243–51. ISSN: 1878-4186. DOI: 10.1016/j.str.2015.10.030.

[74] Y. Gu et al. "Structural basis of outer membrane protein insertion by the BAM complex". In: *Nature* 531.7592 (2016), pp. 64–9. ISSN: 1476-4687. DOI: 10.1038/nature17199.

[75] S. Hussain, J. H. Peterson, and H. D. Bernstein. "Bam complex-mediated assembly of bacterial outer membrane proteins synthesized in an in vitro translation system". In: *Sci Rep* 10.1 (2020), p. 4557. ISSN: 2045-2322. DOI: 10.1038/s41598-020-61431-2.

[76] M. G. Iadanza et al. "Lateral opening in the intact β-barrel assembly machinery captured by cryo-EM". In: *Nat Commun* 7 (2016), p. 12865. ISSN: 2041-1723. DOI: 10.1038/ncomms12865.

[77] R. Rodríguez-Alonso et al. "Structural insight into the formation of lipoprotein-β-barrel complexes". In: *Nat Chem Biol* 16.9 (2020), pp. 1019–1025. ISSN: 1552-4469. DOI: 10.1038/s41589-020-0575-0.

[78] S. E. Rollauer et al. "Outer membrane protein biogenesis in Gram-negative bacteria". In: *Philos Trans R Soc Lond B Biol Sci* 370.1679 (2015). ISSN: 1471-2970. DOI: 10.1098/rstb.2015.0023.

[79] D. Tomasek et al. "Structure of a nascent membrane protein as it folds on the BAM complex". In: *Nature* 583.7816 (2020), pp. 473–478. ISSN: 1476-4687. DOI: 10.1038/s41586-020-2370-1.

[80] X. Wang, J. H. Peterson, and H. D. Bernstein. "Bacterial Outer Membrane Proteins Are Targeted to the Bam Complex by Two Parallel Mechanisms". In: *mBio* 12.3 (2021). ISSN: 2150-7511. DOI: 10.1128/mBio.00597-21.

[81] P. White et al. "The role of membrane destabilisation and protein dynamics in BAM catalysed OMP folding". In: *Nat Commun* 12.1 (2021), p. 4174. ISSN: 2041-1723. DOI: 10.1038/s41467-021-24432-x.

[82] R. Wu et al. "The big BAM theory: An open and closed case?" In: *Biochim Biophys Acta Biomembr* 1862.1 (2020), p. 183062. ISSN: 1879-2642. DOI: 10.1016/j.bbamem.2019.183062.

[83] L. Xiao et al. "Structures of the β-barrel assembly machine recognizing outer membrane protein substrates". In: *FASEB J* 35.1 (2021), e21207. ISSN: 1530-6860. DOI: 10.1096/fj.202001443RR.

[84] M. Braun et al. "In vivo reconstitution of the FhuA transport protein of Escherichia coli K-12". In: *J Bacteriol* 185.18 (2003), pp. 5508–18. ISSN: 0021-9193. DOI: 10.1128/JB.185.18.5508-5518.2003.

[85] A. Garcia-Herrero and H. J. Vogel. "Nuclear magnetic resonance solution structure of the periplasmic signalling domain of the TonB-dependent outer membrane transporter FecA from Escherichia coli". In: *Mol Microbiol* 58.5 (2005), pp. 1226–37. ISSN: 0950-382X. DOI: 10.1111/j.1365-2958.2005.04889.x.

[86] I. J. Passmore et al. "Ferric Citrate Regulator FecR Is Translocated across the Bacterial Inner Membrane via a Unique Twin-Arginine Transport-Dependent Mechanism". In: *J Bacteriol* 202.9 (2020). ISSN: 1098-5530. DOI: 10.1128/JB.00541-19.

[87] K. Hantke. "Regulation of ferric iron transport in Escherichia coli K12: isolation of a constitutive mutant". In: *Mol Gen Genet* 182.2 (1981), pp. 288–92. ISSN: 0026-8925. DOI: 10.1007/BF00269672.

[88] M. D. Lundrigan, W. Köster, and R. J. Kadner. "Transcribed sequences of the Escherichia coli btuB gene control its expression and regulation by vitamin B12". In: *Proc Natl Acad Sci U S A* 88.4 (1991), pp. 1479–83. ISSN: 0027-8424. DOI: 10.1073/pnas.88.4.1479.

[89] G. M. Young and K. Postle. "Repression of tonB transcription during anaerobic growth requires Fur binding at the promoter and a second factor binding upstream". In: *Mol Microbiol* 11.5 (1994), pp. 943–54. ISSN: 0950-382X. DOI: 10.1111/j.1365-2958.1994.tb00373.x.

[90] E. W. Althaus et al. "The ferric uptake regulation (Fur) repressor is a zinc metalloprotein". In: *Biochemistry* 38.20 (1999), pp. 6559–69. ISSN: 0006-2960. DOI: 10.1021/bi982788s.

[91] S. Enz et al. "Surface signaling in ferric citrate transport gene induction: interaction of the FecA, FecR, and FecI regulatory proteins". In: *J Bacteriol* 182.3 (2000), pp. 637–46. ISSN: 0021-9193. DOI: 10.1128/JB.182.3.637-646.2000.

[92] A. D. Ferguson et al. "Signal transduction pathway of TonB-dependent transporters". In: *Proc Natl Acad Sci U S A* 104.2 (2007), pp. 513–8. ISSN: 0027-8424. DOI: 10.1073/pnas.0609887104.

[93] R. J. Kadner and K. J. Heller. "Mutual inhibition of cobalamin and siderophore uptake systems suggests their competition for TonB function". In: *J Bacteriol* 177.17 (1995), pp. 4829–35. ISSN: 0021-9193. DOI: 10.1128/jb.177.17.4829-4835.1995.

[94] O. Mirus et al. "TonB-dependent transporters and their occurrence in cyanobacteria". In: *BMC Biol* 7 (2009), p. 68. ISSN: 1741-7007. DOI: 10.1186/1741-7007-7-68.

[95] K. Schauer, D. A. Rodionov, and H. de Reuse. "New substrates for TonB-dependent transport: do we only see the 'tip of the iceberg'?" In: *Trends Biochem Sci* 33.7 (2008), pp. 330–8. ISSN: 0968-0004. DOI: 10.1016/j.tibs.2008.04.012.

[96] A. J. Glenwright et al. "Structural basis for nutrient acquisition by dominant members of the human gut microbiota". In: *Nature* 541.7637 (2017), pp. 407–411. ISSN: 1476-4687. DOI: 10.1038/nature20828.

[97] R. M. Morris et al. "Comparative metaproteomics reveals ocean-scale shifts in microbial nutrient utilization and energy transduction". In: *ISME J* 4.5 (2010), pp. 673–85. ISSN: 1751-7370. DOI: 10.1038/ismej.2010.4.

[98] T. B. Francis et al. "Changing expression patterns of TonB-dependent transporters suggest shifts in polysaccharide consumption over the course of a spring phytoplankton bloom". In: *ISME J* 15.8 (2021), pp. 2336–2350. ISSN: 1751-7370. DOI: 10.1038/s41396-021-00928-8.

[99] M. Karlsson, K. Hannavy, and C. F. Higgins. "A sequence-specific function for the N-terminal signal-like sequence of the TonB protein". In: *Mol Microbiol* 8.2 (1993), pp. 379–88. ISSN: 0950-382X. DOI: 10.1111/j.1365-2958.1993.tb01581.x.

[100] S. D. Köhler et al. "The proline-rich domain of TonB possesses an extended polyproline II-like conformation of sufficient length to span the periplasm of Gram-negative bacteria". In: *Protein Sci* 19.4 (2010), pp. 625–30. ISSN: 1469-896X. DOI: 10.1002/pro.345.

[101] J. Koedding et al. "Dimerization of TonB is not essential for its binding to the outer membrane siderophore receptor FhuA of Escherichia coli". In: *J Biol Chem* 279.11 (2004), pp. 9978–86. ISSN: 0021-9258. DOI: 10.1074/jbc.M311720200.

[102] J. Ködding et al. "Crystal structure of a 92-residue C-terminal fragment of TonB from Escherichia coli reveals significant conformational changes compared to structures of

smaller TonB fragments". In: *J Biol Chem* 280.4 (2005), pp. 3022–8. ISSN: 0021-9258. DOI: 10.1074/jbc.M411155200.

[103] C. Chang et al. "Crystal structure of the dimeric C-terminal domain of TonB reveals a novel fold". In: *J Biol Chem* 276.29 (2001), pp. 27535–40. ISSN: 0021-9258. DOI: 10.1074/jbc.M102778200.

[104] D. M. Freed et al. "Monomeric TonB and the Ton box are required for the formation of a high-affinity transporter-TonB complex". In: *Biochemistry* 52.15 (2013), pp. 2638–48. ISSN: 1520-4995. DOI: 10.1021/bi3016108.

[105] R. Sean Peacock et al. "The solution structure of the C-terminal domain of TonB and interaction studies with TonB box peptides". In: *J Mol Biol* 345.5 (2005), pp. 1185–97. ISSN: 0022-2836. DOI: 10.1016/j.jmb.2004.11.026.

[106] M. G. Gresock, K. A. Kastead, and K. Postle. "From Homodimer to Heterodimer and Back: Elucidating the TonB Energy Transduction Cycle". In: *J Bacteriol* 197.21 (2015), pp. 3433–45. ISSN: 1098-5530. DOI: 10.1128/JB.00484-15.

[107] A. Sauter, S. P. Howard, and V. Braun. "In vivo evidence for TonB dimerization". In: *J Bacteriol* 185.19 (2003), pp. 5747–54. ISSN: 0021-9193. DOI: 10.1128/JB.185.19.5747-5754.2003.

[108] W. A. Kaserer et al. "Insight from TonB hybrid proteins into the mechanism of iron transport through the outer membrane". In: *J Bacteriol* 190.11 (2008), pp. 4001–16. ISSN: 1098-5530. DOI: 10.1128/JB.00135-08.

[109] Y. W. Lai et al. "Evolution of the Stator Elements of Rotary Prokaryote Motors". In: *J Bacteriol* 202.3 (2020). ISSN: 1098-5530. DOI: 10.1128/JB.00557-19.

[110] H. Celia, N. Noinaj, and S. K. Buchanan. "Structure and Stoichiometry of the Ton Molecular Motor". In: *Int J Mol Sci* 21.2 (2020). ISSN: 1422-0067. DOI: 10.3390/ijms21020375.

[111] A. C. Ratliff, S. K. Buchanan, and H. Celia. "Ton motor complexes". In: *Curr Opin Struct Biol* 67 (2021), pp. 95–100. ISSN: 1879-033X. DOI: 10.1016/j.sbi.2020.09.014.

[112] S. Maki-Yonekura et al. "Hexameric and pentameric complexes of the ExbBD energizer in the Ton system". In: *Elife* 7 (2018). ISSN: 2050-084X. DOI: 10.7554/eLife.35419.

[113] A. A. Ollis and K. Postle. "Identification of functionally important TonB-ExbD periplasmic domain interactions in vivo". In: *J Bacteriol* 194.12 (2012), pp. 3078–87. ISSN: 1098-5530. DOI: 10.1128/JB.00018-12.

[114] A. A. Ollis and K. Postle. "The same periplasmic ExbD residues mediate in vivo interactions between ExbD homodimers and ExbD-TonB heterodimers". In: *J Bacteriol* 193.24 (2011), pp. 6852–63. ISSN: 1098-5530. DOI: 10.1128/JB.06190-11.

[115] N. Cadieux et al. "Identification of the periplasmic cobalamin-binding protein BtuF of Escherichia coli". In: *J Bacteriol* 184.3 (2002), pp. 706–17. ISSN: 0021-9193. DOI: 10.1128/JB.184.3.706-717.2002.

[116] K. J. James et al. "TonB interacts with BtuF, the Escherichia coli periplasmic binding protein for cyanocobalamin". In: *Biochemistry* 48.39 (2009), pp. 9212–20. ISSN: 1520-4995. DOI: 10.1021/bi900722p.

[117] A. Mademidis and W. Köster. "Transport activity of FhuA, FhuC, FhuD, and FhuB derivatives in a system free of polar effects, and stoichiometry of components involved in ferrichrome uptake". In: *Mol Gen Genet* 258.1-2 (1998), pp. 156–65. ISSN: 0026-8925. DOI: 10.1007/s004380050718.

[118] R. N. Hvorup et al. "Asymmetry in the structure of the ABC transporter-binding protein complex BtuCD-BtuF". In: *Science* 317.5843 (2007), pp. 1387–90. ISSN: 1095-9203. DOI: 10.1126/science.1145950.

[119] B. C. Chu et al. "The solution structure, binding properties, and dynamics of the bacterial siderophore-binding protein FepB". In: *J Biol Chem* 289.42 (2014), pp. 29219–34. ISSN: 1083-351X. DOI: 10.1074/jbc.M114.564021.

[120] R. J. Kadner and G. L. Liggins. "Transport of vitamin B12 in Escherichia coli: genetic studies". In: *J Bacteriol* 115.2 (1973), pp. 514–21. ISSN: 0021-9193. DOI: 10.1128/jb.115.2.514-521.1973.

[121] J. C. White et al. "Transport of vitamin B 12 in Escherichia coli. Location and properties of the initial B 12 -binding site". In: *J Biol Chem* 248.11 (1973), pp. 3978–86. ISSN: 0021-9258.

[122] P. J. Bassford and R. J. kadner. "Genetic analysis of components involved in vitamin B12 uptake in Escherichia coli". In: *J Bacteriol* 132.3 (1977), pp. 796–805. ISSN: 0021-9193. DOI: 10.1128/jb.132.3.796-805.1977.

[123] D. P. Chimento et al. "Substrate-induced transmembrane signaling in the cobalamin transporter BtuB". In: *Nat Struct Biol* 10.5 (2003), pp. 394–401. ISSN: 1072-8368. DOI: 10.1038/nsb914.

[124] D. D. Shultis et al. "Outer membrane active transport: structure of the BtuB:TonB complex". In: *Science* 312.5778 (2006), pp. 1396–9. ISSN: 1095-9203. DOI: 10.1126/science.1127694.

[125] V. Cherezov et al. "In meso structure of the cobalamin transporter, BtuB, at 1.95 A resolution". In: *J Mol Biol* 364.4 (2006), pp. 716–34. ISSN: 0022-2836. DOI: 10.1016/j.jmb.2006.09.022.

[126] O. Sharma et al. "Structure of the complex of the colicin E2 R-domain and its BtuB receptor. The outer membrane colicin translocon". In: *J Biol Chem* 282.32 (2007), pp. 23163–70. ISSN: 0021-9258. DOI: 10.1074/jbc.M703004200.

[127] G. Kurisu et al. “The structure of BtuB with bound colicin E3 R-domain implies a translocon”. In: *Nat Struct Biol* 10.11 (2003), pp. 948–54. ISSN: 1072-8368. DOI: 10.1038/nsb997.

[128] D. M. Freed et al. “Conformational exchange in a membrane transport protein is altered in protein crystals”. In: *Biophys J* 99.5 (2010), pp. 1604–10. ISSN: 1542-0086. DOI: 10.1016/j.bpj.2010.06.026.

[129] D. M. Freed et al. “Molecular origin of electron paramagnetic resonance line shapes on β-barrel membrane proteins: the local solvation environment modulates spin-label configuration”. In: *Biochemistry* 50.41 (2011), pp. 8792–803. ISSN: 1520-4995. DOI: 10.1021/bi200971x.

[130] W. M. Yau et al. “The preference of tryptophan for membrane interfaces”. In: *Biochemistry* 37.42 (1998), pp. 14713–8. ISSN: 0006-2960. DOI: 10.1021/bi980809c.

[131] N. Cadieux, N. Barekzi, and C. Bradbeer. “Observations on the calcium dependence and reversibility of cobalamin transport across the outer membrane of Escherichia coli”. In: *J Biol Chem* 282.48 (2007), pp. 34921–8. ISSN: 0021-9258. DOI: 10.1074/jbc.M707426200.

[132] Q. Xu et al. “Substrate-dependent unfolding of the energy coupling motif of a membrane transport protein determined by double electron-electron resonance”. In: *Biochemistry* 45.36 (2006), pp. 10847–54. ISSN: 0006-2960. DOI: 10.1021/bi061051x.

[133] T. D. Nilaweera, D. A. Nyenhuis, and D. S. Cafiso. “Structural intermediates observed only in intact Escherichia coli indicate a mechanism for TonB-dependent transport”. In: *Elife* 10 (2021). ISSN: 2050-084X. DOI: 10.7554/eLife.68548.

[134] D. P. Chimento, R. J. Kadner, and M. C. Wiener. “Comparative structural analysis of TonB-dependent outer membrane transporters: implications for the transport cycle”. In: *Proteins* 59.2 (2005), pp. 240–51. ISSN: 1097-0134. DOI: 10.1002/prot.20416.

[135] L. D. Jordan et al. “Energy-dependent motion of TonB in the Gram-negative bacterial inner membrane”. In: *Proc Natl Acad Sci U S A* 110.28 (2013), pp. 11553–8. ISSN: 1091-6490. DOI: 10.1073/pnas.1304243110.

[136] S. J. Hickman et al. “Gating of TonB-dependent transporters by substrate-specific forced remodelling”. In: *Nat Commun* 8 (2017), p. 14804. ISSN: 2041-1723. DOI: 10.1038/ncomms14804.

[137] R. H. Flores Jiménez and D. S. Cafiso. “The N-terminal domain of a TonB-dependent transporter undergoes a reversible stepwise denaturation”. In: *Biochemistry* 51.17 (2012), pp. 3642–50. ISSN: 1520-4995. DOI: 10.1021/bi300118a.

[138] T. Pieńko and J. Trylska. “Extracellular loops of BtuB facilitate transport of vitamin B12 through the outer membrane of E. coli”. In: *PLoS Comput Biol* 16.7 (2020), e1008024. ISSN: 1553-7358. DOI: 10.1371/journal.pcbi.1008024.

[139] C. Balusek and J. C. Gumbart. “Role of the Native Outer-Membrane Environment on the Transporter BtuB”. In: *Biophys J* 111.7 (2016), pp. 1409–1417. ISSN: 1542-0086. DOI: 10.1016/j.bpj.2016.08.033.

[140] J. Gumbart, M. C. Wiener, and E. Tajkhorshid. “Mechanics of force propagation in TonB-dependent outer membrane transport”. In: *Biophys J* 93.2 (2007), pp. 496–504. ISSN: 0006-3495. DOI: 10.1529/biophysj.107.104158.

[141] M. G. Gresock et al. “Death of the TonB Shuttle Hypothesis”. In: *Front Microbiol* 2 (2011), p. 206. ISSN: 1664-302X. DOI: 10.3389/fmicb.2011.00206.

[142] R. L. Baldwin. “Early days of protein hydrogen exchange: 1954-1972”. In: *Proteins* 79.7 (2011), pp. 2021–6. ISSN: 1097-0134. DOI: 10.1002/prot.23039.

[143] A. HVIDT et al. “Exchange of deuterium and 18O between water and other substances. I. Methods”. In: *C R Trav Lab Carlsberg Chim* 29.9 (1954), pp. 129–57.

[144] S. W. ENGLANDER. "A HYDROGEN EXCHANGE METHOD USING TRITIUM AND SEPHADEX: ITS APPLICATION TO RIBONUCLEASE". In: *Biochemistry* 2 (1963), pp. 798–807. ISSN: 0006-2960. DOI: 10.1021/bi00904a030.

[145] S. O. NIELSEN, W. P. BRYAN, and K. MIKKELSEN. "Hydrogen-deuterium exchange of small peptides in aqueous solution". In: *Biochim Biophys Acta* 42 (1960), pp. 550–2. ISSN: 0006-3002. DOI: 10.1016/0006-3002(60)90842-8.

[146] S. W. Englander et al. "Mechanisms and uses of hydrogen exchange". In: *Curr Opin Struct Biol* 6.1 (1996), pp. 18–23. ISSN: 0959-440X. DOI: 10.1016/s0959-440x(96)80090-x.

[147] I. R. Kleckner and M. P. Foster. "An introduction to NMR-based approaches for measuring protein dynamics". In: *Biochim Biophys Acta* 1814.8 (2011), pp. 942–68. ISSN: 0006-3002. DOI: 10.1016/j.bbapap.2010.10.012.

[148] W. Hu et al. "Stepwise protein folding at near amino acid resolution by hydrogen exchange and mass spectrometry". In: *Proc Natl Acad Sci U S A* 110.19 (2013), pp. 7684–9. ISSN: 1091-6490. DOI: 10.1073/pnas.1305887110.

[149] B. T. Walters et al. "Folding of a large protein at high structural resolution". In: *Proc Natl Acad Sci U S A* 110.47 (2013), pp. 18898–903. ISSN: 1091-6490. DOI: 10.1073/pnas.1319482110.

[150] M. Giladi and D. Khananshvili. "Hydrogen-Deuterium Exchange Mass-Spectrometry of Secondary Active Transporters: From Structural Dynamics to Molecular Mechanisms". In: *Front Pharmacol* 11 (2020), p. 70. ISSN: 1663-9812. DOI: 10.3389/fphar.2020.00070.

[151] G. R. Masson, M. L. Jenkins, and J. E. Burke. "An overview of hydrogen deuterium exchange mass spectrometry (HDX-MS) in drug discovery". In: *Expert Opin Drug Discov* 12.10 (2017), pp. 981–994. ISSN: 1746-045X. DOI: 10.1080/17460441.2017.1363734.

[152] B. Deng, C. Lento, and D. J. Wilson. "Hydrogen deuterium exchange mass spectrometry in biopharmaceutical discovery and development - A review". In: *Anal Chim Acta* 940 (2016), pp. 8–20. ISSN: 1873-4324. DOI: 10.1016/j.aca.2016.08.006.

[153] J. Pan et al. "Hydrogen/deuterium exchange mass spectrometry with top-down electron capture dissociation for characterizing structural transitions of a 17 kDa protein". In: *J Am Chem Soc* 131.35 (2009), pp. 12801–8. ISSN: 1520-5126. DOI: 10.1021/ja904379w.

[154] G. R. Masson et al. "Recommendations for performing, interpreting and reporting hydrogen deuterium exchange mass spectrometry (HDX-MS) experiments". In: *Nat Methods* 16.7 (2019), pp. 595–602. ISSN: 1548-7105. DOI: 10.1038/s41592-019-0459-y.

[155] K. D. Rand et al. "Gas-phase hydrogen/deuterium exchange in a traveling wave ion guide for the examination of protein conformations". In: *Anal Chem* 81.24 (2009), pp. 10019–28. ISSN: 1520-6882. DOI: 10.1021/ac901897x.

[156] U. H. Mistarz and K. D. Rand. "Installation, validation, and application examples of two instrumental setups for gas-phase HDX-MS analysis of peptides and proteins". In: *Methods* 144 (2018), pp. 113–124. ISSN: 1095-9130. DOI: 10.1016/j.ymeth.2018.05.002.

[157] Y. Li et al. "Characterizing protein structure in amorphous solids using hydrogen/deuterium exchange with mass spectrometry". In: *Anal Biochem* 366.1 (2007), pp. 18–28. ISSN: 0003-2697. DOI: 10.1016/j.ab.2007.03.041.

[158] B. S. Moorthy et al. "Solid-State Hydrogen-Deuterium Exchange Mass Spectrometry: Correlation of Deuterium Uptake and Long-Term Stability of Lyophilized Monoclonal Antibody Formulations". In: *Mol Pharm* 15.1 (2018), pp. 1–11. ISSN: 1543-8392. DOI: 10.1021/acs.molpharmaceut.7b00504.

[159] A. Hvidt and S. O. Nielsen. "Hydrogen exchange in proteins". In: *Adv Protein Chem* 21 (1966), pp. 287–386. ISSN: 0065-3233. DOI: 10.1016/s0065-3233(08)60129-1.

[160] Y. Deng, Z. Zhang, and D. L. Smith. "Comparison of continuous and pulsed labeling amide hydrogen exchange/mass spectrometry for studies of protein dynamics". In: *J Am Soc Mass Spectrom* 10.8 (1999), pp. 675–84. ISSN: 1044-0305. DOI: 10.1016/S1044-0305(99)00038-0.

[161] M. Miyagi and T. Nakazawa. "Determination of pKa values of individual histidine residues in proteins using mass spectrometry". In: *Anal Chem* 80.17 (2008), pp. 6481–7. ISSN: 1520-6882. DOI: 10.1021/ac8009643.

[162] J. Pan et al. "Higher-order structural interrogation of antibodies using middle-down hydrogen/deuterium exchange mass spectrometry". In: *Chem Sci* 7.2 (2016), pp. 1480–1486. ISSN: 2041-6520. DOI: 10.1039/c5sc03420e.

[163] R. R. Abzalimov and I. A. Kaltashov. "Controlling hydrogen scrambling in multiply charged protein ions during collisional activation: implications for top-down hydrogen/deuterium exchange MS utilizing collisional activation in the gas phase". In: *Anal Chem* 82.3 (2010), pp. 942–50. ISSN: 1520-6882. DOI: 10.1021/ac9021874.

[164] T. E. Wales et al. "Subzero Celsius separations in three-zone temperature controlled hydrogen deuterium exchange mass spectrometry". In: *J Chromatogr A* 1523 (2017), pp. 275–282. ISSN: 1873-3778. DOI: 10.1016/j.chroma.2017.05.067.

[165] V. Calvaresi et al. "Hydrogen-Deuterium Exchange Mass Spectrometry with Integrated Size-Exclusion Chromatography for Analysis of Complex Protein Samples". In: *Anal Chem* 93.33 (2021), pp. 11406–11414. ISSN: 1520-6882. DOI: 10.1021/acs.analchem.1c01171.

[166] M. J. Watson et al. "Simple Platform for Automating Decoupled LC-MS Analysis of Hydrogen/Deuterium Exchange Samples". In: *J Am Soc Mass Spectrom* 32.2 (2021), pp. 597–600. ISSN: 1879-1123. DOI: 10.1021/jasms.0c00341.

[167] A. Espada et al. “A Decoupled Automation Platform for Hydrogen/Deuterium Exchange Mass Spectrometry Experiments”. In: *J Am Soc Mass Spectrom* 30.12 (2019), pp. 2580–2583. ISSN: 1879-1123. DOI: 10.1007/s13361-019-02331-2.

[168] J. Ahn et al. “Pepsin immobilized on high-strength hybrid particles for continuous flow online digestion at 10,000 psi”. In: *Anal Chem* 84.16 (2012), pp. 7256–62. ISSN: 1520-6882. DOI: 10.1021/ac301749h.

[169] Y. Wu, S. Kaveti, and J. R. Engen. “Extensive deuterium back-exchange in certain immobilized pepsin columns used for H/D exchange mass spectrometry”. In: *Anal Chem* 78.5 (2006), pp. 1719–23. ISSN: 0003-2700. DOI: 10.1021/ac0518497.

[170] Z. Zhang and D. L. Smith. “Determination of amide hydrogen exchange by mass spectrometry: a new tool for protein structure elucidation”. In: *Protein Sci* 2.4 (1993), pp. 522–31. ISSN: 0961-8368. DOI: 10.1002/pro.5560020404.

[171] C. Vorauer et al. “Rapid Assessment of Pepsin Column Activity for Reliable HDX-MS Studies”. In: *J Am Soc Mass Spectrom* 32.9 (2021), pp. 2386–2390. ISSN: 1879-1123. DOI: 10.1021/jasms.1c00080.

[172] L. Cravello, D. Lascoux, and E. Forest. “Use of different proteases working in acidic conditions to improve sequence coverage and resolution in hydrogen/deuterium exchange of large proteins”. In: *Rapid Commun Mass Spectrom* 17.21 (2003), pp. 2387–93. ISSN: 0951-4198. DOI: 10.1002/rcm.1207.

[173] M. Rey et al. “Recombinant immobilized rhizopuspepsin as a new tool for protein digestion in hydrogen/deuterium exchange mass spectrometry”. In: *Rapid Commun Mass Spectrom* 23.21 (2009), pp. 3431–8. ISSN: 1097-0231. DOI: 10.1002/rcm.4260.

[174] M. Rey et al. “Nepenthesin from monkey cups for hydrogen/deuterium exchange mass spectrometry”. In: *Mol Cell Proteomics* 12.2 (2013), pp. 464–72. ISSN: 1535-9484. DOI: 10.1074/mcp.M112.025221.

[175] L. Tsiatsiani et al. "Aspergillus niger Prolyl Endoprotease for Hydrogen-Deuterium Exchange Mass Spectrometry and Protein Structural Studies". In: *Anal Chem* 89.15 (2017), pp. 7966–7973. ISSN: 1520-6882. DOI: 10.1021/acs.analchem.7b01161.

[176] Y. Hamuro and T. Zhang. "High-Resolution HDX-MS of Cytochrome c Using Pepsin/Fungal Protease Type XIII Mixed Bed Column". In: *J Am Soc Mass Spectrom* 30.2 (2019), pp. 227–234. ISSN: 1879-1123. DOI: 10.1007/s13361-018-2087-7.

[177] J. Mullahoo et al. "Dual protease type XIII/pepsin digestion offers superior resolution and overlap for the analysis of histone tails by HX-MS". In: *Methods* 184 (2020), pp. 135–140. ISSN: 1095-9130. DOI: 10.1016/j.ymeth.2020.01.016.

[178] B. T. Walters et al. "Minimizing back exchange in the hydrogen exchange-mass spectrometry experiment". In: *J Am Soc Mass Spectrom* 23.12 (2012), pp. 2132–9. ISSN: 1879-1123. DOI: 10.1007/s13361-012-0476-x.

[179] A. N. Hoofnagle, K. A. Resing, and N. G. Ahn. "Protein analysis by hydrogen exchange mass spectrometry". In: *Annu Rev Biophys Biomol Struct* 32 (2003), pp. 1–25. ISSN: 1056-8700. DOI: 10.1146/annurev.biophys.32.110601.142417.

[180] L. Mayne et al. "Many overlapping peptides for protein hydrogen exchange experiments by the fragment separation-mass spectrometry method". In: *J Am Soc Mass Spectrom* 22.11 (2011), pp. 1898–905. ISSN: 1879-1123. DOI: 10.1007/s13361-011-0235-4.

[181] I. R. Möller et al. "Improving the Sequence Coverage of Integral Membrane Proteins during Hydrogen/Deuterium Exchange Mass Spectrometry Experiments". In: *Anal Chem* 91.17 (2019), pp. 10970–10978. ISSN: 1520-6882. DOI: 10.1021/acs.analchem.9b00973.

[182] E. I. James et al. "Advances in Hydrogen/Deuterium Exchange Mass Spectrometry and the Pursuit of Challenging Biological Systems". In: *Chem Rev* (2021). ISSN: 1520-6890. DOI: 10.1021/acs.chemrev.1c00279.

[183] T. A. Rhomberg et al. “Proteomic analysis of the sarcosine-insoluble outer membrane fraction of the bacterial pathogen Bartonella henselae”. In: *Proteomics* 4.10 (2004), pp. 3021–33. ISSN: 1615-9853. DOI: 10.1002/pmic.200400933.

[184] Z. Y. Kan et al. “ExMS: data analysis for HX-MS experiments”. In: *J Am Soc Mass Spectrom* 22.11 (2011), pp. 1906–15. ISSN: 1879-1123. DOI: 10.1007/s13361-011-0236-3.

[185] Z. Y. Kan et al. “ExMS2: An Integrated Solution for Hydrogen-Deuterium Exchange Mass Spectrometry Data Analysis”. In: *Anal Chem* 91.11 (2019), pp. 7474–7481. ISSN: 1520-6882. DOI: 10.1021/acs.analchem.9b01682.

[186] R. K. Hansen et al. “Hydrogen/deuterium exchange of hydrophobic peptides in model membranes by electrospray ionization mass spectrometry”. In: *J Am Soc Mass Spectrom* 13.12 (2002), pp. 1376–87. ISSN: 1044-0305. DOI: 10.1016/S1044-0305(02)00702-X.

[187] S. Akashi and K. Takio. “Structure of melittin bound to phospholipid micelles studied using hydrogen-deuterium exchange and electrospray ionization Fourier transform ion cyclotron resonance mass spectrometry”. In: *J Am Soc Mass Spectrom* 12.12 (2001), pp. 1247–53. ISSN: 1044-0305. DOI: 10.1016/S1044-0305(01)00314-2.

[188] M. Rey et al. “Effective removal of nonionic detergents in protein mass spectrometry, hydrogen/deuterium exchange, and proteomics”. In: *Anal Chem* 82.12 (2010), pp. 5107–16. ISSN: 1520-6882. DOI: 10.1021/ac100171m.

[189] B. S. Antharavally et al. “Efficient removal of detergents from proteins and peptides in a spin column format”. In: *Anal Biochem* 416.1 (2011), pp. 39–44. ISSN: 1096-0309. DOI: 10.1016/j.ab.2011.05.013.

[190] G. Schnell et al. “Discovery and targeted proteomics on cutaneous biopsies infected by borrelia to investigate lyme disease”. In: *Mol Cell Proteomics* 14.5 (2015), pp. 1254–64. ISSN: 1535-9484. DOI: 10.1074/mcp.M114.046540.

[191] R. Maldonado-Hernández et al. "Sequential purification and characterization of Torpedo californica nAChR-DC supplemented with CHS for high-resolution crystallization studies". In: *Anal Biochem* 610 (2020), p. 113887. ISSN: 1096-0309. DOI: 10.1016/j.ab.2020.113887.

[192] C. M. Hebling et al. "Conformational analysis of membrane proteins in phospholipid bilayer nanodiscs by hydrogen exchange mass spectrometry". In: *Anal Chem* 82.13 (2010), pp. 5415–9. ISSN: 1520-6882. DOI: 10.1021/ac100962c.

[193] K. W. Anderson, E. S. Gallagher, and J. W. Hudgens. "Automated Removal of Phospholipids from Membrane Proteins for H/D Exchange Mass Spectrometry Workflows". In: *Anal Chem* 90.11 (2018), pp. 6409–6412. ISSN: 1520-6882. DOI: 10.1021/acs.analchem.8b00429.

[194] N. M. Duc et al. "Effective application of bicelles for conformational analysis of G protein-coupled receptors by hydrogen/deuterium exchange mass spectrometry". In: *J Am Soc Mass Spectrom* 26.5 (2015), pp. 808–817. ISSN: 1879-1123. DOI: 10.1007/s13361-015-1083-4.

[195] E. Reading et al. "Interrogating Membrane Protein Conformational Dynamics within Native Lipid Compositions". In: *Angew Chem Int Ed Engl* 56.49 (2017), pp. 15654–15657. ISSN: 1521-3773. DOI: 10.1002/anie.201709657.

[196] D. Donnarumma et al. "Native State Organization of Outer Membrane Porins Unraveled by HDx-MS". In: *J Proteome Res* 17.5 (2018), pp. 1794–1800. ISSN: 1535-3907. DOI: 10.1021/acs.jproteome.7b00830.

[197] M. Miethke and M. A. Marahiel. "Siderophore-based iron acquisition and pathogen control". In: *Microbiol Mol Biol Rev* 71.3 (2007), pp. 413–51. ISSN: 1092-2172. DOI: 10.1128/MMBR.00012-07.

[198] C. R. Smallwood et al. "Concerted loop motion triggers induced fit of FepA to ferric enterobactin". In: *J Gen Physiol* 144.1 (2014), pp. 71–80. ISSN: 1540-7748. DOI: 10.1085/jgp.201311159.

[199] N. Noinaj et al. "TonB-dependent transporters: regulation, structure, and function". In: *Annu Rev Microbiol* 64 (2010), pp. 43–60. ISSN: 1545-3251. DOI: 10.1146/annurev.micro.112408.134247.

[200] N. Cadieux and R. J. Kadner. "Site-directed disulfide bonding reveals an interaction site between energy-coupling protein TonB and BtuB, the outer membrane cobalamin transporter". In: *Proc Natl Acad Sci U S A* 96.19 (1999), pp. 10673–8. ISSN: 0027-8424. DOI: 10.1073/pnas.96.19.10673.

[201] P. E. Klebba. "ROSET Model of TonB Action in Gram-Negative Bacterial Iron Acquisition". In: *J Bacteriol* 198.7 (2016), pp. 1013–21. ISSN: 1098-5530. DOI: 10.1128/JB.00823-15.

[202] S. M. Lukasik, K. W. Ho, and D. S. Cafiso. "Molecular basis for substrate-dependent transmembrane signaling in an outer-membrane transporter". In: *J Mol Biol* 370.5 (2007), pp. 807–11. ISSN: 0022-2836. DOI: 10.1016/j.jmb.2007.05.040.

[203] D. A. Nyenhuis, T. D. Nilaweera, and D. S. Cafiso. "Native Cell Environment Constrains Loop Structure in the Escherichia coli Cobalamin Transporter BtuB". In: *Biophys J* 119.8 (2020), pp. 1550–1557. ISSN: 1542-0086. DOI: 10.1016/j.bpj.2020.08.034.

[204] A. Sikora et al. "Allosteric Signaling Is Bidirectional in an Outer-Membrane Transport Protein". In: *Biophys J* 111.9 (2016), pp. 1908–1918. ISSN: 1542-0086. DOI: 10.1016/j.bpj.2016.09.038.

[205] G. S. Moeck et al. "Ligand-induced conformational change in the ferrichrome-iron receptor of Escherichia coli K-12". In: *Mol Microbiol* 22.3 (1996), pp. 459–71. ISSN: 0950-382X. DOI: 10.1046/j.1365-2958.1996.00112.x.

[206] G. E. Fanucci et al. “Competing ligands stabilize alternate conformations of the energy coupling motif of a TonB-dependent outer membrane transporter”. In: *Proc Natl Acad Sci U S A* 100.20 (2003), pp. 11382–7. ISSN: 0027-8424. DOI: 10.1073/pnas.1932486100.

[207] Y. Bai et al. “Primary structure effects on peptide group hydrogen exchange”. In: *Proteins* 17.1 (1993), pp. 75–86. ISSN: 0887-3585. DOI: 10.1002/prot.340170110.

[208] I. Meuskens et al. “A New Strain Collection for Improved Expression of Outer Membrane Proteins”. In: *Front Cell Infect Microbiol* 7 (2017), p. 464. ISSN: 2235-2988. DOI: 10.3389/fcimb.2017.00464.

[209] M. A. Lomize et al. “OPM database and PPM web server: resources for positioning of proteins in membranes”. In: *Nucleic Acids Res* 40.Database issue (2012), pp. D370–6. ISSN: 1362-4962. DOI: 10.1093/nar/gkr703.

[210] S. S. Jaswal and A. D. Miranker. “Scope and utility of hydrogen exchange as a tool for mapping landscapes”. In: *Protein Sci* 16.11 (2007), pp. 2378–90. ISSN: 0961-8368. DOI: 10.1110/ps.072994207.

[211] S. W. Englander and N. R. Kallenbach. “Hydrogen exchange and structural dynamics of proteins and nucleic acids”. In: *Q Rev Biophys* 16.4 (1983), pp. 521–655. ISSN: 0033-5835. DOI: 10.1017/s0033583500005217.

[212] H. Gong, G. Hocky, and K. F. Freed. “Influence of nonlinear electrostatics on transfer energies between liquid phases: charge burial is far less expensive than Born model”. In: *Proc Natl Acad Sci U S A* 105.32 (2008), pp. 11146–51. ISSN: 1091-6490. DOI: 10.1073/pnas.0804506105.

[213] J. L. Sarver et al. “A Dynamic Protein-Protein Coupling between the TonB-Dependent Transporter FhuA and TonB”. In: *Biochemistry* 57.6 (2018), pp. 1045–1053. ISSN: 1520-4995. DOI: 10.1021/acs.biochem.7b01223.

[214] Ashlee Plummer, Dennis Gessmann, and Karen Fleming. "The Role of a Destabilized Membrane for OMP Insertion". In: *The BAM Complex: Methods and Protocols*. Ed. by Susan Buchanan and Nicholas Noinaj. 1st ed. Methods in Molecular Biology. New York Heidelberg Dordrecht London: Humana Press, 2015. Chap. 5, pp. 57–65. DOI: 10.1007/978-1-4939-2871-2.

[215] J. Huerta-Cepas et al. "eggNOG 5.0: a hierarchical, functionally and phylogenetically annotated orthology resource based on 5090 organisms and 2502 viruses". In: *Nucleic Acids Res* 47.D1 (2019), pp. D309–D314. ISSN: 1362-4962. DOI: 10.1093/nar/gky1085.

[216] R. C. Edgar. "MUSCLE: multiple sequence alignment with high accuracy and high throughput". In: *Nucleic Acids Res* 32.5 (2004), pp. 1792–7. ISSN: 1362-4962. DOI: 10.1093/nar/gkh340.

[217] F. Madeira et al. "The EMBL-EBI search and sequence analysis tools APIs in 2019". In: *Nucleic Acids Res* 47.W1 (2019), W636–W641. ISSN: 1362-4962. DOI: 10.1093/nar/gkz268.

[218] P. Sheffield, S. Garrard, and Z. Derewenda. "Overcoming expression and purification problems of RhoGDI using a family of "parallel" expression vectors". In: *Protein Expr Purif* 15.1 (1999), pp. 34–9. ISSN: 1046-5928. DOI: 10.1006/prep.1998.1003.

[219] A. Gudmundsdottir et al. "Point mutations in a conserved region (TonB box) of Escherichia coli outer membrane protein BtuB affect vitamin B12 transport". In: *J Bacteriol* 171.12 (1989), pp. 6526–33. ISSN: 0021-9193. DOI: 10.1128/jb.171.12.6526-6533.1989.

[220] K. C. Usher et al. "The plug domain of FepA, a TonB-dependent transport protein from Escherichia coli, binds its siderophore in the absence of the transmembrane barrel domain". In: *Proc Natl Acad Sci U S A* 98.19 (2001), pp. 10676–81. ISSN: 0027-8424. DOI: 10.1073/pnas.181353398.

[221] S. Nauli et al. “Crystal structures and increased stabilization of the protein G variants with switched folding pathways NuG1 and NuG2”. In: *Protein Sci* 11.12 (2002), pp. 2924–31. ISSN: 0961-8368. DOI: 10.1110/ps.0216902.

[222] J. A. Riback et al. “Innovative scattering analysis shows that hydrophobic disordered proteins are expanded in water”. In: *Science* 358.6360 (2017), pp. 238–241. ISSN: 1095-9203. DOI: 10.1126/science.aan5774.

[223] M. C. Wiener. “TonB-dependent outer membrane transport: going for Baroque?” In: *Curr Opin Struct Biol* 15.4 (2005), pp. 394–400. ISSN: 0959-440X. DOI: 10.1016/j.sbi.2005.07.001.

[224] S. Wang, J. Peng, and J. Xu. “Alignment of distantly related protein structures: algorithm, bound and implications to homology modeling”. In: *Bioinformatics* 27.18 (2011), pp. 2537–45. ISSN: 1367-4811. DOI: 10.1093/bioinformatics/btr432.

[225] C. Woodward, I. Simon, and E. Tüchsen. “Hydrogen exchange and the dynamic structure of proteins”. In: *Mol Cell Biochem* 48.3 (1982), pp. 135–60. ISSN: 0300-8177. DOI: 10.1007/BF00421225.

[226] J. S. Anderson, D. M. LeMaster, and G. Hernández. “Electrostatic potential energy within a protein monitored by metal charge-dependent hydrogen exchange”. In: *Biophys J* 91.11 (2006), pp. L93–5. ISSN: 0006-3495. DOI: 10.1529/biophysj.106.094219.

[227] J. B. Matthew and F. M. Richards. “The pH dependence of hydrogen exchange in proteins”. In: *J Biol Chem* 258.5 (1983), pp. 3039–44. ISSN: 0021-9258.

[228] X. Yan et al. “Deuterium exchange and mass spectrometry reveal the interaction differences of two synthetic modulators of RXRalpha LBD”. In: *Protein Sci* 16.11 (2007), pp. 2491–501. ISSN: 0961-8368. DOI: 10.1110/ps.073019707.

[229] J. J. Skinner et al. “Protein hydrogen exchange: testing current models”. In: *Protein Sci* 21.7 (2012), pp. 987–95. ISSN: 1469-896X. DOI: 10.1002/pro.2082.

[230] R. G. McAllister and L. Konermann. "Challenges in the interpretation of protein h/d exchange data: a molecular dynamics simulation perspective". In: *Biochemistry* 54.16 (2015), pp. 2683–92. ISSN: 1520-4995. DOI: 10.1021/acs.biochem.5b00215.

[231] M. van Rosmalen, M. Krom, and M. Merkx. "Tuning the Flexibility of Glycine-Serine Linkers To Allow Rational Design of Multidomain Proteins". In: *Biochemistry* 56.50 (2017), pp. 6565–6574. ISSN: 1520-4995. DOI: 10.1021/acs.biochem.7b00902.

[232] Y. Hamuro et al. "Rapid analysis of protein structure and dynamics by hydrogen/deuterium exchange mass spectrometry". In: *J Biomol Tech* 14.3 (2003), pp. 171–82. ISSN: 1524-0215.

[233] Y. Bai et al. "Protein folding intermediates: native-state hydrogen exchange". In: *Science* 269.5221 (1995), pp. 192–7. ISSN: 0036-8075. DOI: 10.1126/science.7618079.

[234] Z. Zheng and T. R. Sosnick. "Protein vivisection reveals elusive intermediates in folding". In: *J Mol Biol* 397.3 (2010), pp. 777–88. ISSN: 1089-8638. DOI: 10.1016/j.jmb.2010.01.056.

[235] M. Kim, G. E. Fanucci, and D. S. Cafiso. "Substrate-dependent transmembrane signaling in TonB-dependent transporters is not conserved". In: *Proc Natl Acad Sci U S A* 104.29 (2007), pp. 11975–80. ISSN: 0027-8424. DOI: 10.1073/pnas.0702172104.

[236] D. Cobessi, A. Meksem, and K. Brillet. "Structure of the heme/hemoglobin outer membrane receptor ShuA from Shigella dysenteriae: heme binding by an induced fit mechanism". In: *Proteins* 78.2 (2010), pp. 286–94. ISSN: 1097-0134. DOI: 10.1002/prot.22539.

[237] A. D. Ferguson et al. "Structural basis of gating by the outer membrane transporter FecA". In: *Science* 295.5560 (2002), pp. 1715–9. ISSN: 1095-9203. DOI: 10.1126/science.1067313.

[238] I. D. Sahu. "Conformational Dynamics of the Extracellular Loop of BtuB in Whole Cells". In: *Biophys J* 119.8 (2020), pp. 1470–1471. ISSN: 1542-0086. DOI: 10.1016/j.bpj.2020.09.018.

[239] Z. Cao et al. "Aromatic components of two ferric enterobactin binding sites in Escherichia coli FepA". In: *Mol Microbiol* 37.6 (2000), pp. 1306–17. ISSN: 0950-382X. DOI: 10.1046/j.1365-2958.2000.02093.x.

[240] M. A. Payne et al. "Biphasic binding kinetics between FepA and its ligands". In: *J Biol Chem* 272.35 (1997), pp. 21950–5. ISSN: 0021-9258. DOI: 10.1074/jbc.272.35.21950.

[241] L. Moynié et al. "The complex of ferric-enterobactin with its transporter from Pseudomonas aeruginosa suggests a two-site model". In: *Nat Commun* 10.1 (2019), p. 3673. ISSN: 2041-1723. DOI: 10.1038/s41467-019-11508-y.

[242] S. K. Buchanan et al. "Structure of colicin I receptor bound to the R-domain of colicin Ia: implications for protein import". In: *EMBO J* 26.10 (2007), pp. 2594–604. ISSN: 0261-4189. DOI: 10.1038/sj.emboj.7601693.

[243] L. Moynié et al. "Structure and Function of the PiuA and PirA Siderophore-Drug Receptors from Pseudomonas aeruginosa and Acinetobacter baumannii". In: *Antimicrob Agents Chemother* 61.4 (2017). ISSN: 1098-6596. DOI: 10.1128/AAC.02531-16.

[244] H. M. Zhang et al. "Simultaneous reduction and digestion of proteins with disulfide bonds for hydrogen/deuterium exchange monitored by mass spectrometry". In: *Anal Chem* 82.4 (2010), pp. 1450–4. ISSN: 1520-6882. DOI: 10.1021/ac902550n.

[245] F. Endriss et al. "Mutant analysis of the Escherichia coli FhuA protein reveals sites of FhuA activity". In: *J Bacteriol* 185.16 (2003), pp. 4683–92. ISSN: 0021-9193. DOI: 10.1128/JB.185.16.4683-4692.2003.

[246] L. Ma et al. "Evidence of ball-and-chain transport of ferric enterobactin through FepA". In: *J Biol Chem* 282.1 (2007), pp. 397–406. ISSN: 0021-9258. DOI: 10.1074/jbc.M605333200.

[247] H. A. Eisenhauer et al. "Siderophore transport through Escherichia coli outer membrane receptor FhuA with disulfide-tethered cork and barrel domains". In: *J Biol Chem* 280.34 (2005), pp. 30574–80. ISSN: 0021-9258. DOI: 10.1074/jbc.M506708200.

[248] A. Majumdar et al. "Conformational rearrangements in the N-domain of". In: *J Biol Chem* 295.15 (2020), pp. 4974–4984. ISSN: 1083-351X. DOI: 10.1074/jbc.RA119.011850.

[249] Gong S et al. *An Intra-Molecular Disulfide Cross-Link Stabilizes an Inward-Oriented Transport Intermediate Conformation of the TonB-Dependent Transporters*. Generic. 2015.

[250] T. D. Nilaweera et al. "Disulfide Chaperone Knockouts Enable In Vivo Double Spin Labeling of an Outer Membrane Transporter". In: *Biophys J* 117.8 (2019), pp. 1476–1484. ISSN: 1542-0086. DOI: 10.1016/j.bpj.2019.09.002.

[251] R. I. Hobb et al. "Evaluation of procedures for outer membrane isolation from Campylobacter jejuni". In: *Microbiology (Reading)* 155.Pt 3 (2009), pp. 979–988. ISSN: 1350-0872. DOI: 10.1099/mic.0.024539-0.

[252] W. J. Page and D. E. Taylor. "Comparison of methods used to separate the inner and outer membranes of cell envelopes of Campylobacter spp". In: *J Gen Microbiol* 134.11 (1988), pp. 2925–32. ISSN: 0022-1287. DOI: 10.1099/00221287-134-11-2925.

[253] T. D. Tullius and B. A. Dombroski. "Hydroxyl radical "footprinting": high-resolution information about DNA-protein contacts and application to lambda repressor and Cro protein". In: *Proc Natl Acad Sci U S A* 83.15 (1986), pp. 5469–73. ISSN: 0027-8424. DOI: 10.1073/pnas.83.15.5469.

[254] J. A. Espino and L. M. Jones. "Illuminating Biological Interactions with in Vivo Protein Footprinting". In: *Anal Chem* 91.10 (2019), pp. 6577–6584. ISSN: 1520-6882. DOI: 10.1021/acs.analchem.9b00244.

[255] D. Nguyen et al. “Reference Parameters for Protein Hydrogen Exchange Rates”. In: *J Am Soc Mass Spectrom* 29.9 (2018), pp. 1936–1939. ISSN: 1879-1123. DOI: 10.1007/s13361-018-2021-z.

[256] D. Sparvoli et al. “Diversification of CORVET tethers facilitates transport complexity in”. In: *J Cell Sci* 133.3 (2020). ISSN: 1477-9137. DOI: 10.1242/jcs.238659.

[257] N. Morè et al. “Peptidoglycan Remodeling Enables Escherichia coli To Survive Severe Outer Membrane Assembly Defect”. In: *mBio* 10.1 (2019). ISSN: 2150-7511. DOI: 10.1128/mBio.02729-18.

[258] M. Grabowicz et al. “A mutant Escherichia coli that attaches peptidoglycan to lipopolysaccharide and displays cell wall on its surface”. In: *Elife* 3 (2014), e05334. ISSN: 2050-084X. DOI: 10.7554/eLife.05334.

[259] A. Vermassen et al. “Cell Wall Hydrolases in Bacteria: Insight on the Diversity of Cell Wall Amidases, Glycosidases and Peptidases Toward Peptidoglycan”. In: *Front Microbiol* 10 (2019), p. 331. ISSN: 1664-302X. DOI: 10.3389/fmicb.2019.00331.

[260] M. Mathelié-Guinlet et al. “Lipoprotein Lpp regulates the mechanical properties of the E. coli cell envelope”. In: *Nat Commun* 11.1 (2020), p. 1789. ISSN: 2041-1723. DOI: 10.1038/s41467-020-15489-1.